Cell

Non-canonical odor coding in the mosquito

Graphical abstract

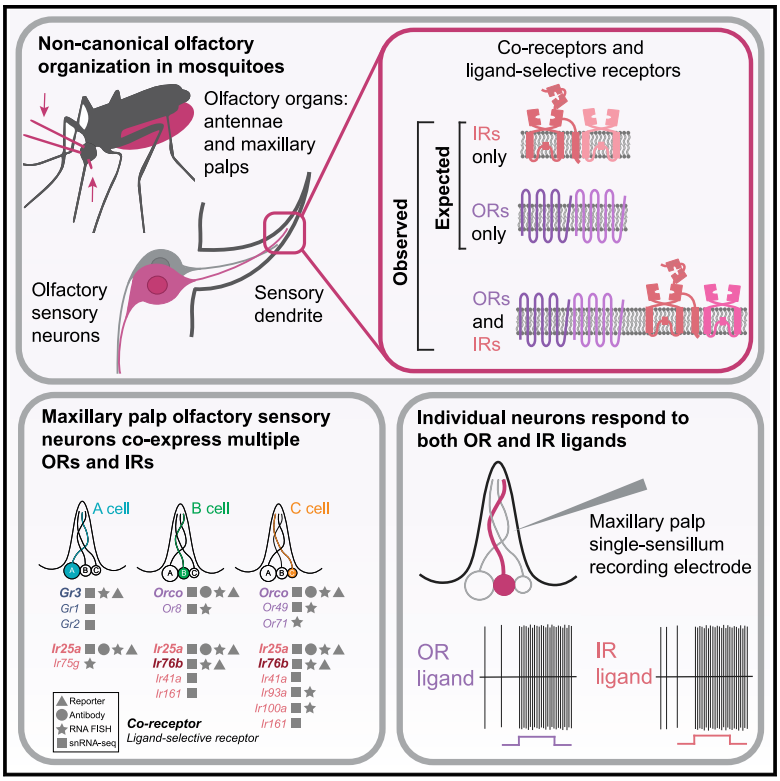

Highlights

- Mosquito olfactory neurons express multiple chemoreceptors
- A given neuron can express multiple members of several chemoreceptor gene families
- Single-nucleus RNA-sequencing points to an unexpectedly large diversity of neurons
- Chemoreceptor co-expression is functionally relevant to odorant responses

Authors

Margaret Herre, Olivia V. Goldman, Tzu-Chiao Lu, ..., Hongjie Li, Leslie B. Vosshall, Meg A. Younger

Correspondence

myounger@bu.edu

In brief

Humans produce a complex blend of odor cues that attract female mosquitoes, and these cues are typically detected by olfactory neurons expressing a single receptor. In female *Aedes aegypti* mosquitos, however, many of these neurons co-express multiple chemosensory receptors directly affecting mosquito behavior and challenging the canonical one-receptor-to-one-neuron organization.

Herre et al., 2022, Cell *185*, 3104–3123
August 18, 2022
https://doi.org/10.1016/j.cell.2022.07.024

CellPress

CellPress
OPEN ACCESS

Cell

Article

Non-canonical odor coding in the mosquito

Margaret Herre,[1,2,3,8] Olivia V. Goldman,[1,2,8] Tzu-Chiao Lu,[4] Gabriela Caballero-Vidal,[5] Yanyan Qi,[4] Zachary N. Gilbert,[1] Zhongyan Gong,[1,9] Takeshi Morita,[1,6] Saher Rahiel,[1] Majid Ghaninia,[5] Rickard Ignell,[5] Benjamin J. Matthews,[1,6,10] Hongjie Li,[4] Leslie B. Vosshall,[1,2,6] and Meg A. Younger[1,2,7,8,11,*]

[1]Laboratory of Neurogenetics and Behavior, The Rockefeller University, New York, NY 10065, USA
[2]Kavli Neural Systems Institute, New York, NY 10065, USA
[3]Weill Cornell/Rockefeller/Sloan Kettering Tri-Institutional MD-PhD Program, New York, NY 10065, USA
[4]Huffington Center on Aging and Department of Molecular and Human Genetics, Baylor College of Medicine, Houston, TX 77030, USA
[5]Disease Vector Group, Unit of Chemical Ecology, Department of Plant Protection Biology, Swedish University of Agricultural Sciences, Alnarp 234 22, Sweden
[6]Howard Hughes Medical Institute, New York, NY 10065, USA
[7]Department of Biology, Boston University, Boston, MA 02215, USA
[8]These authors contributed equally
[9]Present address: Helen Wills Neuroscience Institute, University of California, Berkeley, Berkeley, CA 94720 USA
[10]Present address: University of British Columbia, Department of Zoology, Vancouver, BC V6S 0K3, Canada
[11]Lead contact
*Correspondence: myounger@bu.edu
https://doi.org/10.1016/j.cell.2022.07.024

SUMMARY

Aedes aegypti mosquitoes are a persistent human foe, transmitting arboviruses including dengue when they feed on human blood. Mosquitoes are intensely attracted to body odor and carbon dioxide, which they detect using ionotropic chemosensory receptors encoded by three large multi-gene families. Genetic mutations that disrupt the olfactory system have modest effects on human attraction, suggesting redundancy in odor coding. The canonical view is that olfactory sensory neurons each express a single chemosensory receptor that defines its ligand selectivity. We discovered that *Ae. aegypti* uses a different organizational principle, with many neurons co-expressing multiple chemosensory receptor genes. *In vivo* electrophysiology demonstrates that the broad ligand-sensitivity of mosquito olfactory neurons depends on this non-canonical co-expression. The redundancy afforded by an olfactory system in which neurons co-express multiple chemosensory receptors may increase the robustness of the mosquito olfactory system and explain our long-standing inability to disrupt the detection of humans by mosquitoes.

INTRODUCTION

Increased global travel, a growing world population, and rising temperatures increase the emergence and transmission of novel disease-causing pathogens spread by mosquitoes, ticks, and fleas. Diseases spread by arthropods collectively account for more than 700,000 deaths every year (WHO, 2020). *Ae. aegypti* mosquitoes spread arboviruses including dengue, Zika, yellow fever, and chikungunya. Female mosquitoes require a blood-meal for reproduction (Allan et al., 1987) and prefer to bite humans, which contributes to their effectiveness as a disease vector (Brown et al., 2014; Gouck, 1972; McBride et al., 2014). To identify human hosts, mosquitoes rely heavily on chemosensory cues, including carbon dioxide (CO_2) emitted from breath, and human body odor, which is a mixture of hundreds of different individual odorants including alcohols such as 1-octen-3-ol and volatile amines such as ammonia (Acree et al., 1968; Bernier et al., 2000; Cook et al., 2011; Davis, 1984; Gallagher et al., 2008; Geier et al., 1999; Kline, 1994; Smallegange et al., 2005; Smith et al., 1970). Insects detect chemosensory cues using receptors encoded by three large multi-gene families, odorant receptors (ORs), ionotropic receptors (IRs), and gustatory receptors (GRs). All three gene families encode ionotropic ligand-gated ion channels, in contrast to the metabotropic receptors utilized by vertebrates (Ihara et al., 2013). ORs are odorant-gated ion channels (Butterwick et al., 2018; Del Mármol et al., 2021; Sato et al., 2008; Wicher et al., 2008) that are formed by a heteromultimeric complex of the conserved odorant receptor co-receptor (Orco) and a ligand-selective OR (Benton et al., 2006; Larsson et al., 2004; Neuhaus et al., 2005; Sato et al., 2008). IRs are variant ionotropic glutamate receptors that are formed by one or more of three conserved co-receptors, Ir25a, Ir8a, and Ir76b, and ligand-selective subunits that determine the odorants detected by the receptor complex (Abuin et al., 2011; Benton et al., 2009; Silbering et al., 2011). Although GRs are primarily taste receptors (Clyne et al., 2000; Montell, 2009; Scott et al., 2001), CO_2, the important host cue that activates and attracts mosquitoes (Gillies, 1980) is detected by a

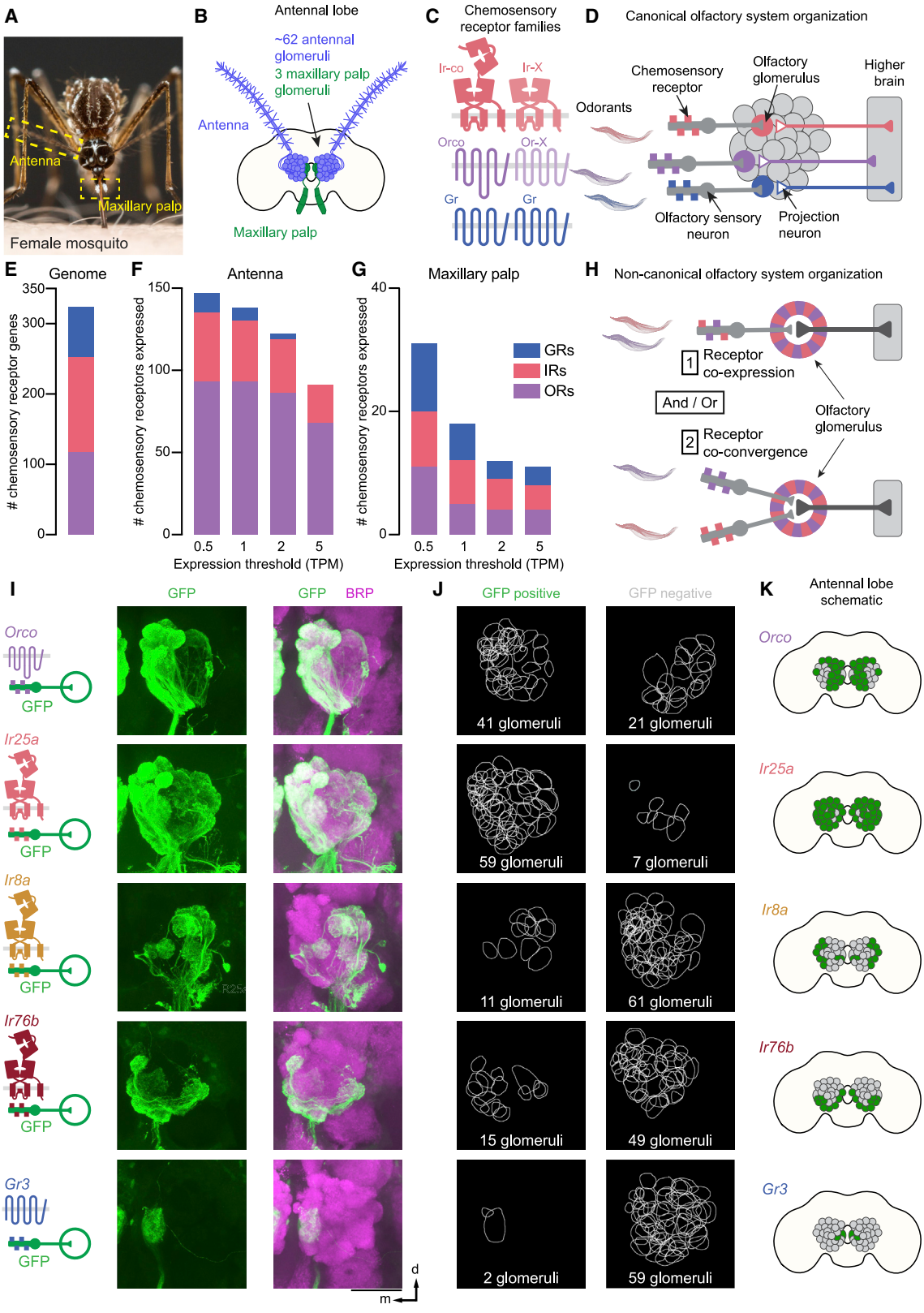

(legend on next page)

heteromultimeric complex of GRs (Jones et al., 2007; Kwon et al., 2007). *Ae. aegypti Gr3* encodes an essential subunit of the CO_2 receptor, and *Gr3* mutant mosquitoes lose all sensitivity to CO_2 (McMeniman et al., 2014).

Because mosquitoes specialize on humans and require blood to reproduce, the drive to find humans is strong and innate. Even mosquitoes missing entire families of chemoreceptors can find and bite people. *Orco* mutants have no functional ORs yet show strong attraction to humans (DeGennaro et al., 2013). Deleting *Ir8a, Ir76b,* or *Ir25a* co-receptors does not eliminate attraction to humans (De Obaldia et al., 2022; Raji et al., 2019). Similarly, while mosquitoes lacking *Gr3* do not respond to CO_2, they are highly effective in finding humans in a naturalistic semi-field setting (McMeniman et al., 2014).

The cloning of the first odorant receptors in 1991 (Buck and Axel, 1991) led to the discovery that each vertebrate olfactory sensory neuron (OSN) expresses a single odorant receptor (Bashkirova and Lomvardas, 2019; Chess et al., 1994). The same organization was originally reported in *Drosophila melanogaster* flies (Clyne et al., 1999; Gao and Chess, 1999; Vosshall et al., 1999), although recent work challenges this (McLaughlin et al., 2021; Task et al., 2022). Decades of evidence supports the model that neurons expressing a given receptor project axons to dedicated olfactory glomeruli in the first sensory processing center in the brain, the antennal lobe in insects (Couto et al., 2005; Fishilevich and Vosshall, 2005, 2000), and the olfactory bulb in vertebrates (Mombaerts et al., 1996; Ressler et al., 1994; Vassar et al., 1994). This ''one-receptor-to-one-neuron-to-one-glomerulus'' organization is believed to be a widespread motif in olfactory systems and is hypothesized to permit the brain to utilize combinatorial coding and parse which subpopulation of olfactory neurons is activated by a given odorant (Bisch-Knaden et al., 2018; Semmelhack and Wang, 2009; Wang et al., 2003).

Consistent with this organization, the number of expressed chemosensory receptors in the OR and IR gene families in many insects roughly corresponds to the number of olfactory glomeruli. This holds true in the honeybee *Apis mellifera* (~180 receptors/~160 glomeruli) (Flanagan and Mercer, 1989; Robertson et al., 2010), the tobacco hornworm *Manduca sexta* (~60 receptors/~70 glomeruli) (Grosse-Wilde et al., 2011), and *D. melanogaster* flies (~60 receptors/~55 glomeruli) (Benton et al., 2009; Laissue et al., 1999; Robertson et al., 2003). In *Ae. aegypti*, however, there is a striking mismatch between the number of expressed chemosensory receptors and the number of glomeruli, with at least twice as many receptors as glomeruli (Bohbot et al., 2007; Ignell et al., 2005; Matthews et al., 2018; Shankar and McMeniman, 2020; Zhao et al., 2022). This raises the question of how the mosquito olfactory system is organized and whether a deviation from rules established in other species explains their exquisite ability to locate human hosts.

In this study, we developed a CRISPR-Cas9-based genetic knock-in strategy to generate *Ae. aegypti* strains that label molecularly distinct populations of OSNs. We discovered that OR- and IR-expressing OSNs frequently innervated the same olfactory glomeruli. To ask if individual olfactory neurons express multiple chemosensory receptors, we profiled endogenous receptor expression in peripheral sensory organs using RNA *in situ* hybridization, immunofluorescence, and single-nucleus RNA sequencing (snRNA-seq). We found that the olfactory system of *Ae. aegypti* is unconventional in co-expressing multiple chemosensory receptors within individual OSNs. To test if multiple receptors function to detect different ligands within the same OSN, we used *in vivo* electrophysiology to examine odorant responses and discovered a class of neurons that expresses members of both the OR and IR gene family and found that both ORs and IRs are required to detect different classes of odorants in the same sensory neuron. This sensory organization, in which multiple receptors responding to different chemosensory stimuli are co-expressed, suggests a redundancy in the code for human odor. We speculate that this unconventional organization underlies the robust, seemingly unbreakable properties of the *Ae. aegypti* olfactory system in detecting human odor in this olfactory specialist.

RESULTS

Mismatch in chemosensory receptor and olfactory glomerulus number suggests a novel olfactory organization

In the mosquito, olfactory cues are sensed by OSNs in the antenna and the maxillary palp, whose axons project to the ipsilateral antennal lobe (Distler and Boeckh, 1997; Ignell et al., 2005) (Figures 1A–1D, S1A, and S1B). Previous studies used morphological criteria to define 50 to 81 (Ignell et al., 2005; Shankar and McMeniman, 2020; Zhao et al., 2022) discrete olfactory glomeruli in the female *Ae. aegypti* antennal lobe. In this study, we define approximately 65 olfactory glomeruli (64.9 ± 0.9, mean ± SEM). This number was obtained by counting glomeruli in the left hemisphere of 12 female *Ae. aegypti* brains stained to reveal synaptic neuropil (Figures 1B, 1I–1K, S1, S2, and S3). The glomerulus count ranged from 60 to 72 glomeruli, indicating a high level of variability in antennal lobe organization.

Figure 1. Mismatch in chemosensory receptor and olfactory glomerulus number

(A) *Ae. aegypti* female sensory structures (yellow boxes).

(B) Approximate number of antennal lobe glomeruli per left brain hemisphere innervated by the indicated sensory structure, quantified from 12 brains in (I–J) and Figure S1, S2, and S3.

(C and D) Cartoons of insect chemosensory gene families (C) and canonical olfactory system organization (D).

(E–G) Stacked bar plots of chemosensory gene number in the *Ae. aegypti* genome (E), and number expressed above indicated TPM thresholds in antenna (F) and maxillary palp (G).

(H) Two models of non-canonical olfactory system organization.

(I) Maximum-intensity projections of confocal z stacks of left antennal lobes of the indicated genotype with immunofluorescent labeling of GFP (green) and the nc82 monoclonal antibody, which recognizes the synaptic marker Brp (magenta). Scale bar: 50 μm. Orientation: d, dorsal; m, medial.

(J) 2D representation of the boundary of each glomerulus in (I) that is GFP positive or GFP negative. See also Figures S1, S2, and S3.

(K) Cartoon of antennal lobe regions receiving projections from OSNs expressing the indicated chemosensory receptor.

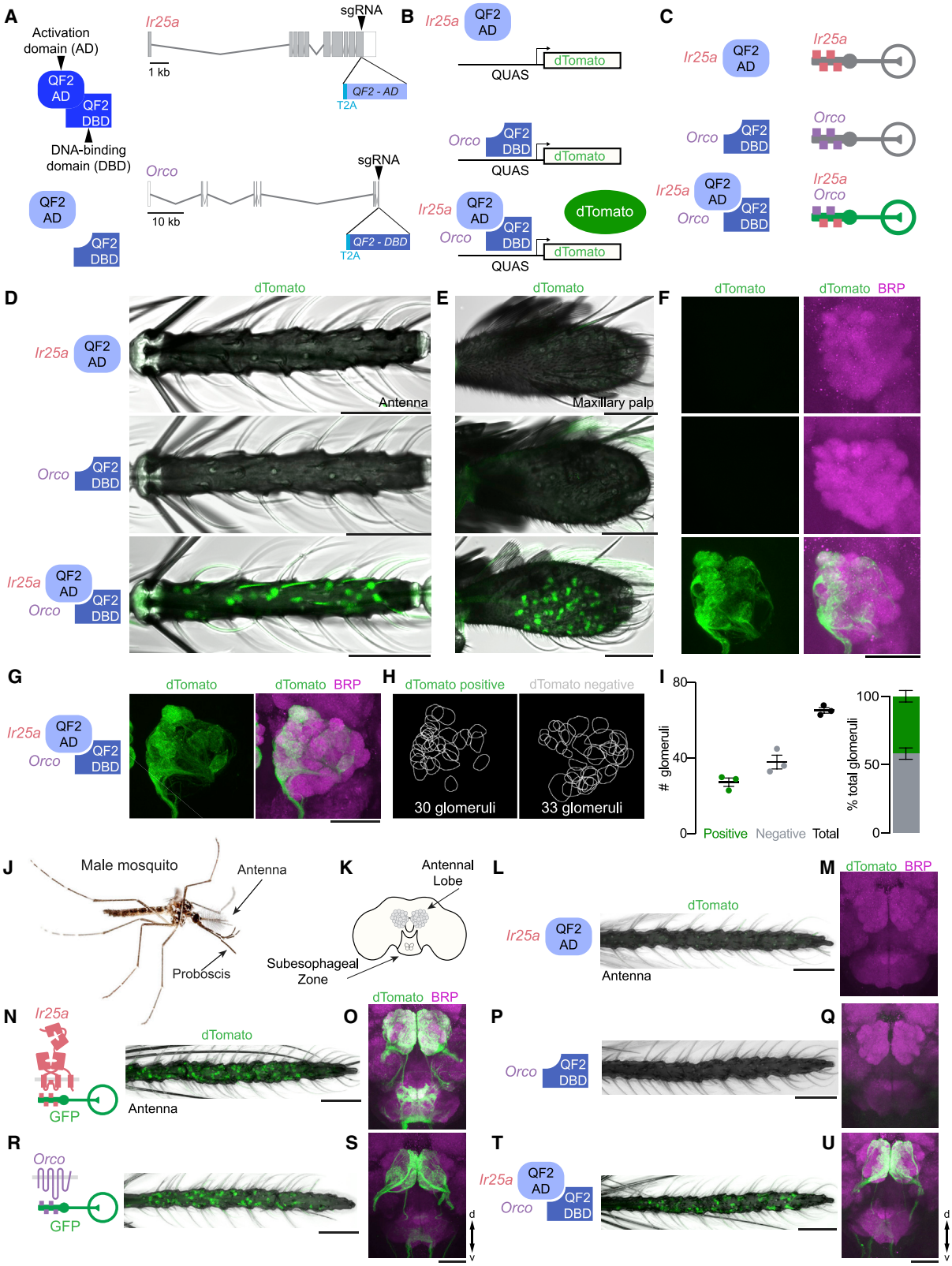

(legend on next page)

Canonical olfactory organization posits that the number of chemosensory receptors should roughly match the number of glomeruli in the antennal lobe (Figure 1D). In *Ae. Aegypti*, there are 324 structural genes for chemosensory receptors (117 OR, 135 IR, and 72 GR genes) (Figure 1E) (Matthews et al., 2018). Analysis of antennal and maxillary palp RNA-seq data (Matthews et al., 2016) demonstrates that even at the conservative threshold of 5 transcripts per million (TPM), the mosquito olfactory system expresses 102 chemosensory receptors. Adjusting the threshold to 2, 1, or 0.5 TPM increases the number of receptors plausibly expressed to 134, 156, and 178, respectively (Figures 1F and 1G). Thus, there are many more chemosensory receptors expressed than antennal lobe glomeruli. This mismatch could be resolved by expressing multiple receptors per neuron or having multiple molecularly distinct neurons co-converge on a single glomerulus or a combination of co-expression and co-convergence (Figure 1H).

To distinguish between these possibilities, we generated CRISPR-Cas9 gene-targeted strains that label subpopulations of olfactory neurons. We used the Q-system, a binary expression system that uses cell-type-specific expression of the QF2 transcription factor, to induce expression of an effector when QF2 binds a *QUAS* enhancer (Potter et al., 2010; Riabinina et al., 2015, 2016). We introduced an in-frame insertion that replaced the stop codon of each of the co-receptors *Orco*, *Ir25a*, *Ir8a*, and *Ir76b*, as well as *Gr3* with the transcription factor *QF2* (Figures 1I, S1, S2, and S3; see Data S1 for a full description of all genotypes by figure) (Matthews et al., 2019; Potter et al., 2010; Riabinina et al., 2016). We crossed these *QF2* driver lines individually to a *QUAS-CD8:GFP* reporter to label neuronal membranes and visualized axonal projection patterns in the antennal lobe.

Orco, *Ir25a*, *Ir8a*, and *Ir76b* co-receptor driver lines exhibited reporter expression in OSNs with distinct projection patterns in the antennal lobe (Figures 1I–1K). Unexpectedly, neurons that expressed *Ir25a* projected to almost all glomeruli in the antennal lobe (89.9 ± 1.4%, mean ± SEM, n = 3) (Figures 1I–1K and S2), and expression overlapped extensively with glomeruli labeled by *Orco* (Figures 1I–1K, S1, and S2). Interindividual expression patterns were not identical, consistent with the variability in glomerular arrangement that we observed. Neurons that detect CO_2 are located in the maxillary palp (Grant et al., 1995; Lu et al., 2007; Omer and Gillies, 1971). *Gr3*-expressing neurons projected to a large glomerulus in the posterior antennal lobe, Glomerulus 1 (Figures 1I–1K), which is also innervated by *Ir25a*-expressing neurons. We noted the presence of a second small glomerulus that was often innervated by *Gr3*-expressing neurons in the antenna (Figures S1O and S1P). These initial findings point to the overlap of projections of *OR*-, *IR*-, and *GR*-expressing neurons in the antennal lobe of *Ae. aegypti*, consistent with recent observations in *D. melanogaster* (Task et al., 2022).

Co-expression of *Orco* and *Ir25a* in the mosquito olfactory system

The high degree of overlap between glomeruli labeled by *Orco*- and *Ir25a*-expressing OSNs suggests that there is either widespread *Orco* and *Ir25a* co-expression within individual neurons or that *Orco* and *Ir25a* are expressed in different neurons whose axons co-converge onto individual antennal lobe glomeruli or both (Figure 1H). To determine if *Orco* and *Ir25a* are co-expressed, we used the Split-QF2 system (Riabinina et al., 2019), which "splits" the transcription factor QF2 into two components, the DNA binding domain (QF2-DBD) and the activation domain (QF2-AD) each tagged with a synthetic leucine zipper (Figures 2A and 2B). When both the QF2-DBD and QF2-AD are co-expressed in the same cell, the two domains associate via the leucine zipper, reconstitute a functional QF2 protein, initiate transcription at the *QUAS* enhancer, and drive expression of a reporter gene (Figure 2C).

When either *Ir25a-QF2-AD* or *Orco-QF2-DBD* was used to drive expression of *dTomato* (Shaner et al., 2004), we did not see fluorescence in the female antenna, maxillary palp, or the antennal lobe (Figures 2D–2F and S4), but when *Orco-QF2-DBD* and *IR25a-QF2-AD* were crossed into the same animal, we saw expression of *dTomato* in antennal and maxillary palp neurons of female mosquitoes, as well as axonal projections in the antennal lobe (Figures 2D–2F and S4). Nearly half of the glomeruli in the antennal lobe were labeled with dTomato (Figures 2G–2I and S4). This points to widespread *Orco* and *Ir25a* co-expression, although these findings do not rule out the possibility that there may also be co-convergence. Male mosquitoes (Figures 2J–2U) showed similar expression and projection patterns to those found in females (Figures 2F, 2G, and 2U).

Another source of olfactory information may derive from olfactory neurons on the proboscis, the mouthpart of the mosquito.

Figure 2. Genetic evidence for widespread *Orco* and *Ir25a* co-expression

(A) Schematic of the Split-QF2 system (left) and *Orco* and *Ir25a* gene loci with exons (gray boxes), introns (gray lines) and CRISPR-Cas9 gRNA site (arrowhead) used to insert *T2A-QF2-AD* (light blue) and *T2A-QF2-DBD* (medium blue). *AD* and *DBD* gene maps are not to scale.

(B and C) Schematic of Split-QF2 system (B) and gene expression in indicated genotypes (C).

(D and E) Maximum-intensity projections of confocal z stacks of female antennae (D) and female maxillary palps (E) of indicated genotypes showing intrinsic dTomato fluorescence, transmitted light overlay. See also Figure S4.

(F and G) Maximum-intensity projections of confocal z stacks of antennal lobes from the indicated genotype with immunofluorescent labeling of dTomato (green) and Brp (magenta). See also Figure S4.

(H and I) 2D representation of each glomerulus in (G) that is GFP positive or GFP negative (H) and quantification (I). Data are mean ± SEM, n = 3. See also Figure S4A.

(J) *Ae. aegypti* male with sensory structures (arrows).

(K) Cartoon of the brain including antennal lobe glomeruli and suboesophageal zone.

(L–U) Maximum-intensity projections of confocal z stacks of male antennae (L, N, P, R, and T) and male brains (M, O, Q, S, and U) of the indicated genotype with immunofluorescent labeling of dTomato (green) and Brp (magenta).

Scale bars: 50 μm. Orientation: proximal left (D, E, L, N, P, R, and T), medial left (F and G); d, dorsal; v, ventral; m, medial.

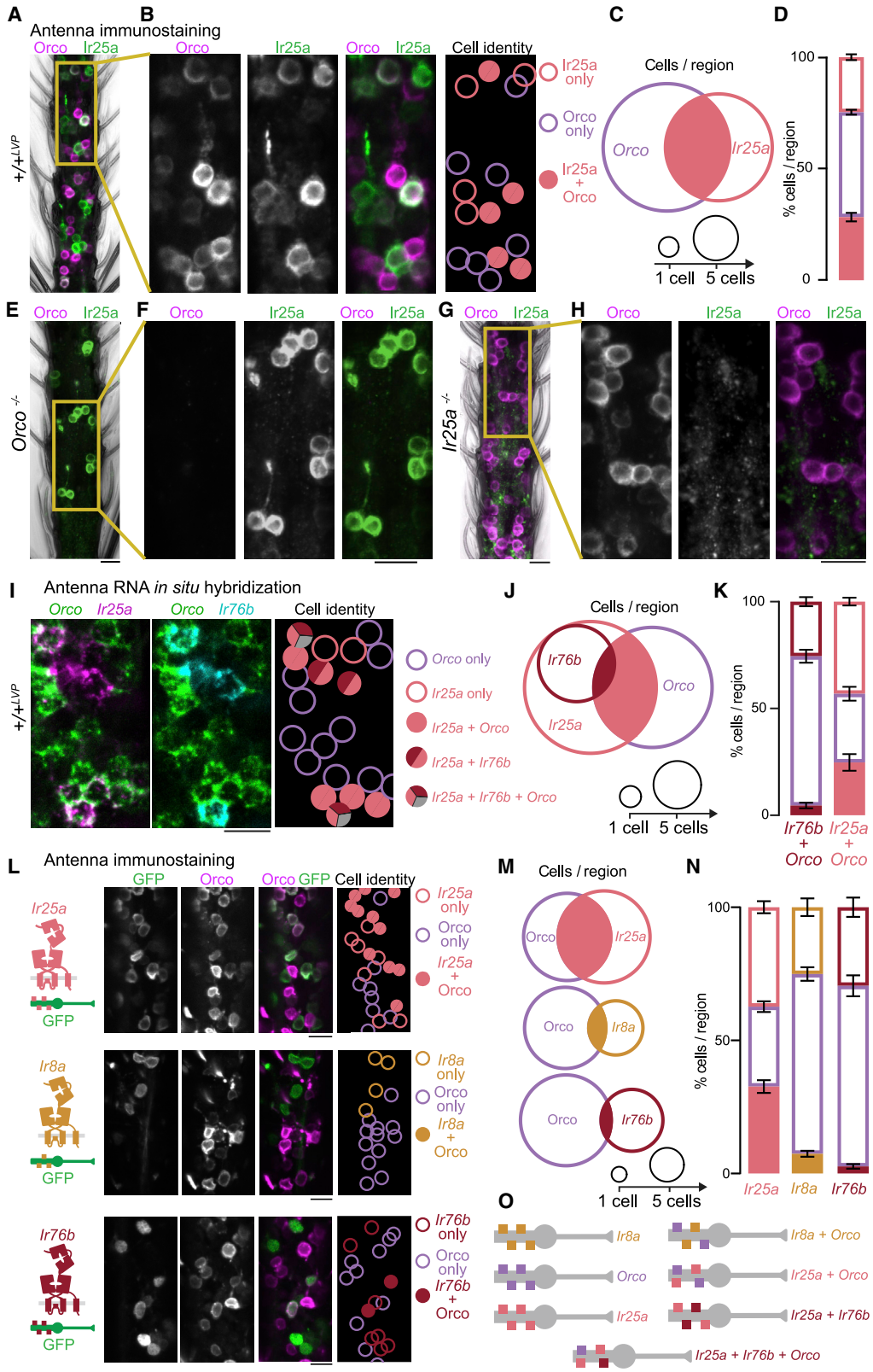

(legend on next page)

We saw extensive expression of both *Orco* and *Ir25a* alone in the proboscis and the subesophageal zone (Figure S4) as well as co-expression of *Orco* and *Ir25a* as defined by dTomato expression in the Split-QF2 animals (Figure S4). It is possible that sensory afferents in the proboscis detect olfactory and gustatory information, or that IRs and ORs both function as olfactory receptors in these neurons.

Extensive co-expression of chemosensory co-receptors in the antenna

To determine if neurons co-express Orco and Ir25a protein, we conducted whole mount antennal immunofluorescence to label endogenous Orco and Ir25a proteins in wild-type mosquito antennae and observed extensive co-expression of Orco and Ir25a (Figures 3A–3D). In addition to neurons that contain both Orco and Ir25a protein, we saw neurons that express either Orco or Ir25a alone (Figures 3A–3D), indicating a mixed population of OR cells, IR cells, and OR + IR cells. Staining was absent in the respective *Orco* and *Ir25a* mutants, confirming the specificity of the antibodies (Figures 3E–3H). To confirm and extend these results, we performed RNA *in situ* hybridization on wild-type antennae with *Orco, Ir76b,* and *Ir25a* probes (Figures 3I–3K) and discovered that almost half of *Orco* cells co-express *Ir25a*, and vice versa. In contrast, few *Orco* cells co-express *Ir76b*.

To study the overlap between Orco and the three major IR co-receptors, we carried out antennal immunofluorescence with antibodies to the endogenous Orco protein and to GFP expressed from each QF2 driver. We confirmed extensive co-expression of Orco and *Ir25a* (Figures 3L–3N) and found that substantially fewer cells co-express either Orco and *Ir8a* or Orco and *Ir76b*, even after accounting for fewer total *Ir76b* and *Ir8a* cells (Figures 3L–3N). In addition to widespread co-receptor co-expression, some olfactory neurons express just one co-receptor (Figure 3O), highlighting the complexity in receptor expression patterns in *Ae. aegypti* antennal neurons.

snRNA-seq reveals a high diversity of antennal neurons and co-expression of multiple ligand-selective receptor subunits

Functional ORs and IRs are composed of co-receptor and ligand-selective receptor subunits. Because there are hundreds of ligand-selective OR and IR genes, it was not feasible to examine combinatorial co-expression of the full complement of receptors by fluorescent RNA *in situ* hybridization or immunofluorescence. Instead, we carried out snRNA-seq (Li et al., 2022; McLaughlin et al., 2021) in mosquito antennae and identified 13,879 total cells (we use the term "cell" to refer to data from a single nucleus) (Figures 4A and S5A–S5G). Unsupervised clustering was used to categorize cells into broad subtypes, which revealed clusters expressing epithelial or glial markers (Figures 4B, S5G, and S5H). We classified neuron clusters based on the expression of at least 3 of 4 neural markers (*cadN*, *brp*, *syt1*, *elav*) in 50% or more of the cells within that cluster, resulting in a total of 5,175 identified neurons (Figure S5I).

We used unsupervised clustering with high resolution on the neuron population to identify chemosensory cell types, here defined as a group of cells expressing the same chemosensory receptor gene or combination of receptor genes (Figure 4C). We classified clusters 2 and 25 as mechanosensory neurons (6.78% of total neurons) based on expression of *LOC5575210*, a homolog of the *D. melanogaster* mechanoreceptor *nompC*. Over 90% of all identified neurons clustered according to distinct patterns of ligand-selective receptor gene expression, comprising at least 35 detectable chemosensory cell types (Figures 4D and S6A).

By averaging receptor gene expression across a cluster, we identified many clusters in which multiple receptors—multiple ORs, multiple IRs, as well as ORs and IRs together—were co-expressed (Figures 4D and S6A). Often individual chemosensory receptors belonged to only one cluster, either expressed alone or within a set of chemosensory receptors. Some receptors appeared in multiple clusters with different sets of co-expression partners, such as *Or82* (Figure 4F). Some clusters contained OSNs that clustered together yet express distinct chemoreceptors, likely due to global transcriptome similarity (Figures 4D and S5L–S5M). This is observed in cluster 0, which expresses *Ir41k*, *Ir41o*, and *Ir41p*, but these genes do not appear to be co-expressed within individual cells (Figure S5M). Thus, we performed cluster-independent analyses to document mutually exclusive expression and co-expression of chemoreceptors.

We defined co-expression of two receptor genes when expression of both occurred in more than 10 cells above a normalized value of 1 (equivalent to an adjusted-unique molecular identifier [UMI] threshold of 2 or higher) (Figures 4E, S6A, and

Figure 3. Extensive chemosensory co-receptor co-expression in the antenna

(A) Maximum-intensity projection of whole-mount wild-type female antennae with immunofluorescent labeling of Orco and Ir25a.

(B) Enlarged view of the yellow rectangle in (A) with cartoon indicating cell identity (right).

(C and D) Quantification of wild-type antennal cells expressing Orco and Ir25a presented as Euler diagrams with area scaled to mean cells/region (C) and stacked bar plots (D). Data are mean ± SEM, n = 7 antennal segments, 48–61 cells/region.

(E and G) Maximum-intensity projection of whole-mount *Orco*$^{16/16}$ mutant (E) and *Ir25a*$^{BamHI/BamHI}$ mutant (G) female antennae with immunofluorescent labeling of Orco and Ir25a.

(F and H) Enlarged view of the yellow rectangles in (E and G).

(I) RNA *in situ* hybridization in wild-type antennae. Probes indicated.

(J and K) Euler plots of wild-type antennal cells expressing the indicated genes with area scaled to mean cells/region (J) and stacked bar plots (K). Data are mean ± SEM, n = 4 antennal segments, 45–63 cells/region.

(L) Maximum-intensity projection of whole-mount Orco and GFP immunofluorescence in female antennae of the indicated genotypes with cartoon schematic indicating cell identity (right).

(M and N) Euler plots of antennal cells of the indicated genotypes co-expressing Orco protein and GFP, area scaled to mean cells/region (M) and stacked bar plots (N). Data are mean ± SEM, n = 6–8 antennal segments, 34–68 cells/region.

(O) Cartoon schematic of OSN populations identified in this figure. Scale bars: 10 μm.

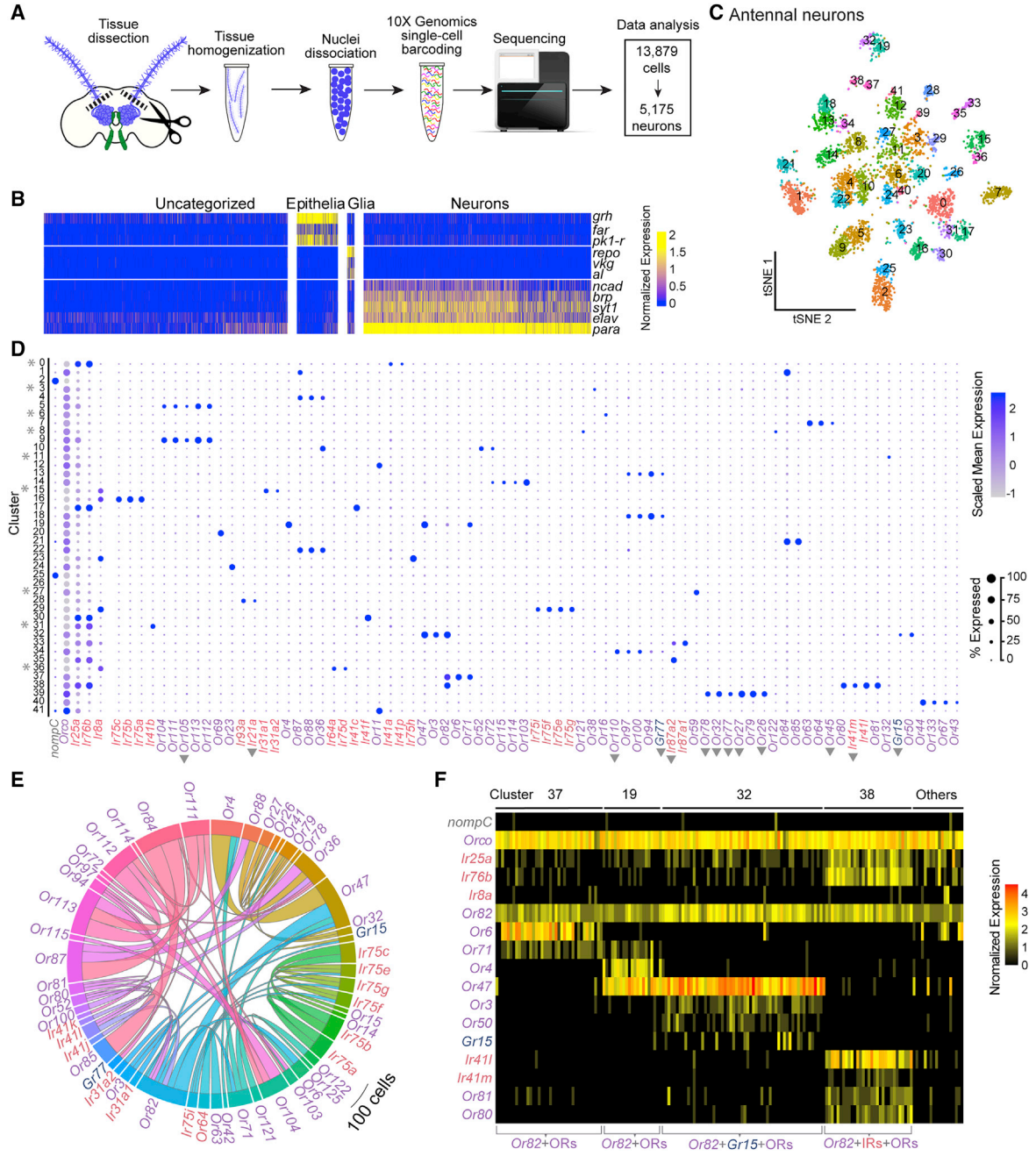

Figure 4. Antennal snRNA-seq reveals complex chemosensory receptor co-expression

(A) Female antenna snRNA-seq workflow.

(B) Heatmap of antenna cells within clusters that express cell-type markers according to normalized expression (unit for normalized expression in antenna data is ln(sctransform-adjusted UMI), see STAR Methods) (see Figure S5H).

(C) t-distributed stochastic neighbor embedding (t-SNE) plot of antennal neurons annotated by cluster (see Figure S5I).

(D) Dot plot illustrating mean scaled expression (*Z* score) of chemosensory receptor expression within each cluster. Note that presence of two chemoreceptor genes expressed in the same cluster does not always indicate that they are co-expressing in the same cells (see Figures S5L–S5M and S6A). Clusters marked with an asterisk exhibit co-clustering without co-expression of some or all of illustrated genes. Genes marked with a triangle may be lower- or sparsely expressed genes that exhibited specific expression to that cluster, but may have not met our defined criteria for expression or co-expression.

(E) Chord plot of co-expressed pairs of chemosensory receptors that meet co-expression criteria for ligand-specific receptors: both genes present in over 10 cells at a sctransform-adjusted UMI value of 2 or greater. (For non-sctransform-adjusted UMIs, see Figure S5J.) Note: normalized expression value of 1 corresponds to sctransform-adjusted UMI of 2 or greater.

(legend continued on next page)

S6B). For *Orco,* which is expressed at an order of magnitude higher than other receptor genes and contributes more to ambient RNA contamination, we used a normalized expression threshold of 2 (Figures S5A, S5F, and S6). Within cells in cluster 38, we observed above-threshold co-expression of *Orco, Ir25a* and ligand-specific receptors *Or82*, *Ir41l*, and other ligand-specific ORs and IRs (Figures 4D and 4F). Co-expression of *Orco* and *Ir25a* appeared in individual cells in over 10% of our neuron population (Figure S5K). For example, in ligand-specific OR-expressing clusters 9 and 5, many cells also express *Ir25a* (Figure S6).

The significance of variable expression levels among receptor genes in their respective cells remains unclear. *Ir41k* is expressed at very high levels, even in relation to co-receptors (Figure S5M and S6A). Using our expression criteria, *Ir41k* is expressed in 59 cells but has a greater number of total counts than *Ir8a*, which is expressed in over four times as many cells (Figure S5F and S6A). These results highlight the diversity of chemoreceptor expression levels in antennal neurons. Future studies may reveal how variability in expression levels may interact with activity.

Coordinated co-expression of chemosensory receptors in the maxillary palp

We next examined receptor co-expression in the maxillary palp, a smaller and simpler olfactory organ that detects important host cues including CO_2 and 1-octen-3-ol (Grant et al., 1995; Lu et al., 2007; McMeniman et al., 2014; Omer and Gillies, 1971). Each female *Ae. aegypti* maxillary palp contains approximately 35 capitate-peg sensilla that each house three chemosensory neurons (McIver, 1982) termed "A," "B," and "C" cells based on their size, from largest to smallest respectively (Figures 5A–5C and S3V).

We hypothesized that these three cell types project to three glomeruli in the antennal lobe, and we used our QF2 and Split-QF2 driver lines to examine this (Figures 5E–5K). We discovered that Glomerulus 1, which is the largest glomerulus in the antennal lobe (Shankar and McMeniman, 2020), received input from *Gr3*- and *Ir25a*-expressing sensory afferents (Figures 5F–5K). Glomerulus 2 and Glomerulus 3 received input from *Orco*-, *Ir25a*-, and *Ir76b*-expressing neurons (Figures 5F–5K). Co-expression of *Orco* and *Ir25a* in neurons that project to these two glomeruli was confirmed using the Split-QF2 system. In *Orco-QF2-DBD*, *IR25a-QF2-AD* animals, Glomerulus 2 and Glomerulus 3 were labeled, but Glomerulus 1 was not (Figure 5E). These findings suggest that the A, B, and C cells express multiple co-receptors, spanning IR-OR and IR-GR classes.

To determine the extent of co-expression of both co-receptors and ligand-selective receptors, we carried out multiplexed whole-mount RNA *in situ* hybridization (Choi et al., 2018) in the maxillary palp (Figures 5L–5P and S3), which expresses only 18 receptors at the 1 TPM threshold compared to 138 in the antenna (Figures 1F and 1G). We performed RNA *in situ* hybridization with probes for 10 of these receptors and visualized gene expression with sufficient sensitivity that even *Or71* and *Ir75g* (present at 1.93 and 1.67 TPM, respectively) were readily detected (Figures S3S and S3T).

We found no overlap in expression of *Orco* and *Gr3*, but *Ir25a* was expressed in all *Orco* and all *Gr3* cells (Figure 5L). Previous work in *Anopheles gambiae* suggested that *Orco*-expressing neurons in the maxillary palp can be evenly divided into two non-overlapping groups: an *Or8* population and an *Or49* population (Lu et al., 2007). The same was assumed in *Ae. aegypti* but has never been shown. We show definitively that *Or8* and *Or49* are expressed in segregated populations of *Orco*-expressing neurons (Figure 5M) and, when combined with the results of the previous experiment (Figure 5L), that these cells are all *Ir25a*-positive. Additional RNA *in situ* hybridization experiments revealed that *Or8*- and *Or49*-expressing cells also often express *Ir76b,* with a bias toward expression in *Or8*-expressing B cells (Figures 5N and S3; Data S1). Therefore, *Orco*-expressing OSNs co-express the co-receptor *Ir25a* and either of the ligand-selective subunits *Or49* or *Or8*, and often co-express the co-receptor *Ir76b.*

When we analyzed IR ligand-selective subunit expression, we found that *Ir100a* and *Ir93a* are selectively expressed in a subset of *Or49*-expressing C cells (Figures 5O, 5P, S3P, and S3Q), suggesting that both functional OR and IR complexes can form in the same neuron and that co-expression may be transcriptionally coordinated. *Or71* and *Or49* were co-expressed, further supporting the idea that multiple ligand-selective ORs can be expressed in an OSN (Figure S3S). We also discovered that the ligand-selective receptor *Ir75g* was expressed in some *Gr3*-expressing cells, which also express *Ir25a* (Figure S3T). It is plausible that *Gr3* neurons can express both functional GRs and IRs.

snRNA-seq of maxillary palp reveals unanticipated neuronal complexity

Our RNA *in situ* hybridization results contradict the current view in the field: that each *Ae. aegypti* maxillary palp has 35 molecularly and functionally identical capitate-peg sensilla (Figure 5A). To expand our analysis, we carried out snRNA-seq using similar methods to those described for the antenna (Figures 6A and S7), which yielded data from 2,298 cells. Using unsupervised clustering, we identified some clusters as epithelia, muscle, glia, or neurons (Figure 6B, 6C, and S7E–S7G). The neuron clusters contained 630 cells that were subdivided into four classes with remarkable correspondence to cell classes previously described in the maxillary palp (Figures 6C, 6D, S7F, S7G, S7L, and S7O). Cluster 4 consists of putative mechanosensory neurons marked by expression of *nompC* and *hamlet*. Clusters 1, 2, and 3 were enriched for *Gr3*, *Or8*, or *Or49*, and likely correspond to A, B, and C cells, respectively (Figures 6D, 6F, 6J, 6K, S7L, and

(F) Heatmap of all cells within neuron population expressing *Or82* above a normalized expression value of 1. Receptors are indicated in rows and cells indicated in columns. Cluster assignment of cells indicated above heatmap. "Others" denotes small groups of cells that belonged to 12 other clusters apart from the ones labeled. *nompC* included for non-quantitative reference of potential background signal. Heatmap colors represent normalized expression. Visually identified cell types are offset with brackets listing the chemosensory receptors expressed in that cell type.
See also Figures S5 and S6.

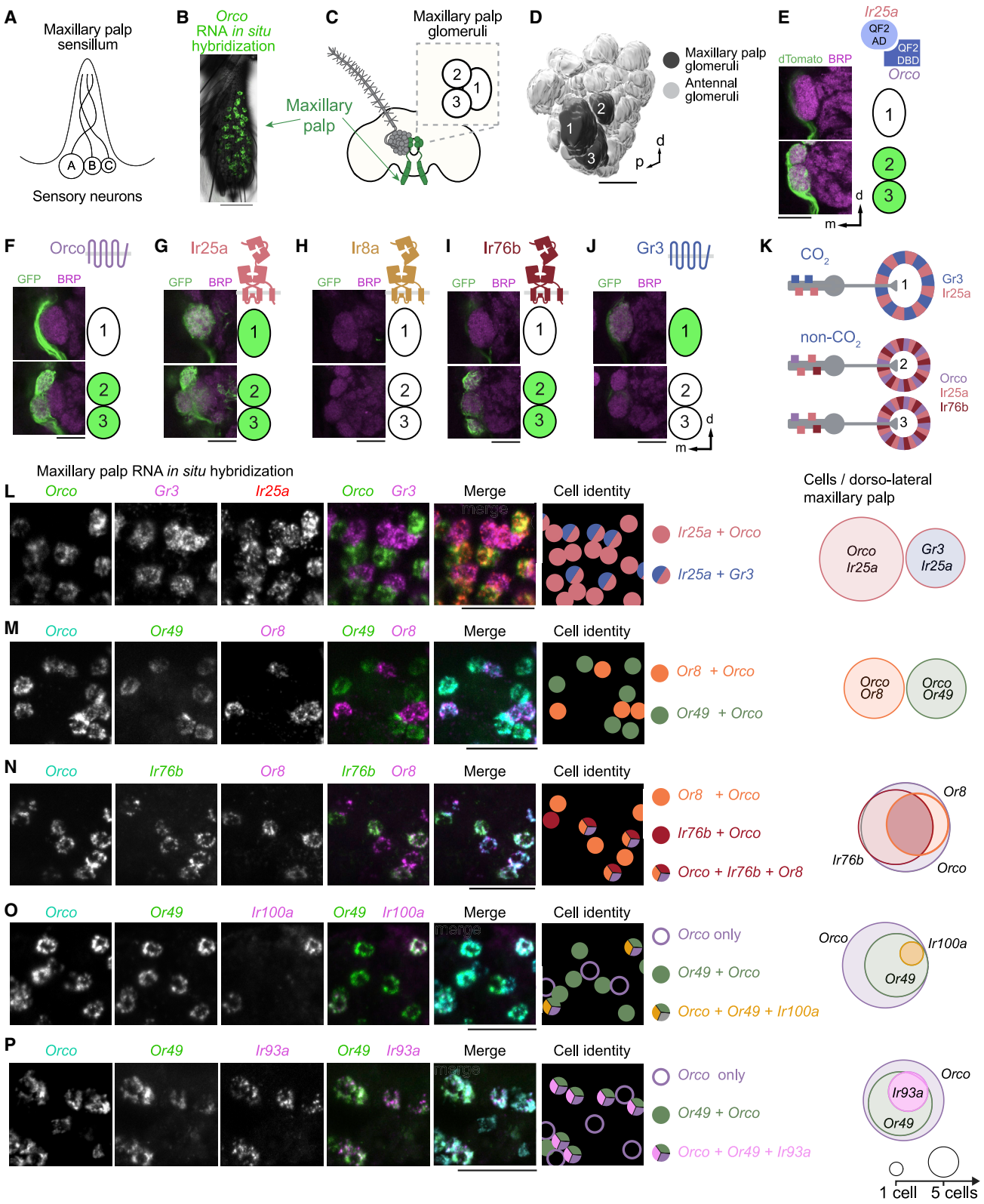

(legend on next page)

S7O). Applying similar parameters for receptor co-expression as for the antenna, we found that *Or49* sometimes co-expressed with *Ir93a* (Figure 6E), in accordance with our RNA *in situ* hybridization results.

Because the maxillary palp data had both fewer neurons and chemoreceptors, as well as sparser expression than in the antenna, we framed our analysis on the three known cell classes. We established expression within a cell class such that a receptor was present in at least 10 cells within the corresponding cluster above a normalized expression value of 1 (Figure 6Q). We used feature plots to visualize the expression of ligand-specific receptors within the clusters of maxillary palp neurons. snRNA-seq data showed expression of *Ir41a* and *Ir161* in both the *Or8*-expressing B and *Or49*-expressing C clusters (Figures 6J, 6K, 6O, and 6P), as well as the *Or49*-expressing *C* cluster sometimes expressed *Ir100a* (Figure 6M). As we saw in the RNA *in situ* hybridization findings, cells expressing *Or49*, *Or8*, or *Gr3* can but do not always express certain ligand-specific IRs, indicating that these classes are likely to be heterogeneous.

Ir25a appeared in a high percentage of cells in all three clusters, accompanied by *Ir76b* in only the B and C cell clusters (Figures 6H, 6I, S7L, and S7O). Abundant chemoreceptors such as *Gr2*, *Orco*, and *Or8* were expressed highly in their expected cell classes (Figures 6G, 6J, and S7K–S7O). Lower-level expression of these genes was also present in a high percentage of cells from other clusters. The significance of this is unclear.

A summary and interpretation of maxillary palp chemosensory receptor gene expression is presented in Figure 6Q. These data suggest that many B and C cells have all the necessary subunits to form both functional ORs and IRs (Figures 6F–6P), representing a departure from the current view.

Receptor co-expression expands the functional responses of olfactory neurons

We next asked whether chemosensory receptor co-expression allows maxillary palp neurons to respond to odorants detected by both ORs and IRs. We used single sensillum recording to measure odorant responses of the OSNs housed in maxillary palp capitate-peg sensilla. This method of *in vivo* extracellular electrophysiology enables the simultaneous recordings of A, B, and C cells in response to odorant stimuli in an intact mosquito. Spike sorting is used to discriminate activity of these neurons. The diameter of the cell positively correlates with the spike amplitude (Zhang et al., 2019). The largest A cell responds to CO_2, whereas the smaller B cell responds to 1-octen-3-ol (Bohbot and Dickens, 2009; Cook et al., 2011; Grant et al., 1995; Majeed et al., 2017; Syed and Leal, 2007). The smallest C cell has no characteristic ligands in *Ae. aegypti* and was therefore excluded from our analysis (Figures 7A–7E).

To determine which family of receptors—GRs, ORs, or IRs—detects a given ligand, we recorded odorant responses in wild-type mosquitoes as well as mosquitoes with mutations in *Gr3*, *Orco*, or *Ir25a*. Because the *Gr3* and *Orco* receptor mutants were generated in a different wild-type strain ($+/+^{ORL}$) than the *Ir25a* mutant ($+/+^{LVP}$) (De Obaldia et al., 2022), all analyses were conducted in two different wild-type background strains, which consistently showed similar odorant responses (Figures 7A–7E).

As previously seen (McMeniman et al., 2014), the A cell responded to CO_2 in a dose-dependent manner, but the B cell did not. The A cell CO_2 response was abolished in *Gr3* mutants (Figure 7A). CO_2-sensing neurons in the mosquito maxillary palp respond to multiple odorants (Lu et al., 2007; Tauxe et al., 2013; Turner et al., 2011), and it has been proposed that *Gr3* is a broadly tuned receptor that responds to many odorants. We examined the response to a recently identified A cell agonist, acetone (Ghaninia et al., 2019), which also activated the A cell but not the B cell (Figure 7B). The response to acetone was abolished in the *Gr3* mutant (Figure 7B), which suggests that the CO_2 receptor interacts with non-CO_2 ligands.

The host-emitted odorant 1-octen-3-ol has been shown to activate the B cell, as well as *Ae. aegypti* and *An. gambiae* Or8-Orco when expressed in heterologous cells (Bohbot and Dickens, 2009; Lu et al., 2007). We found that firing of the B cell, but not the A cell, increased in the presence of 1-octen-3-ol, and this response was abolished in the *Orco* mutant, but not in *Gr3* or *Ir25a* mutants (Figure 7C), consistent with the role of Or8-Orco in detecting this compound.

Volatile amines, including polyamines, have been proposed to be IR ligands in *D. melanogaster* (Geier et al., 1999; Hussain et al., 2016; Min et al., 2013; Silbering et al., 2011). We therefore examined the response of maxillary palp neurons to two volatile amines, hexyl amine, and triethyl amine. We found that both amines activated the B cell in wild type, *Gr3* mutants, and *Orco* mutants (Figures 7D–7F). Average responses to hexyl amine and triethyl amine were strongly reduced but not abolished in the *Ir25a* mutant. When we scrutinized the raw data, we noted that the majority of *Ir25a* mutant neurons did not respond to these stimuli at all, but a few neurons responded to both stimuli even more robustly than wild type (Data S1).

Figure 5. Coordinated co-expression of chemosensory receptors in the maxillary palp

(A) Maxillary palp capitate-peg sensillum with A, B, and C cells.

(B) Maxillary palp expression of Orco in the fourth maxillary palp segment revealed by whole-mount RNA *in situ* hybridization. Orientation: proximal up.

(C) Maxillary palp (green) and three glomeruli that it innervates.

(D) 3D antennal lobe reconstruction.

(E–J) Single confocal sections through the center of Glomerulus 1 (top) or Glomerulus 2 and 3 (bottom) in left antennal lobes of the indicated genotypes. Sections are taken from z stacks in Figure 2G (E) and Figure 1I (F–J).

(K) Schematic of sensory neuron gene expression and glomerular convergence based on (E–J).

(L–P) Whole-mount maxillary palp RNA *in situ* hybridization with indicated probes, cartoon schematic indicating cell identity, and quantification of co-expression shown as Euler diagrams, area scaled to mean. n = 5 maxillary palps, 26–65 cells/dorso-lateral maxillary palp.

See also Figure S3.

Scale bars: 50 μm (B), 25 μm (E–J and L–P). Orientation: d, dorsal; m, medial; p, posterior.

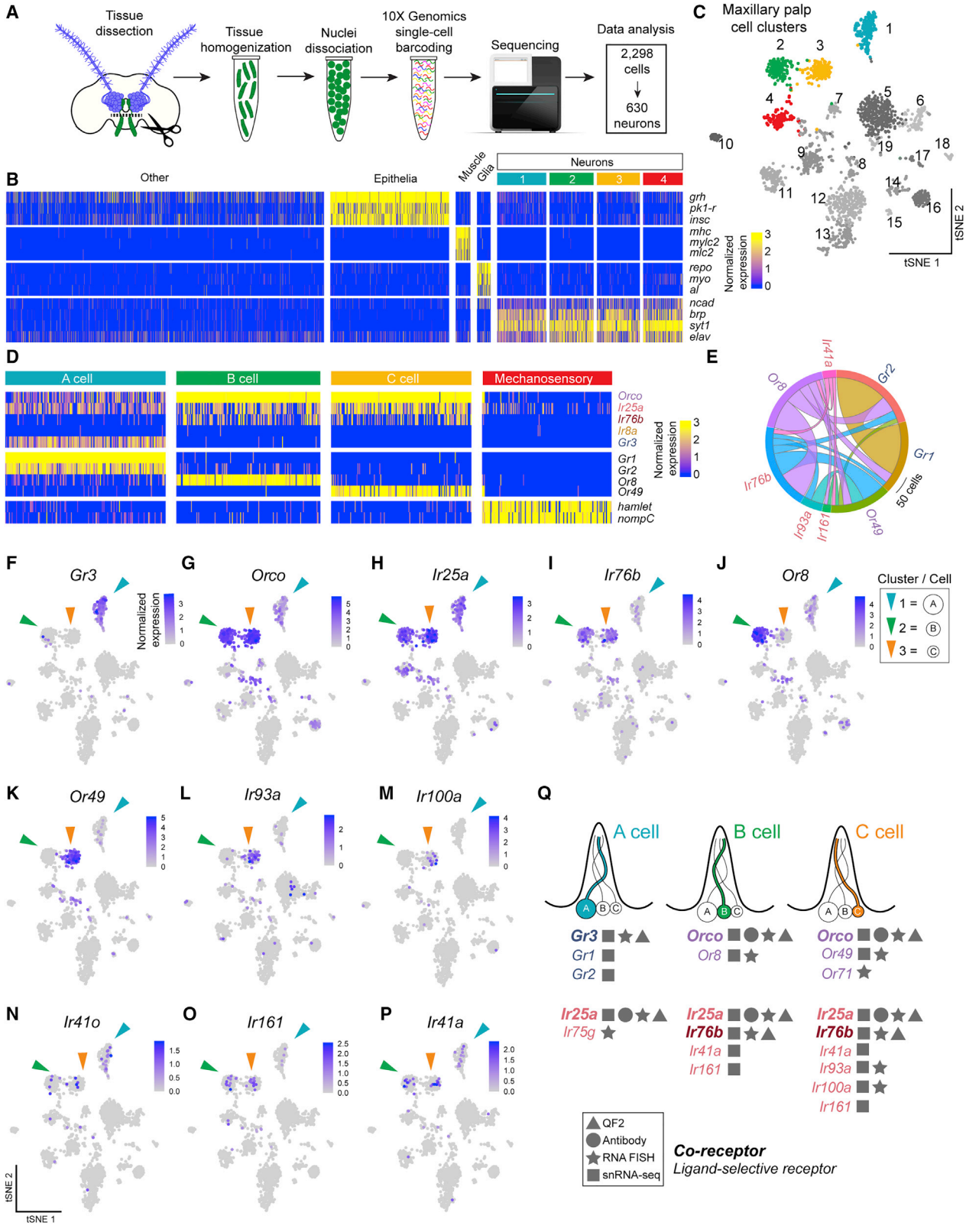

(legend on next page)

To determine if there are two different functional types of B neurons, we generated an independent dataset using these stimuli to examine responses in an additional 17 wild-type (+/+^{LVP}) neurons and 23 *Ir25a* mutant neurons. The response to the water control stimulus never exceeded 30 spikes/s firing frequency in either genotype, and we used this as a threshold to classify neurons as "responders" or "non-responders" (Figures 7G–7I). We found that all +/+^{LVP} neurons responded to triethyl amine, and 16 out of 17 +/+^{LVP} neurons responded to hexyl amine (Figures 7H and 7I). Responses to both amines were significantly higher than the water control in +/+^{LVP}. In contrast, most neurons in the *Ir25a* mutant did not respond to either triethyl amine or hexyl amine (78.3%, n = 23), and neither stimulus elicited significantly different responses from the water control when taking the entire population of 23 neurons into account.

We noted that 5 out of 23 neurons (21.7%) showed strong responses to both amines that exceeded the corresponding response in +/+^{LVP} neurons (Figures 7G–7I). These neurons were considered outliers by a ROUT (robust regression followed by outlier identification) analysis (Q = 1%), consistent with the classification system that we used to categorize neurons as responders or non-responders. Given our discovery of multiple additional IRs and ORs co-expressed along with *Or8* in the B cells (Figure 6Q), we speculate that there are at least two distinct types of B neurons, one that requires *Ir25a* to respond to amines and one that does not. We hypothesize that this second type of B neuron expresses the *Ir76b* co-receptor. Our findings that the B cell responds to 1-octen-3-ol in an *Orco*-dependent manner and to triethyl amine and hexyl amine in an *Ir25a*-dependent manner is consistent with the hypothesis that ORs and IRs are functionally co-expressed in the same neurons.

DISCUSSION

Combinatorial chemosensory receptor co-expression in *Ae. aegypti*

The mismatch between the number of receptors in the *Ae. aegypti* genome and the number of glomeruli in the antennal lobe is resolved in part by co-expression of multiple chemoreceptors in individual OSNs. We found that co-expression is widespread, both between and within OR and IR families, and that the number of receptors expressed in a neuron can vary substantially. While some neurons express only an individual co-receptor and ligand-selective receptor pair, others express "sets" of frequently co-expressed receptor subunits, and in a few cases a single receptor subunit could be co-expressed with completely different combinations of receptor subunits.

Many commonly co-expressed IRs and ORs belong to mosquito gene family expansions. The *Ir41* clade was among the most common of the detected ligand-specific IRs, and *Ir41l* was found to be co-expressed with ORs, which may be indicative of more multi-family co-expression below detection thresholds of the snRNA-seq. This clade is expanded in *Ae. aegypti* relative to *D. melanogaster* (Matthews et al., 2018) and the *D. melanogaster* orthologues, *Ir41a*, *Ir76a*, and *Ir92a*, compose channels that respond to amines (Hussain et al., 2016; Min et al., 2013; Silbering et al., 2011). Volatile amines are enriched in human odor and play an important role in the detection of humans by mosquitoes (Bernier et al., 2000; de Lacy Costello et al., 2014; De Obaldia et al., 2022). It is possible that the *Ir41* clade expansion in *Ae. aegypti* enhances their ability to detect amines in human odor. Many of the commonly co-expressed ORs are also members of gene expansions in *Ae. aegypti* and *An. gambiae* but have no direct orthologues in *D. melanogaster* (Matthews et al., 2018). These may have ligands that are enriched in human odor.

Coordinated co-expression between *IR*, *OR*, and *GR* ligand-selective receptors

Co-receptors and ligand-selective receptor co-expression poses a gene regulatory problem for an olfactory neuron. We have demonstrated that multiple ORs and IRs are expressed in specific receptor "sets." How might this complex receptor co-expression code be regulated? In vertebrates, an epigenetic silencing mechanism ensures that each olfactory neuron stochastically expresses only a single allele of one odorant receptor (Bashkirova and Lomvardas, 2019). In contrast, *D. melanogaster* uses a conventional transcription factor code in which the specification of a neuron and its chemoreceptor is tightly regulated (Jafari and Alenius, 2015; Li et al., 2016; Ray et al., 2008).

Other examples exist of receptor co-expression within a single chemosensory gene family. Polycistronic expression of multiple ORs in *An. gambiae* sensory neurons has been reported (Karner et al., 2015). This differs from *Ae. aegypti*, where co-expressed ORs are not necessarily neighboring genes. In *D. melanogaster* there are rare cases of OR-OR or OR-IR co-expression. These are thought to be the exceptions rather than the rule. *Or49a* and *Or85f* are co-expressed in an OSN population where they play redundant roles in predator avoidance (Ebrahim et al., 2015). *Or35a* is co-expressed with *Ir76b* (Silbering et al., 2011), and while these neurons respond to many odorants (Silbering et al., 2011; Yao et al., 2005), the role of co-expression remains

Figure 6. Maxillary palp snRNA-seq reveals unanticipated neuronal complexity

(A) Female maxillary palp snRNA-seq workflow.

(B) Heatmap of cells in the antenna within clusters that express cell type markers according to normalized expression (unit for normalized expression in maxillary palp data is ln(UMI of gene*10,000/total UMI of cell+1)) (see Figure S7E).

(C) t-SNE plot of maxillary palp nuclei. Identified neuron clusters (1–4) are labeled with color (see Figures S7F and S7G).

(D) Heatmap of normalized expression of selected genes in four identified neuron clusters. See also Figure S7E.

(E) Chord plot of chemosensory receptors (excluding Orco, Ir25a, and Gr3) for which there are at least 10 cells of both genes above a normalized expression value of 1.

(F–P) Normalized expression (ln(UMI of gene*10,000/total UMI of cell+1)) of indicated chemoreceptor genes mapped onto t-SNE plots.

(Q) Summary of chemosensory receptor expression in the maxillary palp based on all experimental data in this study (RNA FISH, fluorescent RNA *in situ* hybridization).

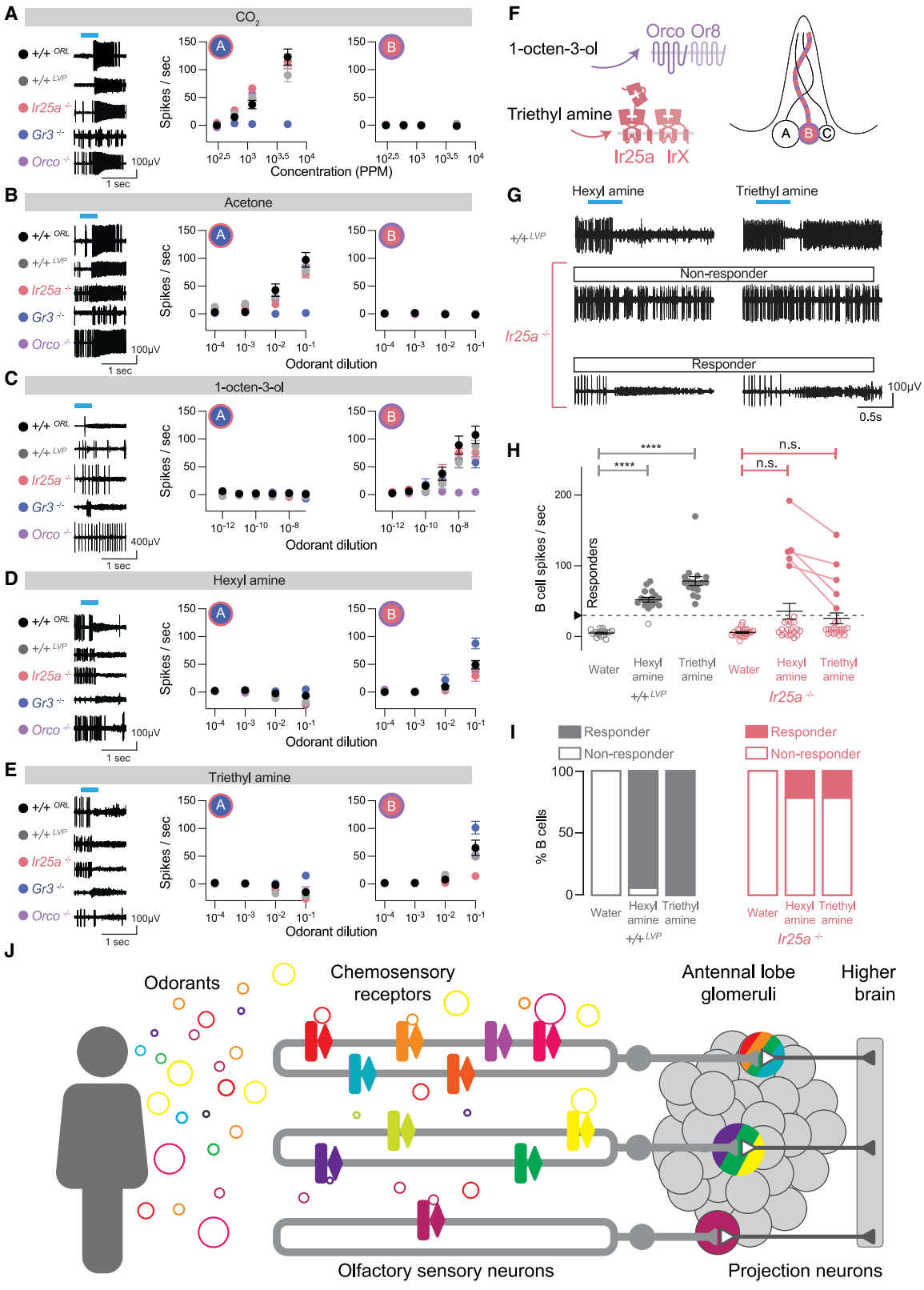

(legend on next page)

unknown. Recent work suggests that there may be more examples to be discovered in flies (McLaughlin et al., 2021; Task et al., 2022).

Our findings are reminiscent of the nematode *Caenorhabditis elegans*, which co-expresses a large number of chemosensory receptor genes in a small number of sensory neurons (Troemel et al., 1995; Vidal et al., 2018). *Ae. aegypti* have many more chemosensory neurons than *C. elegans* and the circuit organization differs dramatically. Extensive olfactory receptor co-expression is also seen in a subpopulation of OSNs in mice that each express multiple MS4a chemosensory receptors and project to the so-called necklace glomeruli that surround the main olfactory bulb (Greer et al., 2016). Interestingly these neurons respond to cues that regulate innate behaviors.

Maxillary palp chemosensory neurons go beyond a simple A, B, and C organization

The maxillary palp is a multi-modal sensory organ that responds to CO_2 (Acree et al., 1968; Gillies, 1980; Grant et al., 1995), temperature (Roth, 1951), mechanical stimuli (Bohbot et al., 2014), attractive monomolecular odorants such as 1-octen-3-ol (Syed and Leal, 2007; Takken and Kline, 1989; Vythilingam et al., 1992), as well as blends of odorants extracted from human hosts (Tauxe et al., 2013). The prior view of the organization of the maxillary palp is that all volatile odorant-detecting capitate-peg sensilla house the sensory dendrites of three neurons that form identical repeating units (Lu et al., 2007; McIver, 1972). It is difficult to reconcile the functional diversity of responses with this simple cellular organization. We demonstrate that the receptor composition of these neurons is far more varied. They can be subdivided into many more than three cell types. Consistent with this idea, we found that B cells can be separated into different types based on their physiological response to volatile amines. This is revealed in *Ir25a* mutant animals, where the response to amines is abolished in most B cells, but a subset of neurons retains their responses. We found that *Ir76b* is expressed in a subset of the *Or8*-expressing B cells, as are *Ir161* and *Ir41a*. It is possible that these IRs mediate amine responses in the subset of *Ir25a* mutant neurons that retain amine responses.

Receptor co-expression as a possible mechanism for robust mosquito attraction to humans

We hypothesize that receptor co-expression is used broadly to detect redundant cues that are present in human odor, a blend that can vary from individual to individual and contains hundreds of different chemicals (Bernier et al., 1999, 2000; De Obaldia et al., 2022). Both volatile amines and 1-octen-3-ol are emitted from human skin (Bernier et al., 2000; Cork and Park, 1996; de Lacy Costello et al., 2014). It is possible that receptor co-expression is used to form a highly redundant detection system for different cues that represent the same ecological target: humans. This motif has the benefit of limiting the number of neurons needed to detect varied odorants with the same meaning. Our study reveals unexpected complexity in the gene expression and functional organization of the mosquito olfactory system that may explain the persistence of mosquitoes in hunting humans. Future attempts to design repellents to ward off mosquitoes or attractant traps to lure them will have to have to reckon with the complexity of this system.

Limitations of the study

We see a variety of OR and IR expression levels in different neurons and have not determined the impact of expression level on *in vivo* receptor function in individual neurons. This study examined the role of receptor co-expression on odor-evoked activity in only a single type of neuron, and odorants were applied above the physiological concentration in human odor. For the snRNA-seq data, we established discrete criteria for expression. However different receptor gene expression levels vary continuously both in individual cells as well as in the tissue at large. This complicates setting a single threshold for determining functional expression for different receptors, especially for those that are rarer or expressed at lower levels. For the mosquito antenna, we lacked validated markers of tissue composition or cell types other than neurons to objectively assess analysis pipeline decisions. Future research into cell populations in the antenna may provide data to further "ground truth" and refine this analysis pipeline. While many of the techniques we used produced consistent results, we sometimes observed inconsistencies in the snRNA-seq data, such as low levels of *Orco* expression in the maxillary palp *Gr3* cluster, an observation at odds with results from the three other methods used in the paper and one that we do not currently understand but that could be due to differences in the sensitivity of detection methods.

STAR★METHODS

Detailed methods are provided in the online version of this paper and include the following:

- KEY RESOURCES TABLE
- RESOURCE AVAILABILITY

Figure 7. Functional consequences of chemosensory receptor co-expression

(A–E) Left, sample traces from maxillary palp single sensillum recordings in indicated genotypes for (A) CO_2, (B) acetone, (C) 1-octen-3-ol, (D) hexyl amine, and (E) triethyl amine. Stimulus delivery: cyan bar. Middle and right, spikes/sec in the A cell (middle) and B cell (right) for indicated concentration of the stimulus. Data are mean ± SEM, n = 4–16 recordings from separate sensilla.

(F) Schematic of an individual sensillum and receptor odorant pairings for the B neuron. The identity of the ligand-selective IrX subunit is unknown.

(G) Sample traces for $+/+^{LVP}$ (top) and $Ir25a^{BamHI/BamHI}$ (bottom) with each indicated stimulus. Stimulus delivery: cyan bar.

(H and I) Dot plots (H) and stacked bar plots (I) showing the percent of total recordings from each genotype that responded to the stimulus (filled circles) and those that did not (open circles), with 30 spikes/s defined as response threshold. Data are mean ± SEM, n = 17 ($+/+^{LVP}$) and n = 23 $Ir25a^{BamHI/BamHI}$ recordings from separate sensilla; n.s., not significant (p = 0.1453 for hexyl amine and p = 0.1642 for triethyl amine), ****p < 0.0001, one-way ANOVA with Kruskal-Wallis test for multiple comparisons.

(J) A revised model of chemosensory coding in *Ae. aegypti* based on this study.

- Lead contact
- Materials availability
- Data and code availability
- EXPERIMENTAL MODEL AND SUBJECT DETAILS
  - Human and animal ethics statement
  - Mosquito rearing and maintenance
- METHOD DETAILS
  - Generation of chemosensory receptor *QF2* and Split-*QF2* knock-in strains
  - *QUAS* transgenic strains
  - Chemosensory receptor mutant strains
  - Transcript abundance estimates of *Ae. aegypti* OR, IR, and GR genes
  - Whole brain fixation and immunofluorescence
  - Purification of nc82/Brp monoclonal antibody
  - Generation of the Ir25a polyclonal antibody
  - Female antennal lobe confocal imaging
  - Male brain and female subesophageal zone confocal imaging
  - Additional technical notes on expression and projection patterns in subesophageal zone
  - Antennal lobe glomerulus quantification
  - Additional technical notes on expression and projection patterns of chemosensory receptor knock-in strains
  - Additional technical notes on expression and projection patterns of Split-QF2 strains
  - Antennal lobe anterograde dye fill
  - Antennal lobe 3D reconstructions
  - Antennal whole mount immunofluorescence
  - Antennal whole-mount immunofluorescence with Ir25a antibody
  - Whole mount antennal and maxillary palp RNA *in situ* hybridization
  - Whole mount antennal, maxillary palp, and proboscis dTomato visualization
  - Antennal and maxillary palp confocal imaging and cell quantification
  - Antenna dissection for snRNA-seq
  - Batch 1 (Rockefeller antenna sample) nuclei extraction
  - Batch 1 (Rockefeller antenna sample): 10X Genomics, library preparation and sequencing
  - Batch 2 (Baylor antenna sample): Nuclei extraction
  - Batch 2 (Baylor antenna sample): FACS sorting, 10X genomics, library preparation, sequencing
  - Maxillary palp dissection, nuclei extraction, FACS sorting, 10X genomics, library preparation, and sequencing
  - snRNA-seq analysis: cell identification, ambient RNA removal, batch combination, and neuron classification
  - Maxillary palp: tSNE, heatmap, chord plot, dot plot, expression feature plot
  - Mosquito preparation for single-sensillum recordings
  - Single-sensillum recordings from maxillary palp capitate peg sensilla
  - Odorant stimulus delivery for single-sensillum recordings
- QUANTIFICATION AND STATISTICAL ANALYSIS

SUPPLEMENTAL INFORMATION

Supplemental information can be found online at https://doi.org/10.1016/j.cell.2022.07.024.

ACKNOWLEDGMENTS

We thank Emily Dennis, Laura Duvall, Itzel Ishida, Philip Kidd, Erica Korb, Carolyn McBride, Christopher Potter, Darya Task, Zhilei Zhao, and members of the Vosshall Lab for comments on the manuscript; Gloria Gordon, Libby Mejia, and Mengistu Dawit Bulo for expert mosquito rearing; Javier Marquina-Solis for assistance with antennal lobe tracing; Priyanka Lakhiani and Julia Deere for troubleshooting mosquito nuclei extraction; Christina Pyrgaki, Carlos Rico, Katarzyna Cialowicz, and Alison North at the Rockefeller Bio-Imaging Resource Center (RRID:SCR_017791) for help with confocal imaging; Helen Duan, Bin Zhang, and Connie Zhao at the Rockefeller Genomics Core for quality control for snRNA-seq samples and 10X Genomics sequencing; Daniel Gross, James Petrillo, and Peer Strogies at the Rockefeller Precision Instrumental Technologies (PIT) Resource Center for advice and fabrication of custom equipment; Olena Riabinina and Christopher Potter for advice and for providing Q-system reagents prior to publication; Carolyn McBride, Matthew De Gennaro, and members of the *Aedes* Toolkit Group for advice and discussion; Caroline Jiang for advice on statistical analysis; Nipun Basrur, Priya Rajasethupathy, Andrea Terceros, Harry Choi, and Molecular Instruments for advice on RNA *in situ* hybridization experiments; Andrea Terceros, Andras Sziraki, Junyue Cao, and 10X Genomics for advice on mosquito nuclei extraction and analysis; Rob A. Harrell II at the Insect Transgenesis Facility at the University of Maryland for embryo injections; Raphael Cohn, Gaby Maimon, Cory Root, Vanessa Ruta, and Ari Zolin for useful discussions; and Dana Pe'er and Roshan Sharma for advice on snRNA-seq data processing. This work was supported in part by grant no. UL1 TR000043 from the National Center for Advancing Translational Sciences (NCATS), National Institutes of Health (NIH) Clinical and Translational Science Award (CTSA) program. Funding for this study was provided by Jane Coffin Childs Postdoctoral Fellowships (M.A.Y. and B.J.M.), The Grass Foundation Grass Fellows Program (M.A.Y.), a Leon Levy Neuroscience Fellowship (M.A.Y.), a Quadrivium Award for Innovative Research in Epigenetics (M.H. and L.B.V.), a pilot grant (M.A.Y.) and postdoctoral (M.A.Y.) and graduate (M.H. and O.V.G.) fellowships from the Kavli Neural Systems Institute, and NIH NIDCD grant F30DC017658 (M.H.). This material is based upon work supported by the National Science Foundation Graduate Research Fellowship under grant No. 1946429 to O.V.G. B.J.M. received support from National Sciences and Engineering Research Council (NSERC) under award RGPIN-2020-05423. M.H. is supported by a Medical Scientist Training Program grant from the National Institute of General Medical Sciences of the NIH under award number T32GM007739 to the Weill Cornell/Rockefeller/Sloan Kettering Tri-Institutional MD-PhD Program. H.L. is a CPRIT Scholar in Cancer Research (RR200063) and supported by National Institute on Aging of the NIH (R00AG062746). R.I. is the recipient of an SLU Vice-Chancellor's Senior Career grant. Antibody purification carried out at the MSKCC Antibody and Bioresource Core Facility was supported by a Cancer Center Core Grant from the National Cancer Institute of the NIH (5 P30 CA008748-56). L.B.V. is an investigator of the Howard Hughes Medical Institute.

AUTHOR CONTRIBUTIONS

M.A.Y. carried out all central tissue immunofluorescence. M.H. carried out all peripheral tissue immunofluorescence and RNA *in situ* hybridization experiments. B.J.M. provided chemosensory gene and transcript analysis. Z.G. cloned and isolated Split-QF2 lines with M.H. Z.N.G. cloned and isolated QF2 stop codon replacement lines with B.J.M. and M.A.Y. S.R. worked with M.H. to generate RNA *in situ* hybridization data. O.V.G. developed the protocol to isolate nuclei and collected all tissue for snRNA-seq together with M.H. and M.A.Y. O.V.G. processed tissue for snRNA-seq experiments at Rockefeller. At Baylor, Y.Q. carried out sample preparation, flow cytometry, and 10X Genomics library preparation. T.-C.L. and O.V.G. carried out snRNA-seq data analysis. T.-C.L. performed read alignment and with O.V.G., carried out quality checking, cell and gene filtering, and data normalization. O.V.G. carried out

additional downstream analysis. O.V.G. together with T.-C.L. generated the figure panels for Figure 4 and Figure 6. H.L. supervised Y.Q and T.-C.L. and oversaw snRNA-seq experimental design and data analysis. The single sensillum recordings in Figures 7A–7E were carried out by M.G., and those in Figures 7F–7I were carried out by G.C.-V. R.I. supervised M.G. and G.C.-V. and analyzed data in Figure 7 together with M.G. and G.C.-V. M.H., M.A.Y., and L.B.V. together conceived the study, designed the figures, and wrote the paper with input from all authors.

DECLARATION OF INTERESTS

The authors declare no competing interests.

Received: November 15, 2020
Revised: January 5, 2022
Accepted: July 20, 2022
Published: August 18, 2022

REFERENCES

Abuin, L., Bargeton, B., Ulbrich, M.H., Isacoff, E.Y., Kellenberger, S., and Benton, R. (2011). Functional architecture of olfactory ionotropic glutamate receptors. Neuron *69*, 44–60. https://doi.org/10.1016/j.neuron.2010.11.042.

Acree, F., Jr., Turner, R.B., Gouck, H.K., Beroza, M., and Smith, N. (1968). L-Lactic acid: a mosquito attractant isolated from humans. Science *161*, 1346–1347. https://doi.org/10.1126/science.161.3848.1346.

Allan, S.A., Day, J.F., and Edman, J.D. (1987). Visual ecology of biting flies. Annu. Rev. Entomol. *32*, 297–314. https://doi.org/10.1146/annurev.en.32.010187.001501.

Bashkirova, E., and Lomvardas, S. (2019). Olfactory receptor genes make the case for inter-chromosomal interactions. Curr. Opin. Genet. Dev. *55*, 106–113. https://doi.org/10.1016/j.gde.2019.07.004.

Basrur, N.S., De Obaldia, M.E., Morita, T., Herre, M., von Heynitz, R.K., Tsitohay, Y.N., and Vosshall, L.B. (2020). *Fruitless* mutant male mosquitoes gain attraction to human odor. Elife *9*, e63982. https://doi.org/10.7554/elife.63982.

Benton, R., Sachse, S., Michnick, S.W., and Vosshall, L.B. (2006). Atypical membrane topology and heteromeric function of *Drosophila* odorant receptors in vivo. PLoS Biol. *4*, e20. https://doi.org/10.1371/journal.pbio.0040020.

Benton, R., Vannice, K.S., Gomez-Diaz, C., and Vosshall, L.B. (2009). Variant ionotropic glutamate receptors as chemosensory receptors in *Drosophila*. Cell *136*, 149–162. https://doi.org/10.1016/j.cell.2008.12.001.

Bernier, U.R., Booth, M.M., and Yost, R.A. (1999). Analysis of human skin emanations by gas chromatography/mass spectrometry. 1. Thermal desorption of attractants for the yellow fever mosquito (*Aedes aegypti*) from handled glass beads. Anal. Chem. *71*, 1–7. https://doi.org/10.1021/ac980990v.

Bernier, U.R., Kline, D.L., Barnard, D.R., Schreck, C.E., and Yost, R.A. (2000). Analysis of human skin emanations by gas chromatography/mass spectrometry. 2. Identification of volatile compounds that are candidate attractants for the yellow fever mosquito (*Aedes aegypti*). Anal. Chem. *72*, 747–756. https://doi.org/10.1021/ac990963k.

Bisch-Knaden, S., Dahake, A., Sachse, S., Knaden, M., and Hansson, B.S. (2018). Spatial representation of feeding and oviposition odors in the brain of a hawkmoth. Cell Rep. *22*, 2482–2492. https://doi.org/10.1016/j.celrep.2018.01.082.

Bohbot, J., Pitts, R.J., Kwon, H.W., Rutzler, M., Robertson, H.M., and Zwiebel, L.J. (2007). Molecular characterization of the *Aedes aegypti* odorant receptor gene family. Insect Mol. Biol. *16*, 525–537. https://doi.org/10.1111/j.1365-2583.2007.00748.x.

Bohbot, J.D., and Dickens, J.C. (2009). Characterization of an enantioselective odorant receptor in the yellow fever mosquito *Aedes aegypti*. PLoS One *4*, e7032. https://doi.org/10.1371/journal.pone.0007032.

Bohbot, J.D., Sparks, J.T., and Dickens, J.C. (2014). The maxillary palp of *Aedes aegypti*, a model of multisensory integration. Insect Biochem. Mol. Biol. *48*, 29–39. https://doi.org/10.1016/j.ibmb.2014.02.007.

Brown, J.E., Evans, B.R., Zheng, W., Obas, V., Barrera-Martinez, L., Egizi, A., Zhao, H., Caccone, A., and Powell, J.R. (2014). Human impacts have shaped historical and recent evolution in *Aedes aegypti*, the dengue and yellow fever mosquito. Evolution *68*, 514–525. https://doi.org/10.1111/evo.12281.

Buck, L., and Axel, R. (1991). A novel multigene family may encode odorant receptors: a molecular basis for odor recognition. Cell *65*, 175–187. https://doi.org/10.1016/0092-8674(91)90418-x.

Butterwick, J.A., Del Marmol, J., Kim, K.H., Kahlson, M.A., Rogow, J.A., Walz, T., and Ruta, V. (2018). Cryo-EM structure of the insect olfactory receptor Orco. Nature *560*, 447–452. https://doi.org/10.1038/s41586-018-0420-8.

Chess, A., Simon, I., Cedar, H., and Axel, R. (1994). Allelic inactivation regulates olfactory receptor gene expression. Cell *78*, 823–834. https://doi.org/10.1016/s0092-8674(94)90562-2.

Choi, H.M.T., Schwarzkopf, M., Fornace, M.E., Acharya, A., Artavanis, G., Stegmaier, J., Cunha, A., and Pierce, N.A. (2018). Third-generation *in situ* hybridization chain reaction: multiplexed, quantitative, sensitive, versatile, robust. Development *145*, dev165753. https://doi.org/10.1242/dev.165753.

Clyne, P.J., Warr, C.G., and Carlson, J.R. (2000). Candidate taste receptors in *Drosophila*. Science *287*, 1830–1834. https://doi.org/10.1126/science.287.5459.1830.

Clyne, P.J., Warr, C.G., Freeman, M.R., Lessing, D., Kim, J., and Carlson, J.R. (1999). A novel family of divergent seven-transmembrane proteins: candidate odorant receptors in *Drosophila*. Neuron *22*, 327–338. https://doi.org/10.1016/s0896-6273(00)81093-4.

Cook, J.I., Majeed, S., Ignell, R., Pickett, J.A., Birkett, M.A., and Logan, J.G. (2011). Enantiomeric selectivity in behavioural and electrophysiological responses of *Aedes aegypti* and *Culex quinquefasciatus* mosquitoes. Bull. Entomol. Res. *101*, 541–550. https://doi.org/10.1017/s0007485311000162.

Cork, A., and Park, K.C. (1996). Identification of electrophysiologically-active compounds for the malaria mosquito, *Anopheles gambiae*, in human sweat extracts. Med. Vet. Entomol. *10*, 269–276. https://doi.org/10.1111/j.1365-2915.1996.tb00742.x.

Couto, A., Alenius, M., and Dickson, B.J. (2005). Molecular, anatomical, and functional organization of the *Drosophila* olfactory system. Curr. Biol. *15*, 1535–1547. https://doi.org/10.1016/j.cub.2005.07.034.

Davis, E.E. (1984). Regulation of sensitivity in the peripheral chemoreceptor systems for host-seeking behavior by a haemolymph-borne factor in *Aedes aegypti*. J. Insect Physiol. *30*, 179–183. https://doi.org/10.1016/0022-1910(84)90124-0.

de Lacy Costello, B., Amann, A., Al-Kateb, H., Flynn, C., Filipiak, W., Khalid, T., Osborne, D., and Ratcliffe, N.M. (2014). A review of the volatiles from the healthy human body. J. Breath Res. *8*, 014001. https://doi.org/10.1088/1752-7155/8/1/014001.

De Obaldia, M.E., Morita, T., Dedmon, L.C., Boehmler, D.J., Jiang, C.S., Zeledon, E.V., Cross, J.R., and Vosshall, L.B. (2022). Differential mosquito attraction to humans is associated with skin-derived carboxylic acid levels. Preprint at bioRxiv. https://doi.org/10.1101/2022.01.05.475088.

DeGennaro, M., McBride, C.S., Seeholzer, L., Nakagawa, T., Dennis, E.J., Goldman, C., Jasinskiene, N., James, A.A., and Vosshall, L.B. (2013). *orco* mutant mosquitoes lose strong preference for humans and are not repelled by volatile DEET. Nature *498*, 487–491. https://doi.org/10.1038/nature12206.

Del Mármol, J., Yedlin, M.A., and Ruta, V. (2021). The structural basis of odorant recognition in insect olfactory receptors. Nature *597*, 126–131. https://doi.org/10.1038/s41586-021-03794-8.

Distler, P., and Boeckh, J. (1997). Central projections of the maxillary and antennal nerves in the mosquito *Aedes aegypti*. J. Exp. Biol. *200*, 1873–1879. https://doi.org/10.1242/jeb.200.13.1873.

Ebrahim, S.A.M., Dweck, H.K.M., Stokl, J., Hofferberth, J.E., Trona, F., Weniger, K., Rybak, J., Seki, Y., Stensmyr, M.C., Sachse, S., et al. (2015). *Drosophila* avoids parasitoids by sensing their semiochemicals via a dedicated olfactory circuit. PLoS Biol. *13*, e1002318. https://doi.org/10.1371/journal.pbio.1002318.

Fishilevich, E., and Vosshall, L.B. (2005). Genetic and functional subdivision of the *Drosophila* antennal lobe. Curr. Biol. *15*, 1548–1553. https://doi.org/10.1016/j.cub.2005.07.066.

Flanagan, D., and Mercer, A.R. (1989). An atlas and 3-D reconstruction of the antennal lobes in the worker honey bee, *Apis mellifera* L. (Hymenoptera : Apidae). Int. J. Insect Morphol. Embryol. *18*, 145–159. https://doi.org/10.1016/0020-7322(89)90023-8.

Gallagher, M., Wysocki, C.J., Leyden, J.J., Spielman, A.I., Sun, X., and Preti, G. (2008). Analyses of volatile organic compounds from human skin. Br. J. Dermatol. *159*, 780–791. https://doi.org/10.1111/j.1365-2133.2008.08748.x.

Gao, Q., and Chess, A. (1999). Identification of candidate *Drosophila* olfactory receptors from genomic DNA sequence. Genomics *60*, 31–39. https://doi.org/10.1006/geno.1999.5894.

Geier, M., Bosch, O.J., and Boeckh, J. (1999). Ammonia as an attractive component of host odour for the yellow fever mosquito, *Aedes aegypti*. Chem. Senses *24*, 647–653. https://doi.org/10.1093/chemse/24.6.647.

Ghaninia, M., Majeed, S., Dekker, T., Hill, S.R., and Ignell, R. (2019). Hold your breath - Differential behavioral and sensory acuity of mosquitoes to acetone and carbon dioxide. PLoS One *14*, e0226815. https://doi.org/10.1371/journal.pone.0226815.

Gillies, M.T. (1980). The role of carbon dioxide in host-finding by mosquitoes (Diptera: Culicidae): a review. Bull. Entomol. Res. *70*, 525–532. https://doi.org/10.1017/s0007485300007811.

Gouck, H.K. (1972). Host preferences of various strains of *Aedes aegypti* and *Aedes simpsoni* as determined by an olfactometer. Bull World Health Org *47*, 680–683.

Grabe, V., Strutz, A., Baschwitz, A., Hansson, B.S., and Sachse, S. (2015). Digital in vivo 3D atlas of the antennal lobe of *Drosophila melanogaster*. J. Comp. Neurol. *523*, 530–544. https://doi.org/10.1002/cne.23697.

Grant, A.J., Wigton, B.E., Aghajanian, J.G., and O'Connell, R.J. (1995). Electrophysiological responses of receptor neurons in mosquito maxillary palp sensilla to carbon dioxide. J Comp Physiol [A] *177*, 389–396. https://doi.org/10.1007/bf00187475.

Greer, P.L., Bear, D.M., Lassance, J.M., Bloom, M.L., Tsukahara, T., Pashkovski, S.L., Masuda, F.K., Nowlan, A.C., Kirchner, R., Hoekstra, H.E., and Datta, S.R. (2016). A family of non-GPCR chemosensors defines an alternative logic for mammalian olfaction. Cell *165*, 1734–1748. https://doi.org/10.1016/j.cell.2016.05.001.

Griffiths, J.A., Richard, A.C., Bach, K., Lun, A.T.L., and Marioni, J.C. (2018). Detection and removal of barcode swapping in single-cell RNA-seq data. Nat. Commun. *9*, 2667. https://doi.org/10.1038/s41467-018-05083-x.

Grosse-Wilde, E., Kuebler, L.S., Bucks, S., Vogel, H., Wicher, D., and Hansson, B.S. (2011). Antennal transcriptome of *Manduca sexta*. Proc. Natl. Acad. Sci. U S A *108*, 7449–7454. https://doi.org/10.1073/pnas.1017963108.

Hafemeister, C., and Satija, R. (2019). Normalization and variance stabilization of single-cell RNA-seq data using regularized negative binomial regression. Genome Biol. *20*, 296. https://doi.org/10.1186/s13059-019-1874-1.

Hussain, A., Zhang, M., Üçpunar, H.K., Svensson, T., Quillery, E., Gompel, N., Ignell, R., and Grunwald Kadow, I.C. (2016). Ionotropic chemosensory receptors mediate the taste and smell of polyamines. PLoS Biol. *14*, e1002454. https://doi.org/10.1371/journal.pbio.1002454.

Ignell, R., Dekker, T., Ghaninia, M., and Hansson, B.S. (2005). Neuronal architecture of the mosquito deutocerebrum. J. Comp. Neurol. *493*, 207–240. https://doi.org/10.1002/cne.20800.

Ihara, S., Yoshikawa, K., and Touhara, K. (2013). Chemosensory signals and their receptors in the olfactory neural system. Neuroscience *254*, 45–60. https://doi.org/10.1016/j.neuroscience.2013.08.063.

Ito, K., Shinomiya, K., Ito, M., Armstrong, J., Boyan, G., Hartenstein, V., Harzsch, S., Heisenberg, M., Homberg, U., Jenett, A., et al. (2014). A systematic nomenclature for the insect brain. Neuron *81*, 755–765. https://doi.org/10.1016/j.neuron.2013.12.017.

Jafari, S., and Alenius, M. (2015). Cis-regulatory mechanisms for robust olfactory sensory neuron class-restricted odorant receptor gene expression in *Drosophila*. PLoS Genet. *11*, e1005051. https://doi.org/10.1371/journal.pgen.1005051.

Jones, W.D., Cayirlioglu, P., Grunwald Kadow, I., and Vosshall, L.B. (2007). Two chemosensory receptors together mediate carbon dioxide detection in *Drosophila*. Nature *445*, 86–90. https://doi.org/10.1038/nature05466.

Jové, V., Gong, Z., Hol, F.J., Zhao, Z., Sorrells, T.R., Carroll, T.S., Prakash, M., McBride, C.S., and Vosshall, L.B. (2020). Sensory discrimination of blood and floral nectar by *Aedes aegypti* mosquitoes. Neuron *108*, 1163–1180.e12. https://doi.org/10.1016/j.neuron.2020.09.019.

Karner, T., Kellner, I., Schultze, A., Breer, H., and Krieger, J. (2015). Co-expression of six tightly clustered odorant receptor genes in the antenna of the malaria mosquito *Anopheles gambiae*. Front Ecol Evol *3*. https://doi.org/10.3389/fevo.2015.00026.

Kistler, K., Vosshall, L., and Matthews, B. (2015). Genome engineering with CRISPR-Cas9 in the mosquito *Aedes aegypti*. Cell Rep. *11*, 51–60. https://doi.org/10.1016/j.celrep.2015.03.009.

Kline, D.L. (1994). Olfactory attractants for mosquito surveillance and control: 1-octen-3-ol. J. Am. Mosq. Control Assoc. *10*, 280–287.

Korsunsky, I., Millard, N., Fan, J., Slowikowski, K., Zhang, F., Wei, K., Baglaenko, Y., Brenner, M., Loh, P.R., and Raychaudhuri, S. (2019). Fast, sensitive and accurate integration of single-cell data with Harmony. Nat. Methods *16*, 1289–1296. https://doi.org/10.1038/s41592-019-0619-0.

Kwon, H.W., Lu, T., Rutzler, M., and Zwiebel, L.J. (2006). Olfactory responses in a gustatory organ of the malaria vector mosquito *Anopheles gambiae*. Proc. Natl. Acad. Sci. U S A *103*, 13526–13531. https://doi.org/10.1073/pnas.0601107103.

Kwon, J.Y., Dahanukar, A., Weiss, L.A., and Carlson, J.R. (2007). The molecular basis of CO_2 reception in *Drosophila*. Proc. Natl. Acad. Sci. U S A *104*, 3574–3578. https://doi.org/10.1073/pnas.0700079104.

Laissue, P.P., Reiter, C., Hiesinger, P.R., Halter, S., Fischbach, K.F., and Stocker, R.F. (1999). Three-dimensional reconstruction of the antennal lobe in *Drosophila melanogaster*. J. Comp. Neurol. *405*, 543–552. https://doi.org/10.1002/(sici)1096-9861(19990322)405:4<543::aid-cne7>3.0.co;2-a.

Larsson, M.C., Domingos, A.I., Jones, W.D., Chiappe, M., Amrein, H., and Vosshall, L.B. (2004). *Or83b* encodes a broadly expressed odorant receptor essential for *Drosophila* olfaction. Neuron *43*, 703–714. https://doi.org/10.1016/j.neuron.2004.08.019.

Li, H., Janssens, J., De Waegeneer, M., Kolluru, S.S., Davie, K., Gardeux, V., Saelens, W., David, F., Brbić, M., Leskovec, J., et al. (2022). Fly Cell Atlas: a single-cell transcriptomic atlas of the adult fruit fly. Science *375*, eabk2432. https://doi.org/10.1126/science.abk2432.

Li, Q., Barish, S., Okuwa, S., Maciejewski, A., Brandt, A.T., Reinhold, D., Jones, C.D., and Volkan, P.C. (2016). A functionally conserved gene regulatory network module governing olfactory neuron diversity. PLoS Genet. *12*, e1005780. https://doi.org/10.1371/journal.pgen.1005780.

Lu, T., Qiu, Y.T., Wang, G., Kwon, J., Rutzler, M., Kwon, H.W., Pitts, R.J., van Loon, J.J., Takken, W., Carlson, J.R., and Zwiebel, L.J. (2007). Odor coding in the maxillary palp of the malaria vector mosquito *Anopheles gambiae*. Curr. Biol. *17*, 1533–1544. https://doi.org/10.1016/j.cub.2007.07.062.

Majeed, S., Hill, S.R., Birgersson, G., and Ignell, R. (2016). Detection and perception of generic host volatiles by mosquitoes modulate host preference: context dependence of (R)-1-octen-3-ol. R. Soc. Open Sci. *3*, 160467. https://doi.org/10.1098/rsos.160467.

Majeed, S., Hill, S.R., Dekker, T., and Ignell, R. (2017). Detection and perception of generic host volatiles by mosquitoes: responses to CO2 constrains host-seeking behaviour. R. Soc. Open Sci. *4*, 170189. https://doi.org/10.1098/rsos.170189.

Manning, L., and Doe, C.Q. (2017). Immunofluorescent antibody staining of intact *Drosophila* larvae. Nat. Protoc. *12*, 1–14. https://doi.org/10.1038/nprot.2016.162.

Matthews, B.J., Dudchenko, O., Kingan, S.B., Koren, S., Antoshechkin, I., Crawford, J.E., Glassford, W.J., Herre, M., Redmond, S.N., Rose, N.H., et al. (2018). Improved reference genome of *Aedes aegypti* informs arbovirus vector control. Nature *563*, 501–507. https://doi.org/10.1038/s41586-018-0692-z.

Matthews, B.J., McBride, C.S., DeGennaro, M., Despo, O., and Vosshall, L.B. (2016). The neurotranscriptome of the *Aedes aegypti* mosquito. BMC Genom. *17*, 32. https://doi.org/10.1186/s12864-015-2239-0.

Matthews, B.J., Younger, M.A., and Vosshall, L.B. (2019). The ion channel *ppk301* controls freshwater egg-laying in the mosquito *Aedes aegypti*. Elife *8*, e43963. https://doi.org/10.7554/elife.43963.

McBride, C.S., Baier, F., Omondi, A.B., Spitzer, S.A., Lutomiah, J., Sang, R., Ignell, R., and Vosshall, L.B. (2014). Evolution of mosquito preference for humans linked to an odorant receptor. Nature *515*, 222–227. https://doi.org/10.1038/nature13964.

McGinnis, C.S., Murrow, L.M., and Gartner, Z.J. (2019). DoubletFinder: Doublet Detection in Single-Cell RNA Sequencing Data Using Artificial Nearest Neighbors. Cell Syst *8*, 329–337.e4. e324. https://doi.org/10.1016/j.cels.2019.03.003.

McIver, S.B. (1972). Fine structure of pegs on the palps of female culicine mosquitoes. Can. J. Zool. *50*, 571–576. https://doi.org/10.1139/z72-078.

McIver, S.B. (1982). Sensilla mosquitoes (Diptera: Culicidae). J. Med. Entomol. *19*, 489–535. https://doi.org/10.1093/jmedent/19.5.489.

McLaughlin, C.N., Brbić, M., Xie, Q., Li, T., Horns, F., Kolluru, S.S., Kebschull, J.M., Vacek, D., Xie, A., Li, J., et al. (2021). Single-cell transcriptomes of developing and adult olfactory receptor neurons in *Drosophila*. Elife *10*, e63856. https://doi.org/10.7554/elife.63856.

McMeniman, C., Corfas, R., Matthews, B., Ritchie, S., and Vosshall, L. (2014). Multimodal integration of carbon dioxide and other sensory cues drives mosquito attraction to humans. Cell *156*, 1060–1071. https://doi.org/10.1016/j.cell.2013.12.044.

Min, S., Ai, M., Shin, S.A., and Suh, G.S.B. (2013). Dedicated olfactory neurons mediating attraction behavior to ammonia and amines in *Drosophila*. Proc. Natl. Acad. Sci. U S A *110*, E1321–E1329. https://doi.org/10.1073/pnas.1215680110.

Mombaerts, P., Wang, F., Dulac, C., Chao, S.K., Nemes, A., Mendelsohn, M., Edmondson, J., and Axel, R. (1996). Visualizing an olfactory sensory map. Cell *87*, 675–686. https://doi.org/10.1016/s0092-8674(00)81387-2.

Montell, C. (2009). A taste of the *Drosophila* gustatory receptors. Curr. Opin. Neurobiol. *19*, 345–353. https://doi.org/10.1016/j.conb.2009.07.001.

Neuhaus, E.M., Gisselmann, G., Zhang, W., Dooley, R., Stortkuhl, K., and Hatt, H. (2005). Odorant receptor heterodimerization in the olfactory system of *Drosophila melanogaster*. Nat. Neurosci. *8*, 15–17. https://doi.org/10.1038/nn1371.

Omer, S.M., and Gillies, M.T. (1971). Loss of response to carbon dioxide in palpectomized female mosquitoes. Ent Exp & Appl *14*, 251–252.

Potter, C.J., Tasic, B., Russler, E.V., Liang, L., and Luo, L. (2010). The Q system: a repressible binary system for transgene expression, lineage tracing, and mosaic analysis. Cell *141*, 536–548. https://doi.org/10.1016/j.cell.2010.02.025.

Prieto-Godino, L.L., Rytz, R., Cruchet, S., Bargeton, B., Abuin, L., Silbering, A.F., Ruta, V., Dal Peraro, M., and Benton, R. (2017). Evolution of acid-sensing olfactory circuits in Drosophilids. Neuron *93*, 661–676.e6. e666. https://doi.org/10.1016/j.neuron.2016.12.024.

Raji, J.I., Melo, N., Castillo, J.S., Gonzalez, S., Saldana, V., Stensmyr, M.C., and DeGennaro, M. (2019). *Aedes aegypti* mosquitoes detect acidic volatiles found in human odor using the *IR8a* pathway. Curr. Biol. *29*, 1253–1262.e7. e1257. https://doi.org/10.1016/j.cub.2019.02.045.

Ray, A., van Naters, W.v. d.G., and Carlson, J.R. (2008). A regulatory code for neuron-specific odor receptor expression. PLoS Biol. *6*, e125. https://doi.org/10.1371/journal.pbio.0060125.

R Core Team (2021). R: A Language and Environment for Statistical Computing (R Foundation for Statistical Computing). https://www.R-project.org/.

Ressler, K.J., Sullivan, S.L., and Buck, L.B. (1994). Information coding in the olfactory system: evidence for a stereotyped and highly organized epitope map in the olfactory bulb. Cell *79*, 1245–1255. https://doi.org/10.1016/0092-8674(94)90015-9.

Riabinina, O., Luginbuhl, D., Marr, E., Liu, S., Wu, M.N., Luo, L., and Potter, C.J. (2015). Improved and expanded Q-system reagents for genetic manipulations. Nat. Methods *12*, 219–222. https://doi.org/10.1038/nmeth.3250.

Riabinina, O., Task, D., Marr, E., Lin, C.C., Alford, R., O'Brochta, D.A., and Potter, C.J. (2016). Organization of olfactory centres in the malaria mosquito *Anopheles gambiae*. Nat. Commun. *7*, 13010. https://doi.org/10.1038/ncomms13010.

Riabinina, O., Vernon, S.W., Dickson, B.J., and Baines, R.A. (2019). Split-QF system for fine-tuned transgene expression in *Drosophila*. Genetics *212*, 53–63. https://doi.org/10.1534/genetics.119.302034.

Robertson, H.M., Gadau, J., and Wanner, K.W. (2010). The insect chemoreceptor superfamily of the parasitoid jewel wasp *Nasonia vitripennis*. Insect Mol. Biol. *19*, 121–136. https://doi.org/10.1111/j.1365-2583.2009.00979.x.

Robertson, H.M., Warr, C.G., and Carlson, J.R. (2003). Molecular evolution of the insect chemoreceptor gene superfamily in *Drosophila melanogaster*. Proc. Natl. Acad. Sci. U S A *100*, 14537–14542. https://doi.org/10.1073/pnas.2335847100.

Roth, L.M. (1951). Loci of sensory end-organs used by mosquitoes (*Aedes aegypti* (L.) and *Anopheles quadrimaculatus say*) in receiving host stimuli. Ann. Entomol. Soc. Am. *44*, 59–74. https://doi.org/10.1093/aesa/44.1.59.

R Studio Team (2020). Integrated Development for R. R Studio. http://www.rstudio.com/.

Satija, R., Farrell, J.A., Gennert, D., Schier, A.F., and Regev, A. (2015). Spatial reconstruction of single-cell gene expression data. Nat. Biotechnol. *33*, 495–502. https://doi.org/10.1038/nbt.3192.

Sato, K., Pellegrino, M., Nakagawa, T., Nakagawa, T., Vosshall, L.B., and Touhara, K. (2008). Insect olfactory receptors are heteromeric ligand-gated ion channels. Nature *452*, 1002–1006. https://doi.org/10.1038/nature06850.

Schaefer, M.L., Finger, T.E., and Restrepo, D. (2001). Variability of position of the P2 glomerulus within a map of the mouse olfactory bulb. J. Comp. Neurol. *436*, 351–362. https://doi.org/10.1002/cne.1072.

Schindelin, J., Arganda-Carreras, I., Frise, E., Kaynig, V., Longair, M., Pietzsch, T., Preibisch, S., Rueden, C., Saalfeld, S., Schmid, B., et al. (2012). Fiji: an open-source platform for biological-image analysis. Nat. Methods *9*, 676–682. https://doi.org/10.1038/nmeth.2019.

Scott, K., Brady, R., Jr., Cravchik, A., Morozov, P., Rzhetsky, A., Zuker, C., and Axel, R. (2001). A chemosensory gene family encoding candidate gustatory and olfactory receptors in *Drosophila*. Cell *104*, 661–673. https://doi.org/10.1016/s0092-8674(01)00263-x.

Semmelhack, J.L., and Wang, J.W. (2009). Select *Drosophila* glomeruli mediate innate olfactory attraction and aversion. Nature *459*, 218–223. https://doi.org/10.1038/nature07983.

Shaner, N.C., Campbell, R.E., Steinbach, P.A., Giepmans, B.N.G., Palmer, A.E., and Tsien, R.Y. (2004). Improved monomeric red, orange and yellow fluorescent proteins derived from *Discosoma sp.* red fluorescent protein. Nat. Biotechnol. *22*, 1567–1572. https://doi.org/10.1038/nbt1037.

Shankar, S., and McMeniman, C.J. (2020). An updated antennal lobe atlas for the yellow fever mosquito *Aedes aegypti*. PLoS Negl Trop Dis *14*, e0008729. https://doi.org/10.1371/journal.pntd.0008729.

Silbering, A.F., Rytz, R., Grosjean, Y., Abuin, L., Ramdya, P., Jefferis, G.S.X.E., and Benton, R. (2011). Complementary function and integrated wiring of the evolutionarily distinct *Drosophila* olfactory subsystems. J. Neurosci. *31*, 13357–13375. https://doi.org/10.1523/jneurosci.2360-11.2011.

Smallegange, R.C., Qiu, Y.T., van Loon, J.J., and Takken, W. (2005). Synergism between ammonia, lactic acid and carboxylic acids as kairomones in the host-seeking behaviour of the malaria mosquito *Anopheles gambiae sensu stricto* (Diptera: Culicidae). Chem. Senses *30*, 145–152. https://doi.org/10.1093/chemse/bji010.

Smith, C.N., Smith, N., Gouck, H.K., Weidhaas, D.E., Gilbert, I.H., Mayer, M.S., Smittle, B.J., and Hofbauer, A. (1970). L-lactic acid as a factor in the attraction of *Aedes aegypti* (Diptera: Culicidae) to human hosts. Ann. Entomol. Soc. Am. *63*, 760–770. https://doi.org/10.1093/aesa/63.3.760.

Stocker, R.F., Lienhard, M.C., Borst, A., and Fischbach, K.F. (1990). Neuronal architecture of the antennal lobe in *Drosophila melanogaster*. Cell Tissue Res. *262*, 9–34. https://doi.org/10.1007/bf00327741.

Strotmann, J., Conzelmann, S., Beck, A., Feinstein, P., Breer, H., and Mombaerts, P. (2000). Local permutations in the glomerular array of the mouse olfactory bulb. J. Neurosci. *20*, 6927–6938. https://doi.org/10.1523/jneurosci.20-18-06927.2000.

Syed, Z., and Leal, W.S. (2007). Maxillary palps are broad spectrum odorant detectors in *Culex quinquefasciatus*. Chem. Senses *32*, 727–738. https://doi.org/10.1093/chemse/bjm040.

Takken, W., and Kline, D.L. (1989). Carbon dioxide and 1-octen-3-ol as mosquito attractants. J. Am. Mosq. Control Assoc. *5*, 311–316.

Tanaka, N.K., Endo, K., and Ito, K. (2012). Organization of antennal lobe-associated neurons in adult *Drosophila melanogaster* brain. J. Comp. Neurol. *520*, 4067–4130. https://doi.org/10.1002/cne.23142.

Task, D., Lin, C.C., Vulpe, A., Afify, A., Ballou, S., Brbic, M., Schlegel, P., Raji, J., Jefferis, G., Li, H., et al. (2022). Chemoreceptor co-expression in *Drosophila melanogaster* olfactory neurons. Elife *11*, e72599. https://doi.org/10.7554/elife.72599.

Tauxe, G., MacWilliam, D., Boyle, S., Guda, T., and Ray, A. (2013). Targeting a dual detector of skin and CO_2 to modify mosquito host seeking. Cell *155*, 1365–1379. https://doi.org/10.1016/j.cell.2013.11.013.

Troemel, E.R., Chou, J.H., Dwyer, N.D., Colbert, H.A., and Bargmann, C.I. (1995). Divergent seven transmembrane receptors are candidate chemosensory receptors in *C. elegans*. Cell *83*, 207–218. https://doi.org/10.1016/0092-8674(95)90162-0.

Turner, S.L., Li, N., Guda, T., Githure, J., Carde, R.T., and Ray, A. (2011). Ultra-prolonged activation of CO_2-sensing neurons disorients mosquitoes. Nature *474*, 87–91. https://doi.org/10.1038/nature10081.

Vassar, R., Chao, S.K., Sitcheran, R., Nunez, J.M., Vosshall, L.B., and Axel, R. (1994). Topographic organization of sensory projections to the olfactory bulb. Cell *79*, 981–991. https://doi.org/10.1016/0092-8674(94)90029-9.

Vidal, B., Aghayeva, U., Sun, H., Wang, C., Glenwinkel, L., Bayer, E.A., and Hobert, O. (2018). An atlas of *Caenorhabditis elegans* chemoreceptor expression. PLoS Biol. *16*, e2004218. https://doi.org/10.1371/journal.pbio.2004218.

Vosshall, L.B., Amrein, H., Morozov, P.S., Rzhetsky, A., and Axel, R. (1999). A spatial map of olfactory receptor expression in the *Drosophila* antenna. Cell *96*, 725–736. https://doi.org/10.1016/s0092-8674(00)80582-6.

Vosshall, L.B., Wong, A.M., and Axel, R. (2000). An olfactory sensory map in the fly brain. Cell *102*, 147–159. https://doi.org/10.1016/s0092-8674(00)00021-0.

Vythilingam, I., Chiang, G.L., and Chan, S.T. (1992). Evaluation of carbon dioxide and 1-octen-3-ol as mosquito attractants. Southeast Asian J Trop Med Public Health *23*, 328–331.

Wagh, D.A., Rasse, T.M., Asan, E., Hofbauer, A., Schwenkert, I., Dürrbeck, H., Buchner, S., Dabauvalle, M.C., Schmidt, M., Qin, G., et al. (2006). Bruchpilot, a protein with homology to ELKS/CAST, is required for structural integrity and function of synaptic active zones in *Drosophila*. Neuron *51*, 275. https://doi.org/10.1016/j.neuron.2006.06.022.

Wang, J.W., Wong, A.M., Flores, J., Vosshall, L.B., and Axel, R. (2003). Two-photon calcium imaging reveals an odor-evoked map of activity in the fly brain. Cell *112*, 271–282. https://doi.org/10.1016/s0092-8674(03)00004-7.

Wang, Z., Yang, S., Koga, Y., Corbett, S.E., Johnson, W.E., Yajima, M., and Campbell, J.D. (2021). Celda: A Bayesian model to perform co-clustering of genes into modules and cells into subpopulations using single-cell RNA-seq data. bioRxiv *2020*, 11–16. 373274.

WHO (2020). Fact Sheet: Vector-Borne Diseases (World Health Organization). https://www.who.int/en/news-room/fact-sheets/detail/vector-borne-diseases.

Wicher, D., Schafer, R., Bauernfeind, R., Stensmyr, M.C., Heller, R., Heinemann, S.H., and Hansson, B.S. (2008). *Drosophila* odorant receptors are both ligand-gated and cyclic-nucleotide-activated cation channels. Nature *452*, 1007–1011. https://doi.org/10.1038/nature06861.

Wickham, H. (2016). ggplot2: Elegant Graphics for Data Analysis (Springer-Verlag). https://ggplot2.tidyverse.org.

Yao, C.A., Ignell, R., and Carlson, J.R. (2005). Chemosensory coding by neurons in the coeloconic sensilla of the *Drosophila* antenna. J. Neurosci. *25*, 8359–8367. https://doi.org/10.1523/jneurosci.2432-05.2005.

Zhang, Y., Tsang, T.K., Bushong, E.A., Chu, L.A., Chiang, A.S., Ellisman, M.H., Reingruber, J., and Su, C.Y. (2019). Asymmetric ephaptic inhibition between compartmentalized olfactory receptor neurons. Nat. Commun. *10*, 1560. https://doi.org/10.1038/s41467-019-09346-z.

Zhao, Z., Zung, J.L., Hinze, A., Kriete, A.L., Iqbal, A., Younger, M.A., Matthews, B.J., Merhof, D., Thiberge, S., Ignell, R., et al. (2022). Mosquito brains encode unique features of human odour to drive host seeking. Nature *605*, 706–712. https://doi.org/10.1038/s41586-022-04675-4.

Zou, D.J., Chesler, A., and Firestein, S. (2009). How the olfactory bulb got its glomeruli: a just so story? Nat. Rev. Neurosci. *10*, 611–618. https://doi.org/10.1038/nrn2666.

STAR★METHODS

KEY RESOURCES TABLE

REAGENT or RESOURCE	SOURCE	IDENTIFIER
Antibodies		
Mouse monoclonal anti-brp	Developmental Studies Hybridoma Bank, see purification in STAR Methods	nc82; RRID AB_2314866
Rabbit polyclonal anti-GFP	Life Technologies	Cat# A-11122; RRID AB_221569
Rabbit polyclonal anti-Ir25a	This study	N/A
Rabbit polyclonal anti-Orco	Larsson et al. (2004)	N/A
Mouse monoclonal anti-Orco	Basrur et al. (2020)	N/A
Chicken anti-GFP	Aves Labs	Cat# GFP-1020; RRID AB_10000240
Goat anti-mouse Cy5	Life Technologies	Cat# A-10524
Goat anti-rabbit Alexa Fluor 488	Life Technologies	Cat# A-11034
Goat anti-mouse Alexa Fluor 488	Life Technologies	Cat# A-11001
Goat anti-mouse Alexa Fluor 594	Life Technologies	Cat# A-11005
Goat anti-rabbit Alexa Fluor 555 plus	Life Technologies	Cat# A-32732
Goat anti-chicken Alexa Fluor 488	Life Technologies	Cat# A-11039
Chemicals, peptides, and recombinant proteins		
Texas red conjugated dextran	Molecular Probes	Cat# D3328
TO-PRO-3 Iodide	Thermo Fisher	Cat# T3605
Chitinase	Sigma Aldrich	Cat# C6137
Chymotrypsin	Sigma Aldrich	Cat# CHY5S
Slowfade Diamond	Thermo Fisher	Cat# S36972
Proteinase K	Thermo Fisher	Cat# AM2548
200 μL filter tip	TipOne	Cat# 11,821,830
RNAse away	Thermo Fisher	Cat# 7000TS1
40 μm Flowmi filter	Bel-Art	Cat# H13680-0040
RNAse inhibitor	Roche	Cat# RNAINH-RO
Propidium Iodide	Logos Biosystems	Cat# LGBD10012
Hoechst-33342	Thermo Fisher	Cat# 62,249
Dimethyl sulfoxide (DMSO)	Sigma Aldrich	Cat# 472,301
Magnesium chloride, 1M	Thermo Fisher	Cat# AM9530G
Triton X-100, 10%	Sigma Aldrich	Cat# 93,443
HEPES, 1M	Sigma Aldrich	Cat# H0887
Calcium chloride, 1M	Sigma Aldrich	Cat# 21,115
Sodium chloride, 5M	Thermo Fisher	Cat# AM9760G
Potassium chloride, 2M	Thermo Fisher	Cat# AM9640G
Normal Goat Serum	Jackson ImmunoResearch	Cat# 005-000-001
R-(−)-1-octen-3-ol	Penta Manufacturing	Cat#15–18900; CID: 6,992,244
Acetone	Sigma Aldrich	Cat#A4206; CID: 180
Hexyl amine	Sigma Aldrich	Cat#219703; PCID: 8102
Triethyl amine	Sigma Aldrich	Cat# T0886; CID: 1146
Paraffin oil	EMD Millipore	PX0045-3
Critical commercial assays		
HCR RNA *in situ* probes, amplifiers, buffers	Molecular Instruments	Data S1

(*Continued on next page*)

Continued

REAGENT or RESOURCE	SOURCE	IDENTIFIER
Deposited data		
Antenna and maxillary palp raw snRNA-sequencing	This study	NCBI BioProject: PRJNA794050
Experimental models: Cell lines		
Mouse hybridoma cell line expressing monoclonal antibody nc82, which recognizes *Drosophila melanogaster* brp	Wagh et al. (2006)	Antibody Registry ID: AB_2314866
Experimental models: Organisms/strains		
Wild-type Liverpool (LVP)	Vosshall lab	N/A
Wild-type Orlando (ORL)	Vosshall lab	N/A
Ir25a$^{BamHI/BamHI}$	De Obaldia et al. (2022)	N/A
Orco$^{16/16}$	DeGennaro et al. (2013)	N/A
Gr3$^{4/4}$	McMeniman et al. (2014)	N/A
Ir25a-T2A-QF2	This study	N/A
Ir76b-T2A-QF2	This study	N/A
Ir8a-T2A-QF2	This study	N/A
Gr3-T2A-QF2	This study	N/A
Orco-T2A-QF2	This study	N/A
Ir25a-T2A-QF2-AD	This study	N/A
Orco-T2A-QF2-DBD	This study	N/A
QUAS-CD8-GFP	Matthews et al. (2019)	N/A
QUAS-dTomato-GCaMP6s	Jové et al. (2020)	N/A
Oligonucleotides		
sgRNA targeting *Ir25a*: GTTTGTGTGCGTGTCCGTA TGG	This study	N/A
sgRNA targeting *Ir76b*: GTATTACACTTATCTAAATA TGG	This study	N/A
sgRNAs targeting *Ir8a*: GTCACGCTTGTTGTACAGGG CGG, GAACAATTTGAACAAGGTCG TGG	This study	N/A
sgRNA targeting *Gr3*: GTTAGTGATGCATAATATGA CGG	This study	N/A
sgRNA targeting *Orco*: GTCACCTACTTCATGGTGT TGG	This study	N/A
Recombinant DNA		
Ir8a-T2A-QF2	This study	Addgene #162520
Gr3-T2A-QF2	This study	Addgene #162511
Ir25a-T2A-QF2	This study	Addgene #162522
Ir76b-T2A-QF2	This study	Addgene #162523
Orco-T2A-QF2	This study	Addgene #162524
Orco-T2A-QF2-DBD	This study	Addgene #162525
Ir25a-T2A-QF2-AD	This study	Addgene #162526
Software and algorithms		
Cell Ranger	10X Genomics	https://support.10xgenomics.com/single-cell-gene-expression/software/pipelines/latest/what-is-cell-ranger
Celda	Wang et al. (2021)	https://github.com/campbio/celda
DropletUtils	Griffiths et al. (2018)	https://github.com/MarioniLab/DropletUtils
DoubletFinder	McGinnis et al. (2019)	https://github.com/chris-mcginnis-ucsf/DoubletFinder
Harmony	Korsunsky et al. (2019)	https://github.com/immunogenomics/harmony
Sctransform	Hafemeister and Satija (2019)	https://github.com/satijalab/sctransform
Seurat	Satija et al. (2015)	https://satijalab.org/seurat/
ggplot2	Wickham (2016)	https://ggplot2.tidyverse.org/

(*Continued on next page*)

Continued

REAGENT or RESOURCE	SOURCE	IDENTIFIER
R	R Core Team (2021)	https://www.r-project.org/
R studio	RStudio Team, 2020	https://www.rstudio.com/
FIJI	Schindelin et al. (2012)	https://imagej.net/software/fiji/
Prism	GraphPad	https://www.graphpad.com/
Other		
Additional raw data, plots, analysis, scripts, descriptive statistics and analysis	This study	https://github.com/VosshallLab/Younger_Herre_Vosshall2020
Additional antenna snRNA-seq data formats (e.g., Seurat Objects)	This study	https://doi.org/10.5281/zenodo.5818542
Additional maxillary palp snRNA-seq data formats (e.g., Seurat Objects)	This study	https://doi.org/10.5281/zenodo.5818951

RESOURCE AVAILABILITY

Lead contact

Further information and requests for resources and reagents should be directed to and will be fulfilled by the lead contact, Meg Younger (myounger@bu.edu).

Materials availability

Plasmids generated in this study have been deposited to Addgene (accession #162520–162526).

Data and code availability

- snRNA-seq data have been deposited as an NCBI BioProject and are publicly available under the accession number listed in the key resources table.
- All original code and custom scripts, along with additional raw data not found in Data S1 as well as plots and additional analysis have been deposited at Github and at Zenodo and are publicly available. DOIs are listed in the key resources table.
- Microscopy data reported in this paper will be shared by the lead contact upon request.
- Any additional information required to reanalyze the data reported in this paper is available from the lead contact upon request.

EXPERIMENTAL MODEL AND SUBJECT DETAILS

Human and animal ethics statement

Blood-feeding procedures and behavioral experiments with live hosts were approved and monitored by The Rockefeller University Institutional Animal Care and Use Committee (IACUC protocol 17,018) and Institutional Review Board (IRB protocol LV-0652), respectively. Human volunteers gave their written informed consent to participate.

Mosquito rearing and maintenance

Ae. aegypti wild-type laboratory strains (Liverpool and Orlando), CRISPR-Cas9 knock-in, and piggyBAC *QUAS* transgenic strains were maintained and reared at 25–28°C, 70–80% relative humidity with a photoperiod of 14 h light: 10 h dark as previously described (DeGennaro et al., 2013). Adult mosquitoes were provided constant access to 10% sucrose. For routine strain maintenance, animals were primarily blood-fed on live mice and occasionally on live human volunteers. Newly generated strains were blood-fed on human volunteers until they were established. All experiments except those in Figures 2J–2T were conducted on adult female mosquitoes. Detailed genotypes used in each figure can be found in Data S1.

METHOD DETAILS

Generation of chemosensory receptor *QF2* and Split-*QF2* knock-in strains

T2A-QF2 gene-sparing stop codon replacement lines were generated using the strategy outlined in Matthews et al. (2019). sgRNAs were placed as close to the stop codon as possible and donor constructs were designed to remove the stop codon and replace it with an in-frame cassette containing the *T2A* ribosomal skipping sequence and the *QF2* transcription factor or Split-*QF2* domains, comprising the *QF2* activation domain *QF2-AD*, or the *QF2* DNA-binding domain *QF2-DBD*. This strategy spares the function of the gene at the locus being targeted, expresses *QF2* or Split-*QF2* domains in the cells specified by enhancers at the locus. Insertions were marked by the *3xP3* enhancer expressing a fluorescent protein. To identify effective sgRNAs, 5 candidate sgRNAs per gene

were first injected into separate pools of 500 Liverpool embryos and CRISPR-Cas9-mediated cut rate was evaluated as previously described (Kistler et al., 2015). Either a single sgRNA or 2 sgRNAs with the highest cut rates were then chosen to be injected with donor plasmids to target chemosensory gene loci using homology-directed repair. sgRNAs targeted the respective gene near the stop codon, target sequence with protospacer adjacent motif (PAM) underlined:

Ir25a: GTTTGTGTGCGTGTCCGTA TGG
Ir76b: GTATTACACTTATCTAAATA TGG
Ir8a: GTCACGCTTGTTGTACAGGG CGG, GAACAATTTGAACAAGGTCG TGG
Gr3: GTTAGTGATGCATAATATGA CGG
Orco: GTCACCTACTTCATGGTGT TGG

sgRNA DNA template was prepared by annealing oligonucleotides as described (Kistler et al., 2015). *In vitro* transcription was performed using HiScribe Quick T7 kit (NEB E2050S) following the manufacturer's directions. Following transcription and DNAse treatment for 15 min at 37°C, sgRNA was purified using RNAse-free SPRI beads (Ampure RNAclean, Beckman-Coulter A63987), and eluted in Ultrapure water (Invitrogen, 10,977–015).

Donor plasmids were constructed by Gibson assembly using the following fragments for QF2 lines:

1) *pUC19* digested with XbaI and BamHI
2) Left and right homology arms: *Gr3* (left: 1.9 kb, right: 1.6 kb), *Ir25a* (left: 1.8 kb, right: 1.6 kb), *Ir76b* (left: 1.2 kb, right: 2.2 kb), *Ir8a* (left: 1.7 kb, right: 1.7 kb), *Orco* (left: 1.2 kb, right: 1.3 kb) generated by polymerase chain reaction (PCR) using Liverpool genomic DNA as a template
3) A 2.6 kb fragment containing *T2A-QF2-SV40, 3xP3-dsRed*, PCR-amplified from a previously assembled vector (*ppk10779-T2A-QF2-SV40, 3xP3-dsRed*, Addgene accession #130667)

For Split-QF2 lines, donor plasmids were constructed by generating fragments using PCR from the indicated template with indicated primers in Data S1 and assembled using NEBuilder HiFi DNA Assembly (NEB E5520S):

Ir25a-T2A-QFAD::Zip+-SV40-3xP3-eYFP-SV40 was composed of:

1. Plasmid backbone with *Ir25* homology arms from *Ir25a-T2A-QF2* plasmid (6 kb)
2. *T2A-QFAD::Zip+-SV40* sequence from (Riabinina et al., 2019), fragment synthesized by Genewiz, sequence in Data S1 (1.5 kb)
3. *3xP3-EYFP-SV40* from *pDSAY* (Addgene, #62291) (1.2 kb)

Orco-T2A-Zip−::QFDBD-SV40-3xP3-dsRED-SV40 was composed of:

1. Plasmid backbone with *Orco* homology arms and *3xP3-dsRED-SV40* from *Orco-T2A-QF2* plasmid (6.3 kb)
2. *T2A-Zip−::QFDBD-SV40* synthesized by Genewiz, sequence in Data S1 (1.5 kb)

For all *QF2* and Split-*QF2* constructs, the stop codon of the endogenous gene was removed and the PAM sequences corresponding to the sgRNAs used for injection were modified by PCR mutagenesis during Gibson assembly by introducing synonymous codon substitutions to protect the sequence from Cas9 cleavage while retaining the amino acid identity. Plasmids were isolated using an endotoxin-free plasmid midiprep kit (Macherey-Nagel) for QF2 lines and NucleoBond Xtra Midi Endotoxin-Free plasmid kit (Clontech 740,420.50) for Split-QF2 lines and eluted in ultrapure water prior to injection. Donor plasmids are available at Addgene (accession numbers #162520–162526). Approximately 2,000 wild-type Liverpool strain *Ae. aegypti* embryos were injected with a mix containing recombinant Cas9 protein (PNA Bio, CP01) at 300 ng/μL, sgRNAs at 40 ng/μL and donor DNA plasmid (300 ng/μL for QF2 lines, 600 ng/μL for Split-QF2 lines) at the Insect Transformation Facility at the University of Maryland Institute for Bioscience & Biotechnology Research. Embryos were hatched and surviving G0 males and females were crossed to wild-type Liverpool mosquitoes and their G1 offspring were screened for fluorescence indicating positive stable germ line transformants. For QF2 lines, the fidelity of insertion was verified by PCR and Sanger sequencing. One representative line for each chemosensory receptor QF2 knock-in was selected for further study. QF2-driven expression patterns were examined by crossing to *QUAS-CD8:GFP-3xP3-ECFP* and/or *QUAS-dTomato-T2A-GCaMP6s-3xP3-ECFP*.

A technical problem arose in the construction of the *QUAS-dTomato-T2A-GCaMP6s-3xP3-ECFP* plasmid that caused only a single copy of *dTomato* to be introduced into the mosquito, rather than the brighter *tandem dTomato* or *tdTomato* that is more conventionally used. Nevertheless we found that dTomato is sufficiently bright for our experiments (Shaner et al., 2004).

All lines were outcrossed to wild-type Liverpool mosquitoes for at least 3 generations prior to being used in experiments. For Split-QF2 lines, a single family with the correct insertion was confirmed by PCR and Sanger sequencing for *Ir25a-QF2-AD* and *Orco-QF2-DBD*. To propagate these lines, a male founder was chosen to cross to wild-type Liverpool females. Animals were then back-crossed to Liverpool for at least 2 additional generations. To evaluate if the Split-QF2 system was functional in *Ae. aegypti*, *Ir25a-QF2-AD was crossed to QUAS-dTomato-T2A-GCaMP6s.* The resulting *Ir25a-QF2-AD, QUAS-dTomato-T2A-GCaMP6s* animals were then crossed to *Orco-QF2-DBD*. Expression of the dTomato reporter was observed in larval antennae and subsequently confirmed in adult antennae and brains.

QUAS transgenic strains

QUAS-CD8:GFP-3xP3-ECFP and *QUAS-dTomato-T2A-GCaMP6s-3xP3-ECFP* transgenic strains were described previously (Matthews et al., 2019). Two independent insertions of the *QUAS-dTomato-T2A-GCaMP6s-3xP3-ECFP* reporter line (Jové et al., 2020; Matthews et al., 2019) were used in this study. These are located on different chromosomes and were used according to the crossing scheme needed for a given experiment. See Data S1 for details.

Chemosensory receptor mutant strains

The three chemosensory receptors mutant strains used in this study was previously described: $Ir25a^{BamHI/BamHI}$ (De Obaldia et al., 2022), $Gr3^{4/4}$ (McMeniman et al., 2014), $Orco^{16/16}$ (DeGennaro et al., 2013). $Gr3^{4/4}$ and $Orco^{16/16}$ were generated in the *Orlando* background (here referred to as $+/+^{ORL}$) and the $Ir25a^{BamHI/BamHI}$ mutant was generated in the *Liverpool* background (here referred to as $+/+^{LVP}$). To account for possible difference in genetic background the $+/+^{ORL}$ strain was used as the controls in all experiments where the $Gr3^{4/4}$ and $Orco^{16/16}$ mutants were used, and the $+/+^{LVP}$ strain was used as the control in experiments where the $Ir25a^{BamHI/BamHI}$ mutant was used.

Transcript abundance estimates of *Ae. aegypti* OR, IR, and GR genes

Expression values for adult sugar-fed, non-blood-fed female sensory tissues were retrieved from the *Ae. aegypti* L5 genome GitHub repository (https://github.com/VosshallLab/AGWG-AaegL5) at this link: https://github.com/VosshallLab/AGWG-AaegL5/raw/master/AGWG%20AaegL5%20Chemoreceptor%20TPM.xlsx. These expression values reflect libraries from a previous transcriptome study (Matthews et al., 2016) that had been aligned to the *Ae. aegypti* genome (AaegL5) and chemosensory receptor geneset annotation reported in units of Transcripts Per Million (TPM) (Matthews et al., 2018). The number of genes from each of three gene families (ORs, IRs, and GRs) with expression values above the indicated threshold were plotted in Figures 1F and 1G and are available in Data S1.

Whole brain fixation and immunofluorescence

Dissection of adult brains and immunofluorescence was carried out as previously described (Matthews et al., 2019). 6-14-day-old mosquitoes were anesthetized on wet ice. Heads were carefully removed from the body by pinching at the neck with sharp forceps. Heads were placed in a 1.5 mL tube for fixation with 4% paraformaldehyde, 0.1 M Millonig's Phosphate Buffer (pH 7.4), 0.25% Triton X-100, and nutated for 3 h. Brains were then dissected out of the head capsule in ice-cold Ca^{+2}-, Mg^{+2}-free PBS (PBS, Lonza 17-517Q) and transferred to a 24-well plate. All subsequent steps were done on a low-speed orbital shaker. Brains were washed in PBS containing 0.25% Triton X-100 (PBT) at room temperature 6 times for 15 min. Brains were permeabilized with PBS, 4% Triton X-100, 2% normal goat serum (Jackson ImmunoResearch #005-000-121) for ~48 h (2 nights) at 4 °C. Brains were rinsed once and then washed with PBT at room temperature 6 times for 15 min. Primary antibodies were diluted in PBS, 0.25% Triton X-100, 2% normal goat serum for ~48 h (2 nights) at 4 °C. Brains were rinsed once then washed in PBT at room temperature 6 times for 15 min. Secondary antibodies were diluted in PBS, 0.25% Triton X-100, 2% normal goat serum for ~48 h (2 nights) at 4 °C. Brains were rinsed once then washed in PBT at room temperature 6 times for 15 min. Brains were equilibrated overnight in Vectashield (Vector Laboratories H-1000) and were mounted in Vectashield. The following primary antibodies were used: anti-Brp/nc82 (mouse; 1:50, Developmental Studies Hybridoma Bank – see below) and/or anti-GFP (rabbit: 1:10,000; Life Technologies A-11122). The secondary antibodies used in all experiments except Figures S1A and S1P were anti-mouse-Cy5 (1:250; Life Technologies A-10524) and anti-rabbit-Alexa Fluor 488 (1:500; Life Technologies A-11034). In Figures S1A and S1P, the secondary antibody was anti-mouse-Alexa Fluor 488 (1:500; Life Technologies A-11001) and in Figures S1A and S1P, the secondary antibodies were anti-mouse-Alexa Fluor 594 (1:500; Life Technologies A-11005) and anti-rabbit-Alexa Fluor 488 (1:500; Life Technologies A-11034).

Purification of nc82/Brp monoclonal antibody

Hybridoma cells expressing monoclonal antibody nc82 (Antibody Registry ID: AB_2314866), which recognizes the *D. melanogaster* Brp protein (Wagh et al., 2006) developed by Erich Buchner were obtained from the Developmental Studies Hybridoma Bank, created by the NICHD of the NIH and maintained at The University of Iowa, Department of Biology, Iowa City, IA 52242. Frances Weis-Garcia and the members of the MSKCC Antibody and Bioresource Core Facility subsequently used these hybridoma cells to purify this monoclonal antibody. The hybridoma was adapted to Gibco Hybridoma-SFM (Cat # 12,045,084) and 1% fetal bovine serum prescreened for ultra-low levels of bovine Ig. Antibody expression was confirmed and the adapted hybridoma was inoculated into the cell compartment of the Corning CELLine Disposable Bioreactor (Cat # 353,137) in 15 mL of Hybridoma-SFM + 0.5% fetal bovine serum (production media) at 3 million viable cells/ml. The media compartment of the flask contained 350 mL of production media. The bioreactor was incubated at 37°C with 7% CO_2 for 3 days, at which time the cells and media containing nc82 were harvested. 30 million viable cells from the harvest were re-inoculated back into the cell compartment in 30 mL fresh production media. The media in the media compartment was replaced the following day with 650 mL production media. Three days later, the media in the media compartment was replaced with 1,000 mL production media, with the next harvest 3 days later (7 days after the previous harvest). Cells were harvested weekly and fed biweekly until the desired amount of monoclonal antibody was reached. After the first harvest, each one contained about 3 mg of monoclonal antibody nc82/mL production media. The harvests to be purified were pooled, centrifuged at 12,855 x g for 15 min 6.5 mg/run were loaded onto a Cytiva (formerly GE Life Sciences) 1 mL HiTrap Protein G HP antibody

purification column (Cat # 29,048,581) at 1 mL/min. The column was then washed with 0.02 M Sodium Phosphate (pH 7.0) before the monoclonal antibody was eluted with 0.1 M Glycine-HCl (pH 2.7). One mL fractions were collected and immediately neutralized with 60 mL of 1.0 M Tris-HCl (pH 9.0). The harvest, flow through and fractions from the peak were run on an a 10% SDS-PAGE (Bio-Rad Cat # 345-0010) to confirm purity and determine which should be pooled. The pooled fractions of monoclonal antibody were dialyzed into PBS overnight using dialysis tubing (Spectrum 132,544) with a 50 kDa MWCO. Another 10% SDS-PAGE was run, and the concentration determined using the absorbance at 280 using an extinction coefficient of 1.43.

Generation of the Ir25a polyclonal antibody

Rabbit polyclonal antibodies were raised against Ir25a by Proteintech Group Inc. Antibodies were raised against a protein fusion of the 67 C-terminal amino acids of Ir25a and glutathione S-transferase. cDNA corresponding to the C-terminal region was inserted into the expression vector PGEX-4T using primers TTTTGGATCCAAATACCGCAAGAACGTAAAG and TTTTCTCGAGTTAGAAACGA GATTTAAAGTTG and expressed in bacterial strain BL21. A purified 31 kDA fusion protein was used to immunize 2 rabbits. Serum was affinity purified to a final concentration of 450 μg/mL and tested by whole mount antenna immunofluorescence comparing $+/+^{LVP}$ to $Ir25a^{BamHI/BamHI}$. Antibodies from one of the two rabbits were found to selectively label $+/+^{LVP}$ antennae, and only this antibody was used in all further studies.

Female antennal lobe confocal imaging

All brains were imaged using a Zeiss Inverted LSM 880 laser scanning confocal microscope with a 25x/0.8 NA immersion-corrected objective unless otherwise noted. Glycerol was used as the immersion medium to most closely match the refractive index of the mounting medium Vectashield. Antennal lobes in Figures 1, 2, 5, S1, S2, S3, and S4 were imaged at either 1024 x 1024 or 2048 x 2048 pixel resolution in X and Y with 0.5 μm Z-steps for a final voxel size of either 0.0615 × 0.0615 × 0.5 μm^3 or 0.1230 × 0.1230 × 0.5 μm^3. Both conditions oversampled relative to the objective resolution and no differences were noted between imaging conditions. The laser intensity and gain were adjusted along the z axis to account for a loss of intensity due to depth and care was taken to avoid saturation and ensure that the deepest glomeruli were visible for segmentation. We note that all confocal imaging was conducted in a manner that would maximize our ability to visualize the boundaries between glomeruli and to determine the presence or absence of a given fluorophore in each glomerulus, and was not intended as a quantitative measure of fluorescence intensity. *3xP3* was used as a promoter to express fluorescent proteins as markers for the knock-ins and *QUAS* transgenes used in this study, and care was taken to distinguish expression derived from the *3XP3* promoter from the expression of the QF2 driver and *QUAS* effector lines under investigation. *3xP3* drives expression in the optic lobes, as well as some cells in the dorsal brain. Neither area overlaps with the antennal lobes. As reported previously (Matthews et al., 2019), we saw no *3xP3*-driven expression in the antennal lobes in the reporter lines alone (data not shown). Representative antennal lobe images presented in the figures were cropped to remove *3xP3*-driven expression elsewhere in the brain.

Male brain and female subesophageal zone confocal imaging

All male brains (Figure 2M, 2O, 2Q, 2S, and 2U) and all female subesophageal zones (Figure S4G) were imaged using a Zeiss Inverted LSM 880 laser scanning confocal microscope with a 25x/0.8 NA immersion-corrected objective. Glycerol was used as the immersion medium to most closely match the refractive index of the mounting medium Vectashield. Brains were imaged at 1024 x 1024 pixel resolution in X and Y with 0.5 μm Z-steps for a final voxel size of 0.2372 × 0.2372 × 0.5 μm^3 (male brain) or 0.2076 × 0.2076 × 0.5 μm^3 (female subesophageal zone). The laser intensity and gain were adjusted along the z axis to account for a loss of intensity due to depth and care was taken to avoid saturation and ensure that the deepest regions of the brain were visible. Confocal images of the brain were processed in ImageJ/FIJI (NIH) (Schindelin et al., 2012).

Additional technical notes on expression and projection patterns in subesophageal zone

Ir25a-expressing neurons send extensive projections to the subesophageal zone, with axons terminating in the anterior and posterior regions. There is a small cluster of glomeruli in the central subesophageal zone that receives dense innervation as well (Figure S4). *Orco*-expressing neurons do not project to the anterior region and send sparse projections to the posterior subesophageal zone and subesophageal zone glomeruli (Figure S4). Innervation by the neurons that co-express *Orco* and *Ir25a* send projections only to the posterior-ventral subesophageal zone, with the densest innervation in the medial region and sparser lateral arborizations (Figure S4). *Ir25a* complexes can mediate detection of volatile odorants and gustatory cues.

Antennal lobe glomerulus quantification

Confocal images of the antennal lobes in Figures 1, 2, 5, S1, S2, S3, and S4 were processed in ImageJ/FIJI (NIH) (Schindelin et al., 2012). The number of glomeruli was quantified as follows: a single region of interest (ROI) was manually drawn around each glomerulus at a section approximately central along the z axis. Every glomerulus was outlined and an ROI set was collected that contained the outlines of all glomeruli. Glomeruli were then separated into two groups, GFP-positive and GFP-negative glomeruli, as determined by eye. A count of each was made to determine the number of glomeruli labeled by each line as well as the total number of glomeruli. The ROIs were flattened along the z axis to enable representation of the data in two dimensions in Figures 1, 2, S1, S2, S3, and S4. The left antennal lobe in 3 brains was analyzed for each genotype in Figure 1 except for *Gr3*, for

which the left antennal lobe was analyzed in 1 brain, and both left and right antennal lobes were analyzed in an additional 4 brains in Figure S1. Although we were able to recognize general regions of the antennal lobe, the interindividual variability made it impossible to identify most glomeruli by shape alone. We therefore have not attempted to name and number every glomerulus in *Ae. aegypti* as has been done in previous studies (Ignell et al., 2005; Shankar and McMeniman, 2020). As noted by Ito et al. (2014), there is considerable confusion about the use of coordinate axes in the brains of animals in general and insects in particular. The glomeruli in the antennal lobe of *Ae. aegypti* were originally named by Ignell et al. (2005) using a set of coordinate axes that differ from those consistently used in *D. melanogaster* (Couto et al., 2005; Fishilevich and Vosshall, 2005; Grabe et al., 2015; Laissue et al., 1999; Stocker et al., 1990). A recent study of the antennal lobe of *Ae. aegypti* renamed glomeruli to account for this discrepancy in coordinate axes (Shankar and McMeniman, 2020), and throughout this paper we use the same coordinate axes they have implemented. While Shankar and McMeniman renamed most antennal lobe regions and glomeruli, they chose not to rename the MD (Medio-Dorsal) cluster of glomeruli comprising MD1, MD2, and MD3 whose sensory input derives from the maxillary palp. We have observed in our study that the MD glomeruli are medial, but they are not notably dorsal, and therefore refer to them as Glomerulus 1, Glomerulus 2, and Glomerulus 3 in this paper for simplicity. While there is utility in naming glomeruli, we suspect that the *Ae. aegypti* mosquito antennal lobe atlas will be refined in the future with the advent of new genetic tools that will unambiguously allow the field to distinguish and name genetically identifiable glomeruli. We found that the size, shape, and number of antennal lobe glomeruli in *Ae. aegypti* was variable from animal to animal. It is possible that the boundaries between glomeruli are not easily distinguished by synaptic staining and that specific glomeruli will become identifiable once there are genetic tools available that label smaller populations of OSNs. The anatomical variability we see is consistent with both the original map that identified 50 glomeruli (Ignell et al., 2005), which divided glomeruli into 3 classes based on their variability in location, as well as a recent study that looked specifically at the size and shape of glomeruli across animals (Shankar and McMeniman, 2020) and revised the original map to a count of ~80 glomeruli. Shankar and McMeniman named and numbered these glomeruli across animals, but they noted that they were only able to consistently identify 63 glomeruli. This is similar to the ~65 glomeruli we observed in our work. While there is not yet a clear consensus on the exact number of antennal lobe glomeruli in *Ae. aegypti*, the number of chemosensory receptors expressed in the antenna and maxillary palp is at least twice as large as any of the estimates of glomerulus number. The variability in antennal lobe structure appears at first to contrast with *D. melanogaster*, where each glomerulus can be clearly identified and named. However, we note that the antennal lobe map in *D. melanogaster* has been refined with the advent of new genetic techniques, starting with 35 glomeruli in the original atlas (Stocker et al., 1990), then modified to 40 glomeruli (Laissue et al., 1999), and further refined in numerous studies (Couto et al., 2005; Fishilevich and Vosshall, 2005; Tanaka et al., 2012) including a recent count of 54 (Grabe et al., 2015) and 58 (Task et al., 2022) glomeruli. We have refrained from naming glomeruli in *Ae. aegypti* at this time because we believe that a more stereotyped arrangement will emerge as new genetic lines are generated that allow cell-type-specific labeling. A recent study in the mosquito *An. gambiae* using mosquitoes that label *Orco*-expressing olfactory neurons also noted that the antennal lobe was variable between animals relative to *D. melanogaster* (Riabinina et al., 2016). It is therefore possible that mosquito antennal lobes are more variable than Drosophilids (Grabe et al., 2015; Prieto-Godino et al., 2017). Variability in olfactory bulb structure is seen even in the mouse, *Mus musculus,* where the principles of olfactory organization were first established (Schaefer et al., 2001; Strotmann et al., 2000; Zou et al., 2009). The exact size and location of glomeruli can vary between animals more than initially appreciated and appears to be determined by both genetic factors and activity in OSNs during the early life of the animal. In *D. melanogaster*, glomerulus size is highly genetically determined and correlates strongly with the number of OSNs that innervates each glomerulus (Grabe et al., 2015). Whether the variability in glomerulus size in the mosquito is due to activity-dependent changes in structure or other factors remains to be seen.

Additional technical notes on expression and projection patterns of chemosensory receptor knock-in strains

Orco-QF2>QUAS-mCD8:GFP. We noted that the intensity of GFP varies between glomeruli in this driver line, with some bright and others comparably dim. We speculate that this is due to a combination of the variability in *Orco* expression levels in individual neurons and variability in the density of innervation in individual glomeruli. A large region of the anterior ventral antennal lobe was previously referred to as the Johnston's organ center and was thought to comprise a single large glomerulus (Ignell et al., 2005). In other insect species, Johnston's organ mediates detection of auditory cues. Consistent with a recent study (Shankar and McMeniman, 2020), we segmented this region into multiple glomeruli based on anatomical boundaries revealed with Brp immunofluorescence. Glomeruli in this region are innervated by *Orco*-expressing neurons, calling into doubt the original report that these glomeruli process auditory stimuli and suggesting instead that they serve an olfactory function. In support of this hypothesis, the analogous area of the *An. coluzzii* antennal lobe has been shown to receive projections from *Orco*-expressing OSNs (Riabinina et al., 2016). We also observed GFP projections into the subesophageal zone in *Orco-QF2>QUAS-mCD8:GFP* animals, which appear to derive from expression in the proboscis, the primary taste organ in insects. This is consistent with similar expression in *An. coluzzii* (Riabinina et al., 2016) and functional data in *An. gambiae* showing that olfactory responses are detected in this gustatory organ (Kwon et al., 2006).

Ir25a-QF2>QUAS-mCD8:GFP. The intensity of GFP projections varies between glomeruli in this driver line, with some bright and other comparably dim, as noted for *Orco-QF2*. The brightest glomeruli are primarily medial and anterior. We see the dimmest innervation in the area previously described as Johnston's organ center as well as in the central antennal lobe. Labeling was also seen in other areas of the brain, most notably the subesophageal zone and anterior mechanosensory motor center.

Ir8a-QF2>QUAS-mCD8:GFP. Depending on the brain being analyzed there were either 2 or 3 medial glomeruli labeled in this line. In the cases where there were 3 medial glomeruli, this third medial glomerulus was innervated by a few large-diameter axons. These were larger and sparser than the smaller axons that densely innervated most other glomeruli in this line. We also note that there are 2–3 cell bodies that express GFP located in the cell body rind lateral to the antennal lobe (rALl). We are unable to definitively describe where these cells project without genetic reagents that selectively label these cells, but they appear to send bilateral processes that cross the midline within what appears to be the saddle to innervate the anterior mechanosensory motor center outside the antennal lobe. All naming is in accordance with the new insect brain nomenclature presented in Ito et al. (2014).

Ir76b-QF2>QUAS-mCD8:GFP. In addition to projections to the antennal lobe, this line shows innervation of the subesophageal zone of the brain.

Gr3-QF2>QUAS-mCD8:GFP. All antennal lobes in this line show innervation of a single glomerulus (also referred to as "MD1″ and here referred to as "Glomerulus 1"; (Ignell et al., 2005; Shankar and McMeniman, 2020). In several brains, we saw a second small medial glomerulus that derives its innervation from the antenna and is in a small medial cluster of landmark glomeruli midway down the anterior-posterior axis closest to the center of the brain. Innervation appears to come from only a few axons. This low and variable reporter expression is consistent with the low level of expression of *Gr3* in the antennal transcriptome (Matthews et al., 2016). Because this line only shows innervation of these 1–2 glomeruli, we analyzed all glomeruli only in the single brain in Figure 1I, and additionally analyzed 8 more antennal lobes in 4 brains for the presence or absence of labeling in these two glomeruli. We analyzed both left and right antennal lobes from 4 brains and found that in 3 of the 4 brains there was a second glomerulus in one or both antennal lobes (Figure S1). The presence of the second glomerulus was not specific within a single animal as we found all variations of presence and absence of this glomerulus across both antennal lobes in these 4 animals. In some *Gr3-QF2>QUAS-mCD8:GFP* animals, we detected a small number of processes that extended beyond the antennal lobe and into the higher brain, although the exact termination site varied. We never saw CO_2-evoked activity in the variable second glomerulus or these projections outside the antennal lobe. Images in Figure S1 were taken as described above with the following changes: Secondary antibodies used were anti-mouse-Alexa Fluor 594 (1:500; Life Technologies A-11005) and anti-Rabbit-Alexa Fluor 488 (1:500; Life Technologies A-11034). Images were taken using a Zeiss Inverted LSM 880 laser scanning confocal microscope with a Plan-Apochromat 40x/1.4 Oil DIC objective. Images were taken at 1024 x 1024 in XY to generate images with a final voxel size of 0.1384 × 0.1384 × 0.5 μm^3. Images were scored as containing GFP in one or two glomeruli.

Additional technical notes on expression and projection patterns of Split-QF2 strains

All antennal lobe immunofluorescence in Figures 2, 5, and S4 was carried out as described above with slight modifications to utilize the *15xQUAS-dTomato-T2A-GCaMP6s* effector line. The same primary antibodies were used because of the structural similarity between GCaMP6s and GFP. Intrinsic dTomato was detected without antibody amplification, as it retained fluorescence after fixation and staining. Brp (Cy5), dTomato, and GCaMP6s (Alexa Fluor 488) were imaged as three separate confocal channels as described above. Glomeruli labeled by dTomato completely overlapped with those labeled by GCaMP6s immunofluorescence, so both channels were used during the quantification of positive and negative glomeruli. dTomato labeling was used to generate sample images. There was no staining in the antennal lobes of the individual split effector lines crossed to *15xQUAS-dTomato-T2A-GCaMP6s* (n = 3 per genotype) (Figures 2 and S4).

Antennal lobe anterograde dye fill

For images in Figure S1, mosquitoes were anesthetized on wet ice until immobile and then transferred to a cold dissection dish. A single antenna or maxillary palp was loaded with Texas red conjugated dextran (Molecular Probes D3328) diluted 10 mg in 100 μL external saline (103 mM NaCl, 3 mM KCl, 5 mM 2-[Tris(hydroxymethyl)methyl]-2-aminoethanesulfonic acid (TES), 1.5 mM $CaCl_2$, 4 mM $MgCl_2$, 26 mM $NaHCO_3$, 1 mM NaH_2PO_4, 10 mM trehalose, 10 mM glucose, pH 7.3, osmolality adjusted to 275 mOsm/kg). To load the dye a small drop (approximately 0.5–1 μL) of dye was placed onto the surface of the dish and the animal was moved such that the intended cut-site on a single antenna or maxillary palp was placed in the drop of dye. The antenna or maxillary palp was then removed with sharp forceps and a fine scalpel (F.S.T 10315-12) while it was submerged in the dye. Care was taken to remove the maxillary palp proximal to the fourth segment, to include all the capitate-peg sensilla, and to remove the antenna near the base but to leave the antennal pedicel completely intact. The animal remained immobile on ice with the antenna or maxillary palp submerged and the dye was loaded for 2–5 min. After this time the animal was placed in a small soup cup with access to 10% sucrose and returned to standard rearing conditions overnight to give the dye time to diffuse throughout the neurons and fill the length of the axon. The next morning dissection of adult brains and immunofluorescence was carried out as described above.

Antennal lobe 3D reconstructions

In an attempt to develop a map of the *Ae. aegypti* antennal lobe, 3 brains from the $+/+^{LVP}$ strain were immunolabeled with Brp to identify the boundaries between antennal lobe glomeruli. The left antennal lobe in each brain was independently reconstructed from confocal sections taken with a Plan-Apochromat 63x/1.40NA oil immersion objective, at 1024× 1024 pixel resolution in X and Y with 0.5 μm Z-steps for a final voxel size of either 0.1318 × 0.1318 × 0.5 μm^3 using the software Imaris (Bitplane). Although the area previously termed Johnston's organ center was considered a single glomerulus in a previous study (Ignell et al., 2005), we

noted anatomical boundaries in this region, suggesting that it contains multiple glomeruli. This observation is consistent with recently published work (Shankar and McMeniman, 2020) and this area was segmented by an individual researcher to generate the final reconstructions. Two of these are shown in Figure S1. Each glomerulus was manually segmented into an individual surface using Surpass View. We were consistently able to identify the three glomeruli innervated by the maxillary palp, previously termed MD1, MD2 and MD3 (Ignell et al., 2005) which we refer to in this study as Glomerulus 1, Glomerulus 2, and Glomerulus 3 (Figures 1 and 5). The overall structure of the antennal lobe varied considerably from animal to animal and although we were able to identify certain regions and certain landmark glomeruli including those that are targeted by the maxillary palp, we were unable to assign an unambiguous identity to every glomerulus, as is possible in *D. melanogaster* (Couto et al., 2005; Fishilevich and Vosshall, 2005). This variability makes it essentially impossible to identify a given glomerulus between animals and we therefore have decided to avoid referring to glomeruli by previous naming schemes, including MD1, MD2, MD3. An authoritative atlas of the *Ae. aegypti* antennal lobe awaits genetic reagents that label subpopulations of sensory neurons that will permit the field to refer to glomeruli by their molecular identity.

Antennal whole mount immunofluorescence

Whole-mount immunofluorescence of adult antennae was performed as described (Riabinina et al., 2016) with modifications. 7-11-day-old Liverpool mosquitoes were immobilized on ice, decapitated and heads and placed in 1 mL ZnFA fixative solution (0.25% $ZnCl_2$, 2% paraformaldehyde, 135 mM NaCl, 1.2% sucrose and 0.03% Triton X-100) for 20–24 h at room temperature in the dark. Next, the heads were washed three times for 30 min each with HBS buffer (150 mM NaCl, 5 mM KCl, 25 mM sucrose, 10 mM HEPES, 5 mM $CaCl_2$ and 0.03% Triton X-100). Antennae were carefully removed in HBS on ice and placed in 400 μL HBS in 0.5 mL Eppendorf tubes. After a brief wash in HBS, the tissue was incubated in 400 μL 80% methanol/20% dimethyl sulfoxide (DMSO) solution for 1 h at room temperature, washed for 5 min in 400 μL 0.1 M Tris pH 7.4, 0.03% Triton X-100 solution and incubated in 400 μL blocking solution (PBS, 5% normal goat serum (Jackson 005-000-121), 1% DMSO and 0.3% Triton X-100) for at least 3 h at room temperature or overnight at 4°C. Next, the tissue was placed in a 0.5 mL Eppendorf tubes containing 400 μL blocking solution with primary antibodies [rabbit anti-Orco EC2 (Larsson et al., 2004), 1:50, Vosshall lab; chicken anti-GFP,1:200, Aves GFP-1020] and submerged and held in a water bath sonicator (Branson m1800) for 30 s at the high setting. Next, the tubes were placed on a rotator for 2 days at 4°C in the dark, after which the sonication procedure was repeated. The tubes were placed on a rotator for 2 additional days (for a total of 4 days) at 4°C in the dark. Next, the tissue was washed 5 × 30 min each at room temperature in PBS, 1% DMSO and 0.3% Triton X-100. Secondary antibodies (anti-rabbit Alexa Fluor 555 Plus, 1:200, Thermo Fisher A-32732, anti-chicken Alexa Fluor 488, 1:200, Thermo Fisher A-11039) and nuclear dye (TO-PRO-3 Iodide, 1:400, Thermo Fisher T3605) were added to the blocking solution, and tubes were sonicated as described above and incubated for 4 days at 4°C in the dark with the sonication repeated after 2 days of incubation. The tissue was then washed 5 × 30 min at room temperature in PBS, 1% DMSO and 0.3% Triton X-100, rinsed in PBS and mounted in Slow Fade Diamond for confocal imaging.

Antennal whole-mount immunofluorescence with Ir25a antibody

This protocol was performed as previously described (Basrur et al., 2020) with modifications. Six-to 11-day-old female mosquitoes were anesthetized on wet ice, decapitated, and placed in 1.5 mL 5 U/mL chitinase (Sigma C6137) and 100 U/mL chymotrypsin (Sigma CHY5S) in 119 mM NaCl, 48 mM KCl, 2 mM CaCl2, 2 mM MgCl2, 25 mM HEPES, 1% DMSO buffer on ice. Heads were incubated on a ThermoMixer (Eppendorf 5,382,000,023) at 37 °C for 5 min, followed by 55 min in a rotating hybridization oven at 37 °C. Heads were then rinsed once and fixed in 4% paraformaldehyde, 1X Ca+2, Mg+2 free PBS, and 0.03% Triton X-100 for 24 h at 4 °C on a rotator. All subsequent 4 °C steps used a nutator, and room temperature steps used a rotator. Heads were washed for 30 min at room temperature at least three times in 1X PBS with 0.03% Triton X-100 (0.03% PBT). Antennae were then dissected into 0.5-mL microfuge tubes and dehydrated in 80% methanol/20% DMSO for 1 h at room temperature. Antennae were washed in 0.03% PBT for 30 min at room temperature, and blocked/permeabilized in 1X PBS, 1% DMSO (Sigma 472,301), 5% normal goat serum, 4% Triton X-100 for 24 h at 4 °C. Antennae were washed for 30 min at least five times with 0.03% PBT, 1% DMSO, 5% normal goat serum at 4 °C, and then moved to primary antibody in 1X PBS, 1% DMSO, 5% normal goat serum, 0.03% Triton X-100 for 72 h at 4 °C. Primary antibodies used were mouse anti-*Apocrypta bakeri* Orco monoclonal antibody #15B2 (1:50 dilution, gift of Joel Butterwick and Vanessa Ruta), and rabbit anti-Ir25a (1:50 dilution). Orco monoclonal antibody and Ir25a polyclonal antibody specificities were verified in *Ae. aegypti* by staining *orco* mutant and *Ir25a* mutant antennae, respectively (Figures 3E–3H). Antennae were washed for 30 min at least five times with 0.03% PBT, 1% DMSO at room temperature, and then washed overnight in the same solution. Antennae were then moved to secondary antibody (1:200) in 1X PBS, 1% DMSO, 5% normal goat serum, 0.03% Triton X-100 for 72 h at 4 °C. Secondary antibodies used were goat anti-mouse Alexa Fluor 488 (Thermo A-11001) and goat anti-rabbit Alexa Fluor 555 Plus (Thermo A32732). Antennae were washed for 30 min at least five times with 0.03% PBT, 1% DMSO at room temperature, and then washed overnight in the same solution. Antennae were rinsed in 1X PBS, rinsed three times in Slowfade Diamond (Thermo S36972), and mounted in Slowfade Diamond.

Whole mount antennal and maxillary palp RNA *in situ* hybridization

RNA was detected in whole mount antenna and maxillary palp using the hybridization chain reaction (HCR) technique as previously described (Choi et al., 2018) with modifications. Probes, amplifiers, Probe Hybridization Buffer, Amplification Buffer, and Probe Wash

Buffer were purchased from Molecular Instruments. Full list of probe lot numbers can be found in Data S1. 5-8 day-old Liverpool mosquitoes were anesthetized on wet ice, manually decapitated with forceps, and heads with antennae and the proboscis were digested in a chitinase-chymotrypsin solution (119 mM NaCl, 48 mM KCl, 2 mM $CaCl_2$, 2 mM $MgCl_2$, 25 mM HEPES, 5 U/mL chitinase (Sigma-Aldrich C6137-50UN), 100 U/mL alpha-chymotrypsin (Sigma-Aldrich CHY5S-10VL), 2% DMSO) (Manning and Doe, 2017) at 37°C for 30 min (antennae) or 1 h (maxillary palps) in a Fisher Isotemp oven and subsequently fixed in 4% paraformaldehyde, 1X PBS, 0.03% Triton X-100 on a rotator at 4°C overnight. Heads were washed 4 times on ice for 10 min each in 0.1% PBS-Tween-20. Antennae or maxillary palps were dissected in 0.1% PBS-Tween-20 on ice and dehydrated with a graded series of methanol/0.1% PBS-Tween: 25% methanol in 0.1% PBS-Tween-20 for 10 min on ice, 50% methanol in 0.1% PBS-Tween-20 for 10 min on ice, 75% methanol in 0.1% PBS-Tween-20 for 10 min on ice, and two washes of 100% methanol for 10 min on ice. Tissues were incubated overnight in 100% methanol at −20°C and were subsequently rehydrated with a series of graded methanol/0.1% PBS-Tween-20: 75% methanol in 0.1% PBS-Tween-20 for 10 min on ice, 50% methanol in 0.1% PBS-Tween-20 for 10 min on ice, 25% methanol in 0.1% PBS-Tween-20 for 10 min on ice, and two washes of 0.1% PBS-Tween-20 for 10 min each on ice. Tissue was digested in 20 μg/mL Proteinase K (Thermo Fisher AM2548) in 0.1% PBS-Tween for 30 min at room temperature and washed twice with 0.1% PBS-Tween-20 for 10 min each at room temperature. Tissue was fixed in 4% paraformaldehyde in 0.1% PBS-Tween-20 for 20 min at room temperature and washed 3 times for 10 min each in 0.1% PBS-Tween-20 at room temperature. Tissue was incubated in Probe Hybridization Buffer at room temperature for 5 min and then in 37°C pre-warmed Probe Hybridization Buffer rotating in a hybridization oven for 30 min 8 pmol of each probe set was prepared in 37°C pre-warmed Probe Hybridization Buffer and tissue was incubated in probe solution at 37°C in a hybridization oven for 2 nights. Tissues were washed in 37°C pre-warmed Probe Wash Buffer 5 times for 10 min each at 37°C. Tissues were washed twice in 5X SSC 0.1% Tween 20 at room temperature for 10 min each. Tissues were pre-amplified in room temperature Amplification Buffer for 10 min 18 pmol hairpins were separately prepared by heating 6 μL of 3 μM stock of hairpins H1 and H2 at 95°C for 90 s on an Eppendorf Mastercycler and allowing to cool to room temperature in a dark drawer for 30 min. Hairpins were resuspended in 100 μL amplification buffer and tissues were incubated in this hairpin solution in the dark on a rotator at room temperature overnight. Tissues were washed 5 times for 10 min each in 5X SSC 0.1% Tween 20 and mounted in SlowFade Diamond (Thermo Fisher S36972) on glass slides with coverslips for confocal imaging.

Whole mount antennal, maxillary palp, and proboscis dTomato visualization

7-14-day-old *Ir25a-QF2*, *Orco-QF2*, *Ir25a-QF2AD*, *Orco-QFDBD*, and *Ir25a-QF2AD Orco-QFDBD>15XQUAS-dTomato-T2A-GCaMP6s* mosquitoes were anesthetized on wet ice, manually decapitated with forceps and heads with antennae, proboscises, and maxillary palps were immediately fixed in 1 mL 4% paraformaldehyde, 1X PBS, 0.03% Triton X-100, on a rotator in the dark at 4°C overnight. Heads were washed 3 × 30 min each in 1X PBS, 0.03% Triton X-100 at room temperature, then antennae, proboscises, and maxillary palps were carefully removed and placed in 1X PBS, 0.03% Triton X-100. Next, antennae, proboscises, and maxillary palps were placed in a solution of 1X PBS, 0.03% Triton X-100, 1% DMSO, and a 1:400 dilution of TO-PRO-3 (Thermo Fisher T3605) for 24 h at 4°C in the dark. Antennae, proboscises, and maxillary palps were then washed 5 × 30 min each in 1X PBS, 0.03% Triton X-100 at room temperature in the dark, washed once with 1X PBS, transferred to a well of SlowFade diamond to remove excess PBS, and mounted in SlowFade Diamond for confocal imaging.

Antennal and maxillary palp confocal imaging and cell quantification

Images of peripheral tissues were acquired with a Zeiss Axio Observer Z1 Inverted LSM 880 NLO laser scanning confocal microscope (Zeiss) with a 25x/0.8 NA or 63x/1.4 NA immersion-corrected objective at a resolution of 3096× 3096 pixels or 2048 x 2048 pixels. When comparing dTomato fluorescence across genotypes, image acquisition parameters were kept consistent. When necessary, tiled images were stitched with 20% overlap. We note that all confocal imaging was conducted in a manner that would maximize our ability to visualize the presence or absence of each fluorophore and was not intended as a quantitative measure of fluorescence intensity. Confocal images were processed in ImageJ (NIH). Because the antenna is a cylindrical structure, when whole antennal segments are mounted on a slide and imaged on a confocal microscope, signal can be easily detected from the region closest to the coverslip and confocal objective, but signal is weaker when imaging the side further from the coverslip and objective. For the purposes of consistent quantification, we only quantified cell numbers from the region closest to the coverslip (red rectangle in Figure S3E). For quantifying expression in the maxillary palp, only the dorso-lateral region of the fourth maxillary palp segment was analyzed. (yellow rectangle in Figure S3F). Quantification of co-expression in antennae and maxillary palps was done in ImageJ (NIH) using the Cell Counter plugin. Cells in each channel were manually marked independently of the signal in the other channels. After cells in each channel are marked, and markers were then merged. Cells that were labeled with multiple markers (co-expressing cells) were then marked with a third marker (Figures S3G–S3L). Cell counts were then imported into Microsoft Excel and R for analysis.

Antenna dissection for snRNA-seq

Approximately 100–250 female $+/+^{LVP}$ mosquitoes aged 6–8 days post-eclosion were anesthetized on wet ice for 10 min. Mosquitoes were then placed in a 70 μm cell strainer (Falcon 08-771-1). The cell strainer containing the anesthetized mosquitoes was placed in a 60 mm Petri dish (Corning 430,166), and ice-cold molecular-grade 100% ethanol was gently poured into the cell strainer for 5 s. The cell strainer with ethanol-rinsed mosquitoes was then transferred to a new 60 mm Petri dish and ice-cold Schneider's Medium (Gibco

21,720,024) was poured into the cell strainer to rinse. Approximately 20 mL of ice-cold Schneider's medium was poured into a 100 mm Petri dish (Corning 430,293) on wet ice or reusable ice pack (Cooler Shock, mid-size freeze pack). Schneider's Medium-rinsed mosquitoes were transferred from the cell strainer to the 100 mm Petri dish. A new 70 μm cell strainer (pluriSelect 43–10070) with walls trimmed with a sterile razor blade to a height of 0.5–0.75 cm was placed into the same 100 mm Petri dish. The antennae were then removed using forceps and placed into the cell strainer. Antennae were rinsed approximately every 10 min by agitating the cell strainer and pipetting fresh ice-cold Schneider's Medium into the cell strainer. Dissection of each sample was limited to 90 min to ensure nuclei integrity, and when 90 min elapsed or all mosquitoes dissected, antennae were transferred into a DNA LoBind 1.5 mL tube (Eppendorf 022,431,021) pre-wet with Schneider's Medium. The cell strainer with antennae was inverted with forceps into the tube and approximately 300 μL ice-cold Schneider's Medium was pipetted into the cell strainer to release antennae into the Eppendorf tube. The sample was then flash-frozen in liquid nitrogen and stored at −70°C until ready for nuclei extraction. A total of approximately 750-1300 antennae were collected for each snRNA-seq batch, collected across four 90-min dissection sessions. Two batches of female antennae were processed for the snRNA-seq data presented in this paper. All tissue was collected at Rockefeller University. Batch 1 was processed at Rockefeller University (including nuclei extraction, 10X Genomics run, library preparation and sequencing), and Batch 2 was shipped on dry ice and processed at Baylor College of Medicine.

Batch 1 (Rockefeller antenna sample) nuclei extraction

Nuclei extraction of mosquito antennae was performed as previously described (McLaughlin et al., 2021) with modifications. Dissected antennae were thawed on wet ice, and all subsequent steps were performed on wet ice unless otherwise noted. Once samples were thawed, antennae were centrifuged in a benchtop microcentrifuge for 5–10 s, Schneider's Medium was removed and replaced with 100 μL of homogenization buffer (McLaughlin et al., 2021). Antennae from multiple dissection sessions were combined into a single DNA LoBind 1.5 mL tube using a low-retention repel polymer technology 200 μL filter tip (TipOne 11,821,830), with ~1 mm from the distal end trimmed using a sterilized and RNAse away-treated (Thermo Fisher 7000TS1) razor blade. With no more than 500 μL buffer present in the tube, tissue was ground for 30–60 s with a pellet pestle motor (Kimble 749,540-0000) and RNase-free pestle (Kimble 749,521-0590). The volume of buffer was brought up to 1000 μL with additional ice-cold homogenization buffer. Next, a 1 mL Dounce tissue grinder and pestle set (Wheaton 357,538) that had been autoclaved at 121°C for 4 h the previous day was pre-wetted with homogenization buffer. Using a low-retention (repel polymer technology) 1000 μL filter tip (TipOne 11,821,830), samples were transferred into the Dounce homogenizer. Nuclei were released by homogenizing with 20 strokes of the loose pestle, and 40 strokes of the tight pestle. Next, a low-retention 1000 μL tip was used to remove ~500 μL of the suspension. The suspension was filtered through a 40 μm Flowmi filter (Bel-Art H13680-0040) into a pre-wet 20 μm PluriStrainer (pluriSelect 43-10020-40) in a 1.5 mL LoBind Eppendorf tube. The second ~500 μL antennae nuclei suspension was then filtered the same way into the same Eppendorf tube. The suspension was then divided equally into two 1.5 mL LoBind Eppendorf tubes and centrifuged for 10 min at 500xG at 4°C. The supernatant was gently discarded without disturbing the pellet. Next, pellets were resuspended in 100 μL 1X PBS, 1% BSA, 10 μL/mL RNAse inhibitor (Roche RNAINH-RO) by pipetting 5 times with a low-retention 1000 μL tip, combined and pipetted to re-suspend and break up cell clumps 15 more times. The suspension was then filtered three times by running it through a Flowmi filter into a 10 μm strainer (pluriSelect 43-10010-40) in a 1.5 mL LoBind Eppendorf tube. To ensure nuclei were not clumping, 10 μL of the suspension was removed and stained with acridine orange and propidium iodide (Logos Biosystems, LGBD10012). The concentration of nuclei was determined by counting cells on a Luna FX7 automated cell counter (Logos Biosystems L70001).

Batch 1 (Rockefeller antenna sample): 10X Genomics, library preparation and sequencing

Single cell 3' expression Libraries were generated using Chromium Single Cell 3′ Library & Gel Bead kit Version 3.1 (10X Genomics PN1000269). Standard protocols from 10X Genomics were followed to generate the dual index libraries. Due to the small nucleus size (4–5 μm in diameter), 17 cycles were used for cDNA amplification and 13 cycles for index PCR. The quality and quantity of the libraries were assessed on Agilent TapeStation, the library was sequenced on Illumina NovaSeq 6000 sequencer using 100 cycle SP flowcell and 800 million paired reads were generated (read 1 = 28 bp, read 2 = 90 bp).

Batch 2 (Baylor antenna sample): Nuclei extraction

Nuclei extraction from mosquito antennae were performed as previously described (Li et al., 2022) with modifications. Fresh homogenization buffer (Li et al., 2022) was prepared and kept on ice. Samples were thawed from −80°C on wet ice, spun down in 100 μL Schneider's Medium using a bench top spinner, and as much medium as possible was discarded. Antennae from multiple dissection sessions were combined into a single 1.5 mL Eppendorf tube using a low-retention 200 μL filter tip (Rainin 30,389,240) with ~1 mm from the distal end trimmed using a sterilized and RNAse away-treated (Thermo Fisher 7000TS1) razor blade (VWR 10835-965) and 100 μL Homogenization buffer was added. The sample was ground with a pestle motor (Kimble 6HAZ6) for 30–60 s on wet ice. 900 μL homogenization buffer was added, and 1000 μL homogenized sample was transferred into the 1 mL Dounce tissue grinder set (Wheaton 357,538) that had been autoclaved at 200°C for >5 h or overnight a day in advance. Nuclei were released by 20 strokes with a loose Dounce pestle and 40 with a tight Dounce pestle on ice, taking care to avoid bubbles. 1000 μL of the sample was filtered through a 5 mL cell strainer (35 μm), and then filtered using 40 μm Flowmi (BelArt, H13680-0040) into 1.5 mL EP tube, centrifuged for 10 min at 1000xG at 4°C. The supernatant was discarded with care not to disturb the pellet. The nuclei were resuspended using 500 μL 1xPBS/0.5%BSA with RNase inhibitor (9.5 mL 1x PBS, 0.5 mL 10% BSA, 50 μL RNasin Plusby) pipetting at least 20 times

to completely re-suspend the nuclei. Sample were filtered using 40 μm Flowmi into a new 5 mL fluorescence-activated cell sorting (FACS) tube and kept on wet ice.

Batch 2 (Baylor antenna sample): FACS sorting, 10X genomics, library preparation, sequencing

FACS sorting was done using a BD FACSAria III Cell Sorter to collect nuclei (for FACS plots and gates, see Data S1). Nuclei were stained with Hoechst-33342 (1:1000; >5 min). Hoechst-positive nuclei were collected into 1.5 mL Eppendorf tube with 500 μL 1x PBS with 0.5% BSA as the receiving buffer (RNase inhibitor added). For each 10X Genomics run, all nuclei were collected. Approximately 15,000 nuclei were collected from the antennae. Nuclei were spun for 10 min at 1000XG at 4°C, and then resuspended using 43.2 μL 1x PBS with 0.5% BSA (RNase inhibitor added). Since the yield of nuclei was low, all nuclei were loaded onto a 10X Genomics controller. 10X Genomics sequencing libraries were prepared following the standard protocol from 10X Genomics 3′ v3.1 kit with following settings. All PCR reactions were performed using the Biorad C1000 Touch Thermal cycler with 96-Deep Well Reaction Module. 13 cycles were used for cDNA amplification and 16 cycles were used for sample index PCR. As per 10X Genomics protocol, 1:10 dilutions of amplified cDNA and final libraries were evaluated on Agilent 4200 TapeStation. Single-cell RNA libraries were sequenced on Illumina NovaSeq 6000 sequencer with minimum sequencing depth of 50,000 reads/cell using the read lengths 28bp Read1, 8bp i7 Index, 91bp Read2.

Maxillary palp dissection, nuclei extraction, FACS sorting, 10X genomics, library preparation, and sequencing

Maxillary palp dissections were conducted as described for the antenna. A total of 2,448 total maxillary palps were collected across fifteen 90-min dissection sessions at Rockefeller. These samples were shipped on dry ice and processed at Baylor College of Medicine. Nuclei extraction and FACS was performed at Baylor as described for the Batch 2 antenna sample with approximately 7,000 nuclei collected (for FACS plots and gates, see Data S1). 10X Genomics, library preparation, and sequencing was done as described above for the Batch 2 antenna sample.

snRNA-seq analysis: cell identification, ambient RNA removal, batch combination, and neuron classification

Alignment and initial cell identification: The *Ae. aegypti* genome (AaegL5.0, GCF_002204515.2 on NCBI) was indexed using Cell Ranger (version 6.0.2). FASTQ files generated from 10X Genomics 3′ gene expression libraries were mapped to the indexed genomes and gene counts in each cell were calculated by CellRanger (version 6.0.2). Intron signals were included by specifying the –include-introns parameter for cellranger count. From this point onward, data were further processed and analyzed using R and RStudio (R Core Team, 2021; R Studio Team, 2020).

Ambient RNA removal: DecontX from the Celda package (*antenna:* version 1.10.1, *maxillary palp:* 1.8.1) (Wang et al., 2021) was chosen for removing the ambient RNAs produced during nuclei preparation. Raw and filtered reads generated from Cell Ranger were compared by DecontX to obtain decontaminated reads (Figures S5A and S7A). The decontaminated reads were rounded by the R base:round function and the decontaminated matrices were generated by the DropletUtils package (version 1.14.2) (Griffiths et al., 2018).

Decontaminated expression matrices were loaded into the Seurat package (antenna: version 4.1.0, maxillary palp: 4.0.5) (Satija et al., 2015), filtering for cells with a minimum total features of 200 and genes expressed in a minimum of 3 cells for the maxillary palp, and 12 cells for the antenna (determined by evaluation of the distribution of cells per feature). Multiplets were identified by DoubletFinder (version 2.0.3) (McGinnis et al., 2019). The pK with maximum AUC was chosen for DoubletFinder. The multiplet numbers were estimated by the multiplet rate table on the 10X Genomics website. DoubletFinder-defined multiplets were excluded for the downstream analysis.

Cell filtering (antenna): Cells expressing a total number of features within the lowest 3% of each batch were excluded. As a further precaution against the inclusion of potential multiplets, we only included cells with the number of detective genes less than the median of gene number plus 3 median absolute deviations (MADs) for the analysis. Cells with more than 5% of mitochondrial transcripts were excluded (Figures S5C–S5E).

Cell filtering (maxillary palp): Cells with extreme gene numbers or abundant mitochondria transcripts were removed using Seurat (Satija et al., 2015). We excluded nuclei expressing fewer than 400 or greater than 4000 genes. Nuclei with more than 5% of mitochondrial transcripts were excluded. Genes expressed in fewer than 3 nuclei were removed (Figures S7B–S7D).

Normalization and dimensionality reduction (maxillary palp): Expression matrices of remaining nuclei were loaded into the Seurat package and processed by Seurat (version 4.0.5) (Satija et al., 2015). The analyses applied default parameters of Seurat unless specified. Expression matrices were normalized using NormalizeData() function. Highly variable genes were selected using FindVariableFeatures(). The data were scaled using the ScaleData() function with the vars.to.regress = c('nCount_RNA') parameter to regress out the effect of the total counts. The scaled data were dimensionally reduced using the RunPCA() function. t-distributed stochastic neighbor embedding (t-SNE) was used for visualizing the non-linear dimensionality reduction with 1–50 dimensions. Nuclei were clustered using the Louvain algorithm (Figure 6C).

Normalization, dimensionality reduction, merging and batch correction (antenna): With little previous explicit research on the detailed composition of the mosquito antenna and few known gene markers for mosquito cell types, analysis pipeline decisions on the remaining cells were weighed holistically by the following criteria: (1) interrogating the data for possible technical artifacts, and (2) how well putative chemosensory cell types separated, here defined as a group of cells expressing the same chemosensory

receptor gene or combination of receptor genes. Future research into cell populations in the antenna may uncover information on which to further ''ground-truth'' and refine this analysis pipeline.

Initially, we applied either LogNormalize() and SCTransform() to normalization our data for analysis. Log-normalized data appeared hampered significantly with low UMI gene counts frequently resulting in high normalization scores (data not shown). Additionally, our batches were sequenced at different depths, a technical factor which sctransform is designed to address (Hafemeister and Satija, 2019). Therefore, we applied sctransform for normalization, scaling, and identification of highly variable genes for downstream analysis. Sctransfrom-normalized data were dimensionally reduced using the RunPCA() function. t-distributed stochastic neighbor embedding (t-SNE) was used for visualizing the non-linear dimensionality reduction with 1–50 dimensions. Nuclei were clustered using the Louvain algorithm (Figures S5G and 6C).

We performed two independent snRNA-seq experiments on the antenna to collect a greater number of nuclei for our analysis. After filtering, the two batches were merged and renormalized. To correct principal component analysis (PCA) embeddings and remove the batch effects, we performed either harmony (version 0.1.0) (Korsunsky et al., 2019) or canonical correlation analysis (CCA) implemented in Seurat (Satija et al., 2015), also comparing the resulting clusters to the uncorrected data population (data not shown). The two batches of antenna snRNA-seq data were combined using merge(). For CCA-based integration, batches were split using and SplitObject() functions in Seurat. Split objects were normalized and selected for highly variable genes independently. 3,000 features used for the integration were selected by the SelectIntegrationFeatures() and PrepSCTIntegration() functions in Seurat. Two batches were then integrated using the FindIntegrationAnchors() and IntegrateData() functions. For harmony-based correction, batch-corrected dimensions were obtained using the RunHarmony() function. Batch-corrected samples using both methods were then analyzed following the procedures described in the previous section from scaling to clustering to identify cluster-specific genes. Harmony was selected as the batch-correction the final dataset and the generation of the final figures in this paper. Any subsequent clustering was done on Harmony-corrected PCs.

Neuron cluster identification: Cells were dimensionally reduced as described above and with a clustering resolution of 1. To classify cells as neurons, we first identified genes that are orthologous to the neuronal marker genes used in *D. melanogaster* using BLASTP. Four mosquito genes, LOC5565901, LOC5570204, LOC5564848, and LOC5570381, are orthologous to the *D. melanogaster* neural markers, *synaptotagmin 1* (*syt1*), *embryonic lethal abnormal vision* (*elav*), cadherin-N (*CadN*), and *bruchpilot* (*brp*), respectively. We saw that expression largely overlapped with the OSN co-receptors *Orco*, *Ir25a*, *Ir76b*, and *Ir8a*, consistent with the idea that these are neuronal markers. We defined neural clusters based on the expression of *syt1*, *elav*, *CadN*, and *brp*, and clusters expressing at least three neuronal markers in more than 50% of cells in the corresponding cluster were defined as neural clusters (Figures S5I, S7F, and S7G). The remaining cells were reprocessed using RunUMAP(), RunTSNE(), FindNeighbors() and FindClusters().

Neuron cluster identification (antenna): Before dimensionality reduction of the final neuron population, clusters 3 and 45 were also removed because in some iterations of the pipeline the central neural cluster they did not meet our criteria for classification as ''neurons''. In addition to low expression of neural markers and variable quality control metrics, it was ambiguous whether these were legitimate neural clusters (Figures S5G–S5I). For more data on clusters 3 and 45, see Data S1.

Cluster resolution testing (antenna neurons): FindClusters() was tested using the following resolutions: 0.8, 1.0, 1.2, 1.5, 1.7, 2.0, 2.5, 3.0, 3.2, 3.5, 3.7, 4.0. Between each resolution, cells were assessed for chemoreceptor expression changes in cluster assignment. Cluster separations were evaluated for ''validity'' using heatmaps for chemosensory receptor gene expression – essentially whether a cluster separation identified populations with distinct expression of chemosensory genes. For instance, cluster 3 at resolution 3.7 split at resolution 4.0 into cluster 40, primarily *Or44*-expressing cells and cluster 6, primarily non-*Or44* expressing cells in cluster 6. Some mutually exclusive receptors could not be separated by high clustering resolution, such as asterisk-marked clusters in Figure 4D, in addition to Figures S5L and S5M), indicating that sometimes cluster categorization was driven by general transcriptome characteristics and not solely by chemoreceptor expression. Bulked over the neuron population, 185 chemoreceptor genes had SCT-corrected UMI counts of 2 or above (Figure S5F; full plot in Data S1). 121 were identified as highly variable genes by sctransform when normalized after batch merging. If the remaining 64 chemoreceptors were appended to the highly variable gene list, and principal components re-run, it did not a noticeable difference for cluster identities (data not shown).

Expression criteria (antenna): Neural clusters were then examined for ligand-selective receptor and co-receptor expression. For ligand-selective receptors, we define ''expression'' of a gene within a cell as being expressed above a sctransform normalized expression value of 1 (Figure S6A). Because sctransform performs via adjusting UMI values, this also corresponds to an adjusted UMI value of 2 or above. We define ''co-expression'' as genes that meet this criteria in 10 or more cells within our identified neuron population. The chord plots compare the sctransform-adjusted UMIs (Figure 4E) and non-adjusted UMIs (Figure S5J), with the same but fewer chords appearing in the sctransform chord plot.

Co-receptors *Ir25a*, *Ir76b*, *Ir8a* have similar overall expression levels in the tissue with other highly expressed ligand-selective receptors, so we applied the same criteria for these co-receptors (Figures S5F and S6). *Orco*, conversely, is expressed overall at an order of magnitude higher than other chemoreceptors, likely why it leads to the contamination of other cells, including non-neurons (Figure S5A). Therefore, for *Orco* we raised the definition of ''expression'' to a normalized expression value of 2, corresponding to an sctransform-adjusted UMI value of 6.

Determination of minimum number of chemosensory cell types in antenna: Within our chemosensory neuron population, we define ''cell type'' as a population of neurons expressing the same chemosensory receptors. By examining cluster chemoreceptor

expression, we determined that there are at least 35 chemosensory cell types in the antenna. Clusters with high levels of LOC5575210, a gene orthologous to *D. melanogaster* gene *no mechanoreceptor potential C* (*nompC*), were excluded. High cluster resolution was needed to separate some clusters containing mutually exclusive chemoreceptor expression (see cluster resolution testing above). However sometimes cells with the same chemoreceptor expression were also separated by clustering, resulting in ''duplicate'' clusters, although there may be differences in expression of these clusters for expression of other genes (clusters 4 and 22, clusters 13 and 18, clusters 12 and 41, cluster 9 and 5). Cluster 26 has no apparent ligand-specific chemoreceptor expression (Figure 4D and S6A). We arrived at the total number of cell types according to this scheme: (42 total clusters) - (2 clusters with *nompC*) - (1 cluster with no apparent ligand-specific chemoreceptor expression) - (4 ''duplicate'' clusters) = 35 chemosensory cell types. Figure S6A also illustrates these chemoreceptor expression-defined cell types. 35 is a conservative estimate of chemoreceptor cell types since there are instances of multiple populations of chemosensory cell types co-clusters such as the ligand-specific IR cells in cluster 0 (Figures S5L and S5M). In addition, transcript ''drop outs'' make it difficult to determine if cells within a cluster that have low or sparse expression of a given gene mean that there are additional heterogeneity along distinct subtypes of these lower expressed chemoreceptors, or this is a result of sampling limitation of snRNAseq. Based on this, we believe that there are more than 35 cell types.

Antenna cell marker heatmap (on total cell population): The heatmap in Figure 4B was generated using normalized expression values and the ComplexHeatmap package in R (R Core Team, 2021). Epithelia-, glia-, and neuron-enriched genes in the *D. melanogaster* antenna were considered as references of the corresponding marker genes in *Ae. aegypti*. Mosquito genes LOC5564305, LOC5570152, LOC5576812 were used as markers for epithelia cell clusters and are orthologolous respectively *to D. melanogaster* genes *grainy head* (*grh*), *farkas* (*far*), *pyrokinin 1 receptor* (*pk1-r*). Mosquito genes LOC110678282, LOC110678282, LOC110676862, were used as markers for putative glial cell clusters and are orthologus respectively for *reversed polarity* (*repo*, LOC110678282), *viking* (*vkg*, LOC110678282), *aristaless* (*al*, LOC110676862), were used for glial cell clusters. Neural cell markers *syt1*, *elav*, *CadN*, and *brp*, were used as listed above with the addition of LOC5567355, an orthologue to *paralytic* (*para*).

Antenna tSNE plot: To generate tSNE plots in Figure S5G of all antennal nuclei and Figure 4C of antennal neurons, expression matrices were first normalized, selected for highly variable genes, and scaled using sctransform. Scaled data were applied to the RunTSNE() with 1–50 dimensions. All antenna nuclei and antennal neurons were clustered using the Louvain algorithm with resolutions 1 and 4 respectively.

Antenna dot plot: The dot plot of cluster-enriched chemosensory receptors in Figure 4D was based on the DotPlot() function in Seurat (Satija et al., 2015) and customized using the ggplot2 package (Wickham, 2016). The scaled mean normalized expression and expression percentage of each chemosensory receptor was calculated by the DotPlot() function. The hclust() function was used to cluster genes.

Asterisk-marked clusters: Co-clustering of different cell types within a cluster was marked to indicate that apparent co-expression of chemoreceptors within a cluster is not always indicative of co-expression within individual cells. Inversely a cluster with no apparent chemoreceptor expression may have some cells that express chemoreceptors at low levels. We determined that when cells that exhibited co-clustering but expressed different chemoreceptor cell types were mutually exclusive cell types according to cells' highest expressed receptor within the cluster. For example see clusters 0 and 3 (Figures S5L and S5M). Co-clustering for asterisks-marked clusters can also be observed by looking at clusters in Figure S7A. For cluster heatmaps, see Data S1.

Triangle-marked clusters: Lower or more sparsely expressed chemoreceptors that are co-expressed on a cluster-level or when we looked at the scaled average expression but do not explicitly pass our stated threshold for co-expression are marked with a triangle. These also do not appear in the chord plot in Figure 4E, which depicts only the co-expression relationships that clear our threshold. We used scaled average expression for the dot plot as a means of investigating expression of these chemoreceptors. For instance, *Ir41m* does not meet our co-expression with *Ir41L*. *Ir41m*'s specific expression in cluster 38 appears high on a scaled (*Z* score) of average expression because *Ir41m* has specific expression to cluster 38 (see Figures 4F and S6A). These genes provide important context for other highly expressed genes (e.g., that in cluster 38, *Ir93a* may not be expressed as a singular ligand-specific chemoreceptor, but co-expressed with other genes, potentially *Ir21a*). For this reason, we did not omit these genes from the dot plot.

Antenna chord plot: The chord plot of co-expressed chemosensory receptor in Figures 4E and S5J was generated using the chorddiag package in R (R Core Team, 2021). A list of 184 receptor genes was generated from the matrix data and co-receptors *Orco*, *Ir25a*, *Ir76b* and *Ir8a* were excluded. Receptors that express UMI at 2 or above were considered as positively expressed. Each expressed chemosensory receptor was iteratively compared to the expression of the remaining chemosensory receptors in the corresponding nuclei. If more than 10 nuclei expressed two chemosensory receptors simultaneously, these two receptors were considered as co-expressed chemosensory receptors and visualized using the chorddiag package. Figure 4E uses sctransform-adjusted UMI values, and Figure S5J uses UMI values from the RNA assay in the final Seurat object.

Antenna chemoreceptor scatterplot: The count scatterplot in Figure S5F was generated by summing the counts across all cells within each batch for each chemosensory receptor. The sum counts were plotted using the geom_point() function of the ggplot2 package in R (R Core Team, 2021; Wickham, 2016).

Antenna chemoreceptor expression heatmaps: The heatmaps in Figures 4F, S6A, and S5L–S5P were generating using the DoHeatmap() function on sctransform-normalized expression data. Cells were filtered by either subsetting by cluster identity or for normalized expression of a given gene. Clusters are ordered by co-receptor expression, chemoreceptor genes are ordered by

cluster expression. In Figures S5L and S5M, cells are dimensionally reduced and clusters re-assigned at a resolution of 4 to visualize cell gene expression similarities within a cluster. LOC5575210 expression (ortholog of *D. melanogaster nompC*) is likely to not be expressed in chemosensory cells but expressed in the neural population at a similar level to other highly expressed chemoreceptor genes (Figure S6A; Data S1), thus is included as a non-quantitative demonstration of potential background noise.

Antenna violin plots: Gene expression feature plots were made using the command VlnPlot() on normalized expression values.

Maxillary palp: tSNE, heatmap, chord plot, dot plot, expression feature plot

The tSNE of maxillary palp nuclei in Figure 6C was generated similarly to the antenna tSNE, with cluster resolution adjusted to 2.5. The heatmap of all maxillary palp nuclei in Figures 6B and 6D was plotted as described for the antenna heatmap. The dot plot of all maxillary palp abundant receptors in Figure S7O was plotted as described for the antenna heatmap. The maxillary palp chord plot in Figure 6E was processed similarly to the antenna one. Maxillary palp gene expression feature plots were made using the command FeaturePlot() on normalized expression values.

Maxillary palp scatterplot: The co-expression scatterplot in Figures S7M and S7N was based on the normalization expression from each single nuclei for a pair of chemosensory receptors. The normalization values were plotted using the geom_point() function of the ggplot2 package in R (R Core Team, 2021; Wickham, 2016).

Mosquito preparation for single-sensillum recordings

Female mosquitoes from two wild-type and three mutant strains ($+/+^{ORL}$, $+/+^{LVP}$, $Ir25a^{BamHI/BamHI}$, $Gr3^{4/4}$ and $Orco^{16/16}$) five to seven days post-emergence, were anesthetized on wet ice for 1–2 min. An individual mosquito was then glued onto a piece of double-sided sticky tape on a microscope slide (76 × 26 mm) and secured by a piece of tape covering the thorax and abdomen. The maxillary palps were immobilized using a short segment of human hair placed over the basal part of the maxillary palps. The sensilla of the maxillary palps were subsequently visualized using an Olympus light microscope (BX51WI; LRI Instrument AB, Lund, Sweden) at 750×. A continuous humidified stream of synthetic air (Strandmöllen AB, Ljungby, Sweden) was passed over the maxillary palp (2 L min^{-1}) via a glass tube (7 mm i.d.), terminating 10 mm from the maxillary palps, to avoid desiccation.

Single-sensillum recordings from maxillary palp capitate peg sensilla

Electrophysiological recordings from capitate peg sensilla were made and analyzed according to previously described protocols (Ghaninia et al., 2019; Majeed et al., 2016). In brief, two tungsten microelectrodes, electrolytically sharpened in 10% KNO_2 solution, were used as reference and recording electrodes. The reference electrode was inserted into the eye and the recording electrode was positioned at the base or shaft of the sensillum using a piezo motorized micromanipulator (Märzhäuser Wetzlar GmbH & Co. KG, Wetzlar Germany) until electrical contact was established. Extracellular signals from the OSNs housed in the capitate peg sensilla were amplified and recorded using a high-impedance probe (universal single ended probe) and a USB-acquisition controller (IDAC-4) (Ockenfels Syntech GmbH, Buchenbach, Germany). Extracellular spikes were differentiated based on amplitude as A, B, and C, according to standard nomenclature (Ghaninia et al., 2019; Majeed et al., 2016), and manually counted using Autospike 3.7 (Ockenfels Syntech GmbH). The response to odorant stimuli were analyzed by subtracting the number of spikes 0.5 s post-stimulus from the number of spikes 0.5 s pre-stimulus, and the outcome was multiplied by two to obtain a spike/sec measurement. In cases where the neuronal response was high enough to result in pinching of the spike train (>150 spikes/sec), the number of spikes post-stimulus were counted for the first 100 ms and then multiplied by 5, as the inter-spike frequency is constant once the neuron is activated maximally. Neurons were classified as responders or non-responders based upon whether their odorant response was above or below a 30 spikes/sec threshold, respectively.

Odorant stimulus delivery for single-sensillum recordings

Odorants used in Figure 7 were selected for the highest purity available (>98%): R-(−)-1-octen-3-ol (PubChem CID: 6992244, Penta Manufacturing 15–18900); acetone (PubChem CID: 180 Sigma A4206); hexyl amine (PubChem CID: 8102, Sigma 219,703); triethyl amine (PubChem CID: 1146, Sigma T0886). All odorants were diluted into a large stock solution that was used throughout each entire experiment to avoid variability in concentrations. Serial decadic dilutions of acetone, hexyl amine, and triethyl amine were made in MilliQ ultrapure water (18 MΩ resistance) and 1-octen-3-ol was diluted in paraffin oil (EMD Millipore #PX0045-3). Aliquots of 10 μL of each compound and dilution was pipetted onto a piece of filter paper (5 × 20 mm) placed inside a Pasteur pipette. Similar volumes of MilliQ ultrapure water and paraffin oil were used as controls. Stimulus cartridges were used within 5 min after loading, and only used once. For dose-response analysis using CO_2, gas cylinders containing metered amounts of CO_2 (300, 600, 1200, 4800 ppm) and oxygen (20%), balanced by nitrogen (Strandmöllen AB, Ljungby, Sweden) were used as previously described (Ghaninia et al., 2019). Odorants were introduced by passing a 0.5 s air puff through the Pasteur pipette using a stimulus controller (Ockenfels Syntech GmbH) into the airstream passing over the maxillary palps through a hole in the glass tube, 10 cm upstream from the preparation.

QUANTIFICATION AND STATISTICAL ANALYSIS

All statistical analyses were performed using Prism (GraphPad), Excel (Microsoft) or R version 3.6.3 (R Core Team, 2021). Data are shown as mean ± SEM unless otherwise noted. Details of statistical methods are reported in the figure legends.

CellPress
OPEN ACCESS

Supplemental figures

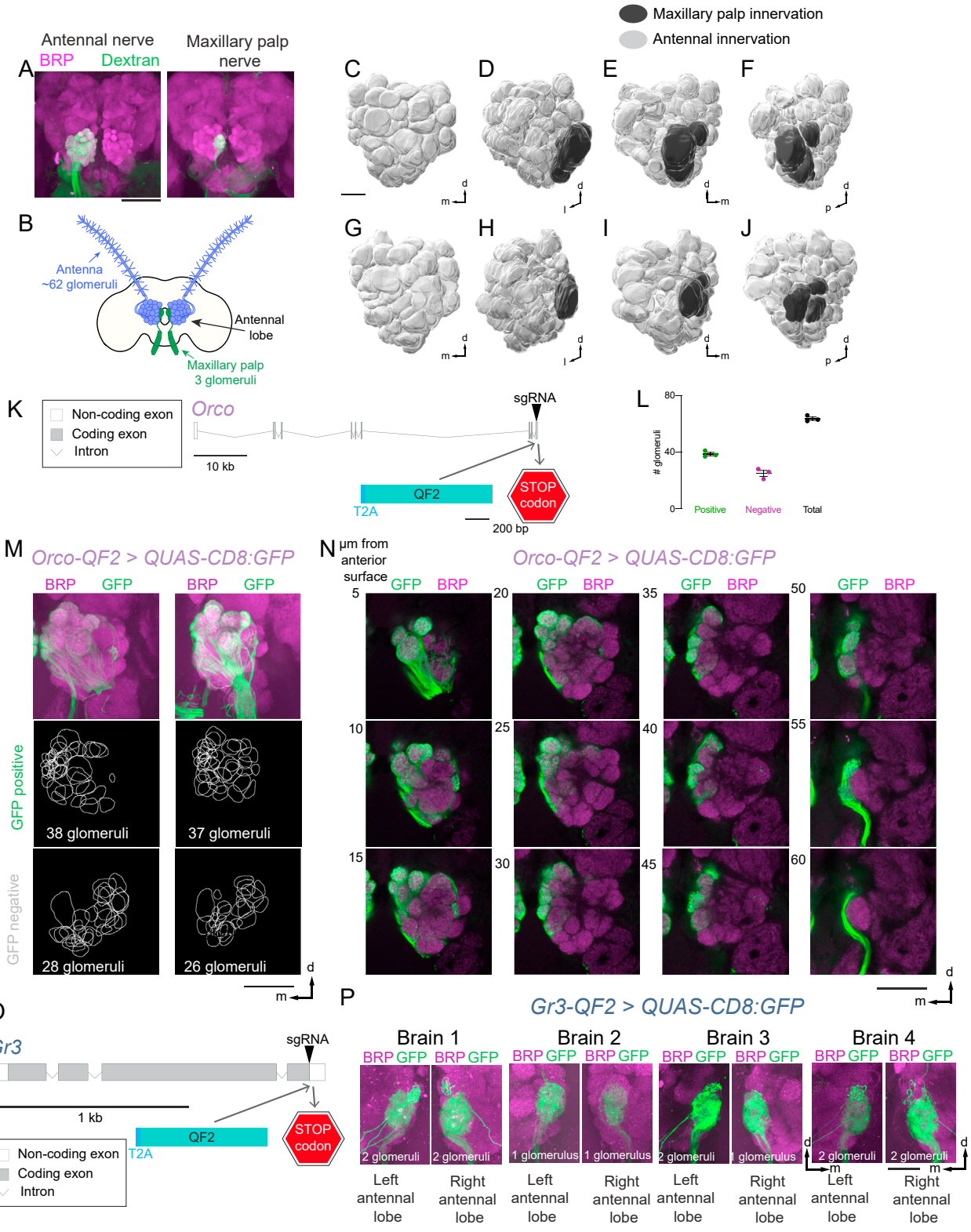

(legend on next page)

Figure S1. Organization of *Ae. aegypti* antennal lobe glomeruli and projections of *Orco-QF2*-expressing neurons and *Gr3-QF2*-expressing neurons, related to Figure 1

(A) Maximum-intensity projections of confocal z stacks of a brain after anterograde dye fill of a single ipsilateral antenna (left) or ipsilateral maxillary palp (right) using a dextran-conjugated fluorophore (green) with immunofluorescent labeling of Brp (synaptic marker, magenta).

(B) Approximate number of antennal lobe glomeruli per brain hemisphere innervated by the indicated sensory structure, derived from quantification of the left antennal lobe in 12 brains presented in Figures 1I–1J, S2, S3, S4, and S5.

(C–J) 3D reconstruction of a single left antennal lobe with 61 (D–G) or 66 (H–K) glomeruli shown at 4 different angles. Glomeruli are colored according to innervation by the indicated sensory appendage.

(K) *Orco* locus with exons (gray boxes), introns (gray lines) and CRISPR-Cas9 gRNA site (arrowhead) used to insert T2A-QF2 (light blue).

(L) Quantification of the number of glomeruli that are GFP positive (green), GFP negative (magenta), and total number of glomeruli (black). Analysis based on brains in (M) and Figures 1I and 1J.

(M) Maximum-intensity projections of confocal z stacks of left antennal lobes from two different brains of the indicated genotype with immunofluorescent labeling of GFP (green) and Brp (synaptic marker, magenta) (top) and 2D representation of the boundary of each glomerulus that is GFP positive and GFP negative (bottom).

(N) Single confocal sections taken from the maximum-intensity projection confocal z stack of the left antennal lobe shown in Figure 1I with immunofluorescent labeling of GFP (green) and Brp (synaptic marker, magenta). A single plane is shown every 5 μm in Z to capture each glomerulus.

(O) *Gr3* locus with exons (gray boxes), introns (gray lines) and CRISPR-Cas9 gRNA site (arrowhead) used to insert T2A-QF2 (light blue).

(P) Maximum-intensity projection confocal z stack through the medial antennal lobes of 4 brains with immunofluorescent labeling of GFP (green) and Brp (synaptic marker, magenta).

Panel (F) is reprinted in Figure 5D. Scale bars: 50 μm (A, M, and N), 20 μm (C–J), 25 μm (P). Orientation: d = dorsal, m = medial, p = posterior.

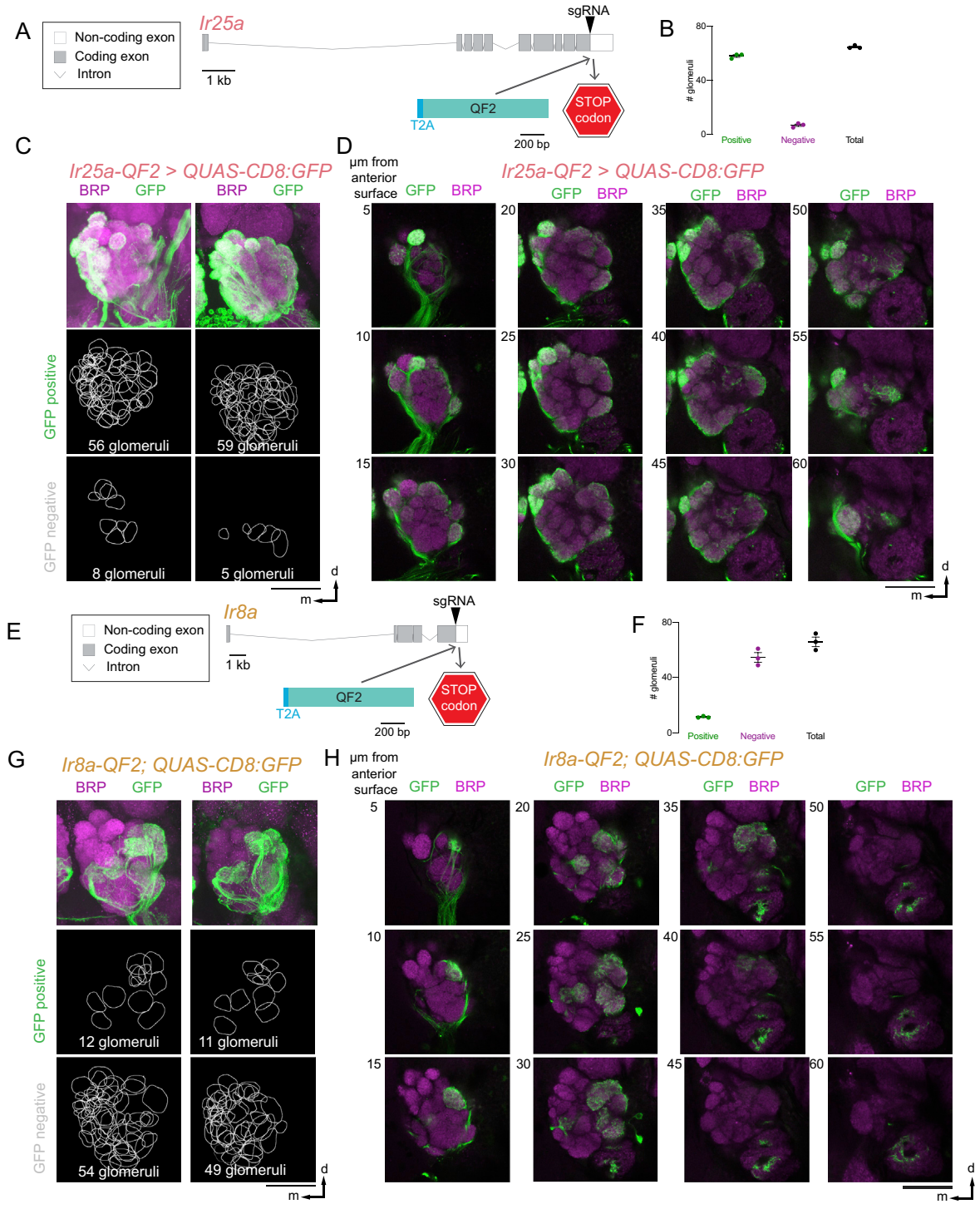

Figure S2. Projections of *Ir25a-QF2*-expressing neurons and *Ir8a-QF2*-expressing neurons in the antennal lobe, related to Figure 1

(A) *Ir25a* locus with exons (gray boxes), introns (gray lines) and CRISPR-Cas9 gRNA site (arrowhead) used to insert T2A-QF2 (light blue).

(B) Quantification of the number of glomeruli that are GFP positive (green), GFP negative (magenta), and total number of glomeruli (black). Analysis based on brains in (C and D) and Figures 1I and 1J.

(C) Maximum-intensity projections of confocal z stacks of left antennal lobes from two different brains of the indicated genotype with immunofluorescent labeling of GFP (green) and Brp (synaptic marker, magenta) (top) and 2D representation of the boundary of each glomerulus that is GFP positive and GFP negative (bottom).

(legend continued on next page)

(D) Single confocal sections taken from the maximum-intensity projection confocal z stack of the left antennal lobe shown in Figure 1I with immunofluorescent labeling of GFP (green) and Brp (synaptic marker, magenta). A single plane is shown every 5 μm in Z to capture each glomerulus.
(E) *Ir8a* locus with exons (gray boxes), introns (gray lines) and CRISPR-Cas9 gRNA site (arrowhead) used to insert T2A-QF2 (light blue).
(F) Quantification of the number of glomeruli that are GFP positive (green), GFP negative (magenta), and total number of glomeruli (black). Analysis based on brains in (C and D) and Figures 1I and 1J.
(G) Maximum-intensity projections of confocal z stacks of left antennal lobes from two different brains of the indicated genotype with immunofluorescent labeling of GFP (green) and Brp (synaptic marker, magenta) (top) and 2D representation of the boundary of each glomerulus that is GFP positive and GFP negative (bottom).
(H) Single confocal sections taken from the maximum-intensity projection confocal z stack of the left antennal lobe shown in Figure 1I with immunofluorescent labeling of GFP (green) and Brp (synaptic marker, magenta). A single plane is shown every 5 μm in Z to capture each glomerulus.
Scale bar (C, D, G, and H): 50 μm. Orientation: d = dorsal, m = medial.

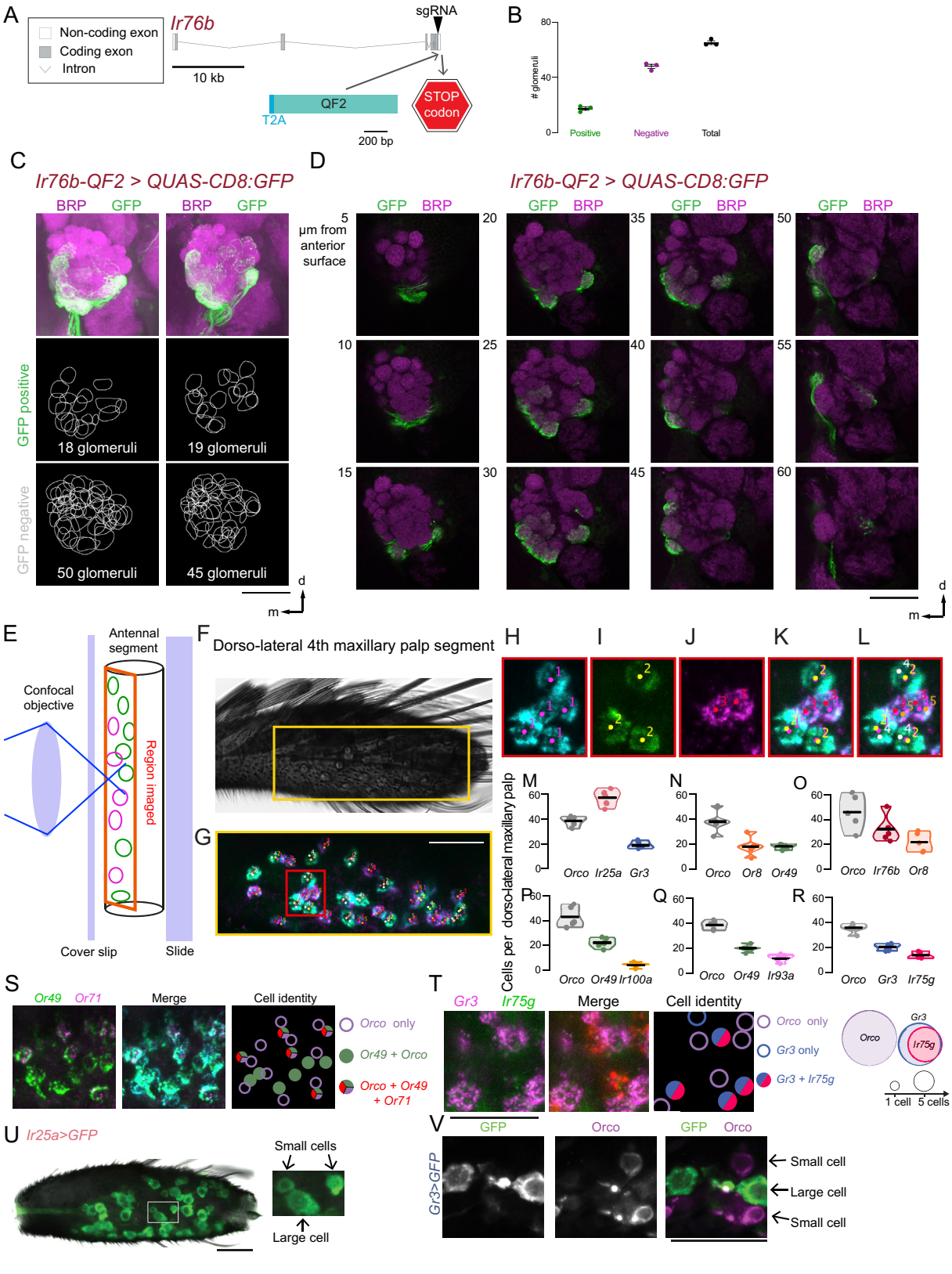

(legend on next page)

Figure S3. Projections of *Ir76b-QF2*-expressing neurons in the antennal lobe and quantification of maxillary palp cell populations, related to Figures 1 and 5

(A) *Ir76b* locus with exons (gray boxes), introns (gray lines) and CRISPR-Cas9 gRNA site (arrowhead) used to insert T2A-QF2 (light blue).

(B) Quantification of the number of glomeruli that are GFP positive (green), GFP negative (magenta), and total number of glomeruli (black). Analysis based on brains in (C and D) and Figures 1I and 1J.

(C) Maximum-intensity projections of confocal z stacks of left antennal lobes from two different brains of the indicated genotype with immunofluorescent labeling of GFP (green) and Brp (synaptic marker, magenta) (top) and 2D representation of the boundary of each glomerulus that is GFP positive and GFP negative (bottom).

(D) Single confocal sections taken from the maximum-intensity projection confocal z stack of the left antennal lobe shown in Figure 1I with immunofluorescent labeling of GFP (green) and Brp (synaptic marker, magenta). A single plane is shown every 5 μm in Z to capture each glomerulus.

(E–L) Workflow for cell quantification. Schematic of antennal region imaged on a confocal microscope (E) and image of maxillary palp with imaged area indicated with the yellow square (F). Whole-mount maxillary palp RNA *in situ* hybridization, yellow region from (F). Cells are manually marked independently as *Orco*+, *Or49*+, or *Or8*+ (red inset from G) using FIJI Cell Counter (Schindelin et al., 2012) (H–J) and markers from each channel are merged (G). Cells with markers 1 and 2 are then scored as *Orco* + *Or49*+ with marker 4, and cells with markers 1 and 3 are then scored as *Orco* + *Or8*+ with marker 5 (L). Counts from each marker for each image are exported into Excel and R for further analysis.

(M–R) Total cell counts from whole mount maxillary palp RNA *in situ* hybridization in Figure 5. Mean with range, n = 5.

(S and T) RNA *in situ* hybridization of whole-mount maxillary palp with the indicated probe and cell identity schematic.

(U and V) Whole-mount maxillary palp immunofluorescence showing *Ir25a* expression in "small" and "large" cells (Q) and *Gr3* expression in "large" cells and Orco protein in "small" cells (R).

Scale bars: 50 μm (C, D, G, and U), 25 μm (H–L, S, T, and V) Orientation: d = dorsal, m = medial. Orientation (B, P): proximal left.

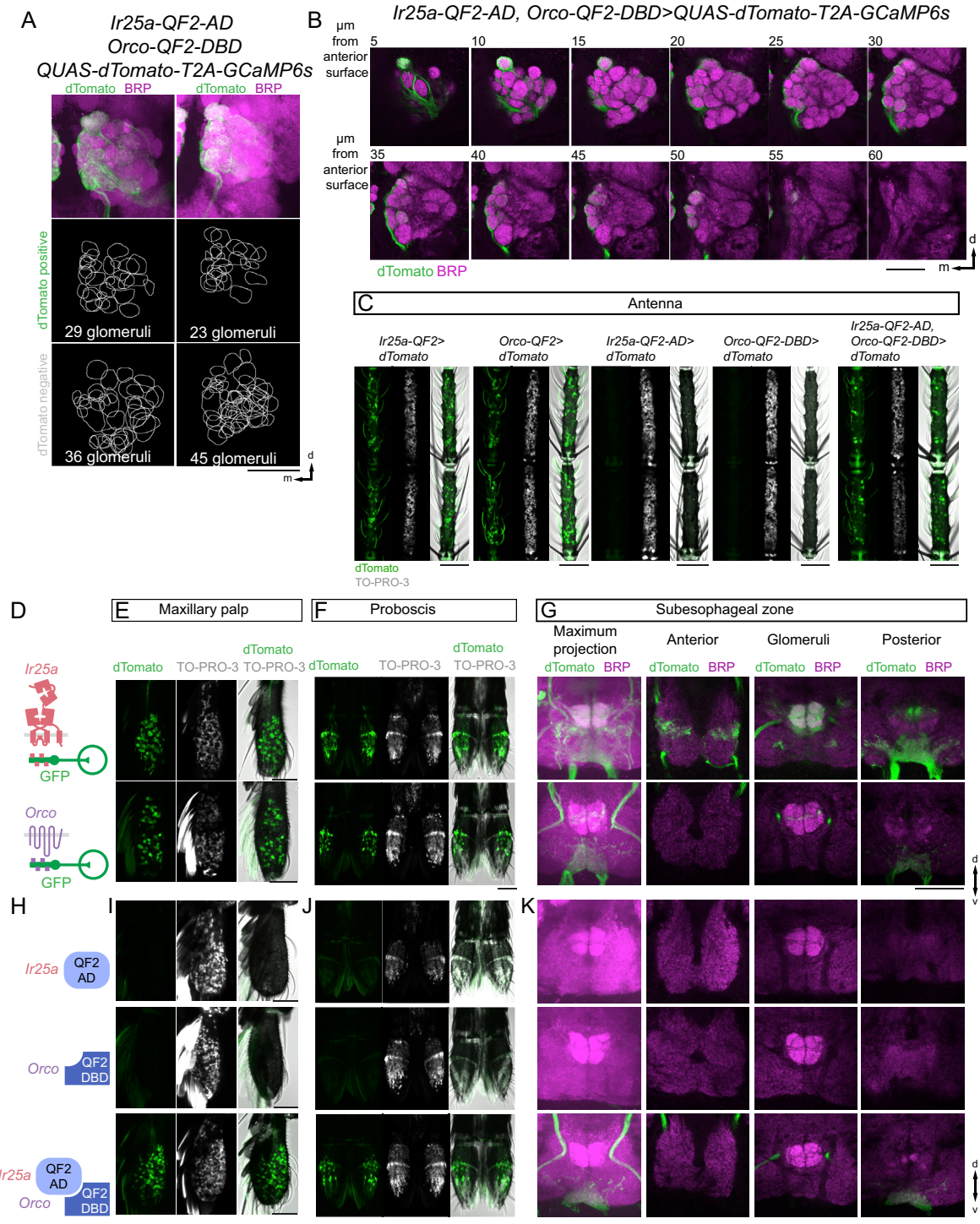

Figure S4. Specificity of Split-QF2 reagents and co-expression in the mosquito taste system, related to Figure 2

(A) Maximum-intensity projections of confocal z stacks of left antennal lobes from two different brains of the indicated genotype with immunofluorescent labeling of dTomato (green) and Brp (synaptic marker, magenta) (top) and 2D representation of the boundary of each glomerulus that is GFP positive and GFP negative (bottom).

(B) Single confocal sections taken from the maximum-intensity projection confocal z stack of the left antennal lobe shown in Figure 2G with immunofluorescent labeling of dTomato (green) and Brp (synaptic marker, magenta). A single plane is shown every 5 µm in Z to capture each glomerulus.

(C–K) Maximum-intensity projections of confocal z stacks of antennae (C), maxillary palps (E and I), and proboscis (F and J) of the indicated genotypes (D and H), showing intrinsic dTomato fluorescence and stained with the nuclear dye TO-PRO-3, with transmitted light overlay.

(legend continued on next page)

(G and K) Left panel, maximum-intensity projections of confocal z stacks of suboesophageal zone from the indicated genotypes with immunofluorescent labeling of dTomato (green) and Brp (synaptic marker, magenta). Right three panels, single confocal sections through indicated areas of the subesophageal zone.
Orientation: proximal up (C, E, and F); d = dorsal, v = ventral, m = medial. Scale bars: 50 μm.

CellPress
OPEN ACCESS

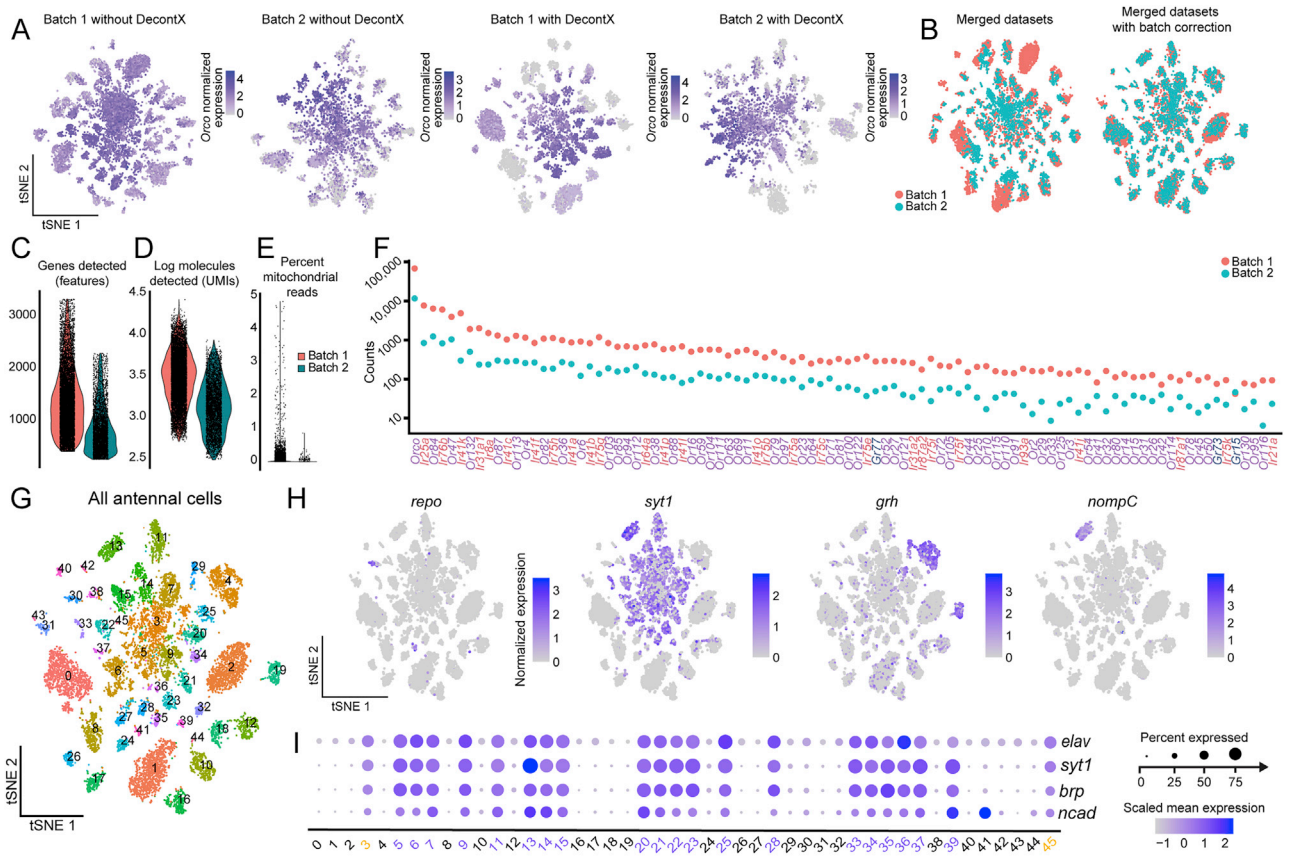

(legend on next page)

Figure S5. Antennal snRNA-seq pipeline and chemoreceptor expression analysis, related to Figure 4

(A) Ambient RNA removal using DecontX was used independently on data from snRNA-seq experiments processed at Rockefeller (Batch 1) and Baylor (Batch 2), illustrated using normalized expression of *Orco* mapped onto t-distributed stochastic neighbor embedding (t-SNE) plots [unit for normalized expression in antenna data is ln(sctransform-adjusted UMI), see STAR Methods].

(B) Independently collected snRNA-seq experiments were merged and batch effects reduced using Harmony.

(C–E) Batch properties and distributions after quality control filtering (see STAR Methods).

(F) Scatterplot of summed counts of chemoreceptor genes within all identified neural cells within each batch. 93 out of 191 chemoreceptor genes with the highest counts shown for space.

(G) Antennal cell clusters after batch effect reduction, visualized using t-SNE.

(H) Normalized expression mapped onto t-SNE plots for *syt1* as a marker for neurons, *nompC* for mechanosensory cells, *repo* for glial cells, and *grh* for epithelial cells.

(I) Dot plot illustrating mean scaled expression (*Z* score) of neural markers used to identify neuron clusters. Clusters were identified as neurons if over 50% of cells within a cluster expressed 3 out of 4 neural markers (*elav*, *syt1*, *brp*, *ncad*). Identified neuron clusters are labeled in purple. Clusters 3 and 45 (labeled in orange) were classified as ambiguous and excluded (see STAR Methods).

(J) Chord plot of co-expressed pairs of chemosensory receptors using RNA counts where both genes are above a normalized expression value of 1 in over 10 cells (for sctransform-adjusted UMIs, see Figure 4E).

(K) Venn diagram depicting percent of neurons co-expressing different combinations of co-receptors according to normalized expression [ln(sctransform-adjusted UMI)]. Threshold for *Orco* is a normalized expression value of 2, threshold for *Ir25a, Ir76b, Ir8a* is a normalized expression value of 1.

(L and M) Heatmaps of all cells in (L) cluster 3 and (M) cluster 0, indicating co-clustering of cells with unique expression of chemoreceptors. Receptors are indicated in rows and cells in columns. Heatmap colors represent normalized expression. Cells are ordered using unsupervised clustering to visualize gene expression similarities of cell subclusters. Receptors are ordered by expression within subclusters.

(N–P) Heatmaps of all cells within neuron population expressing (N) *Or36*, (O) *Or47*, or (P) *Or84* above a normalized expression value of 1. Receptors are indicated in rows, and cells in columns. Cluster assignment of cells indicated above heatmap. "Others" denotes small groups of cells belonging to other clusters apart from the ones labeled. *nompC* is included for non-quantitative reference of potential background signal. Heatmap colors represent normalized expression.

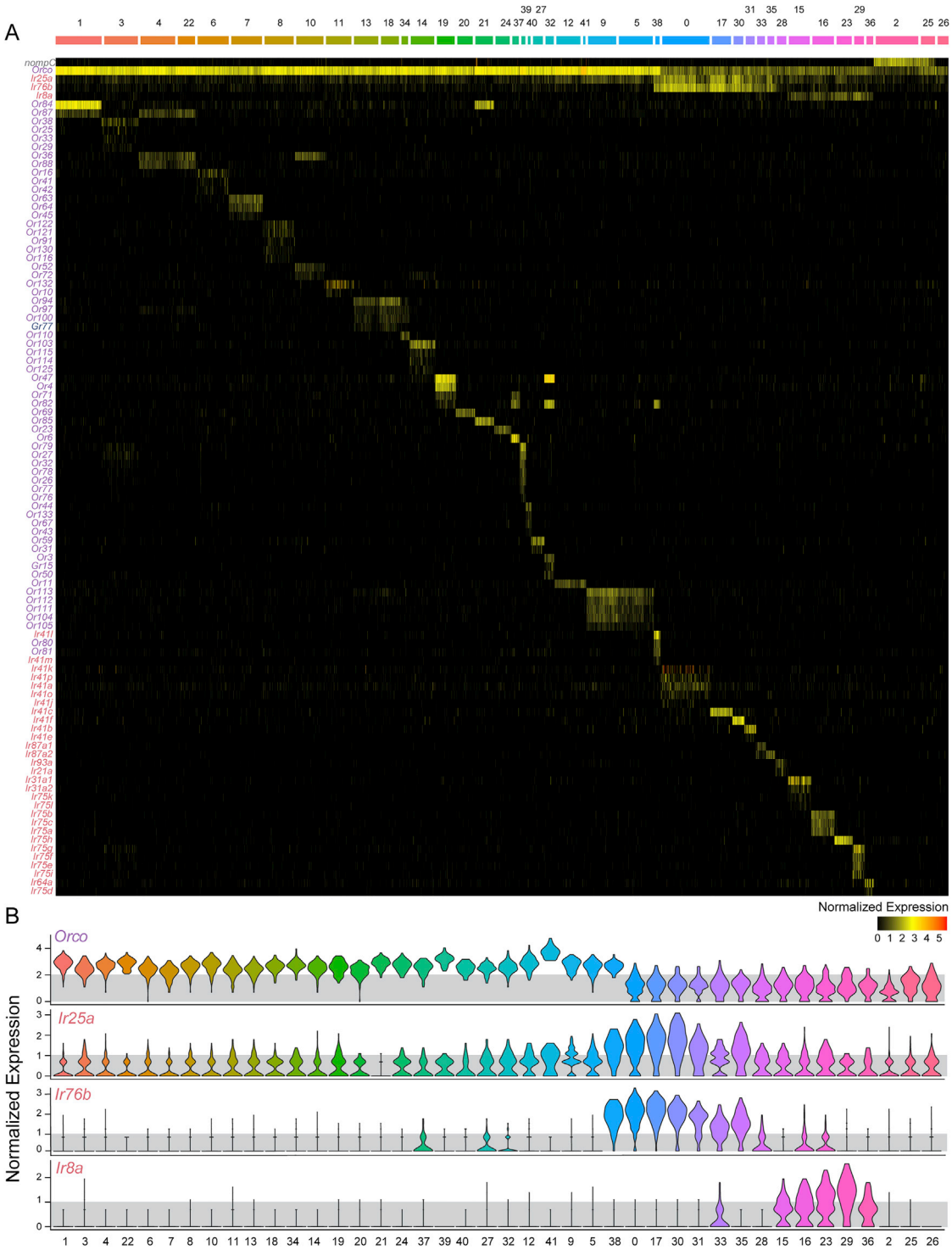

Figure S6. Antennal snRNA-seq cluster chemosensory receptor expression analysis and co-receptor analysis, related to Figure 4

(A) Heatmaps of all identified neurons. Receptors are indicated in rows, and cells in columns. Cluster assignment of cells indicated above heatmap. Clusters are ordered by co-receptor expression, chemoreceptor genes are ordered by cluster expression. Heatmap colors represent normalized expression [unit is ln(sctransform-adjusted UMI)].

(B) Violin plots illustrating distribution of normalized expression of indicated co-receptor within individual cells within each cluster. Cluster labels at the bottom of panel apply to each violin plot vertically above it.

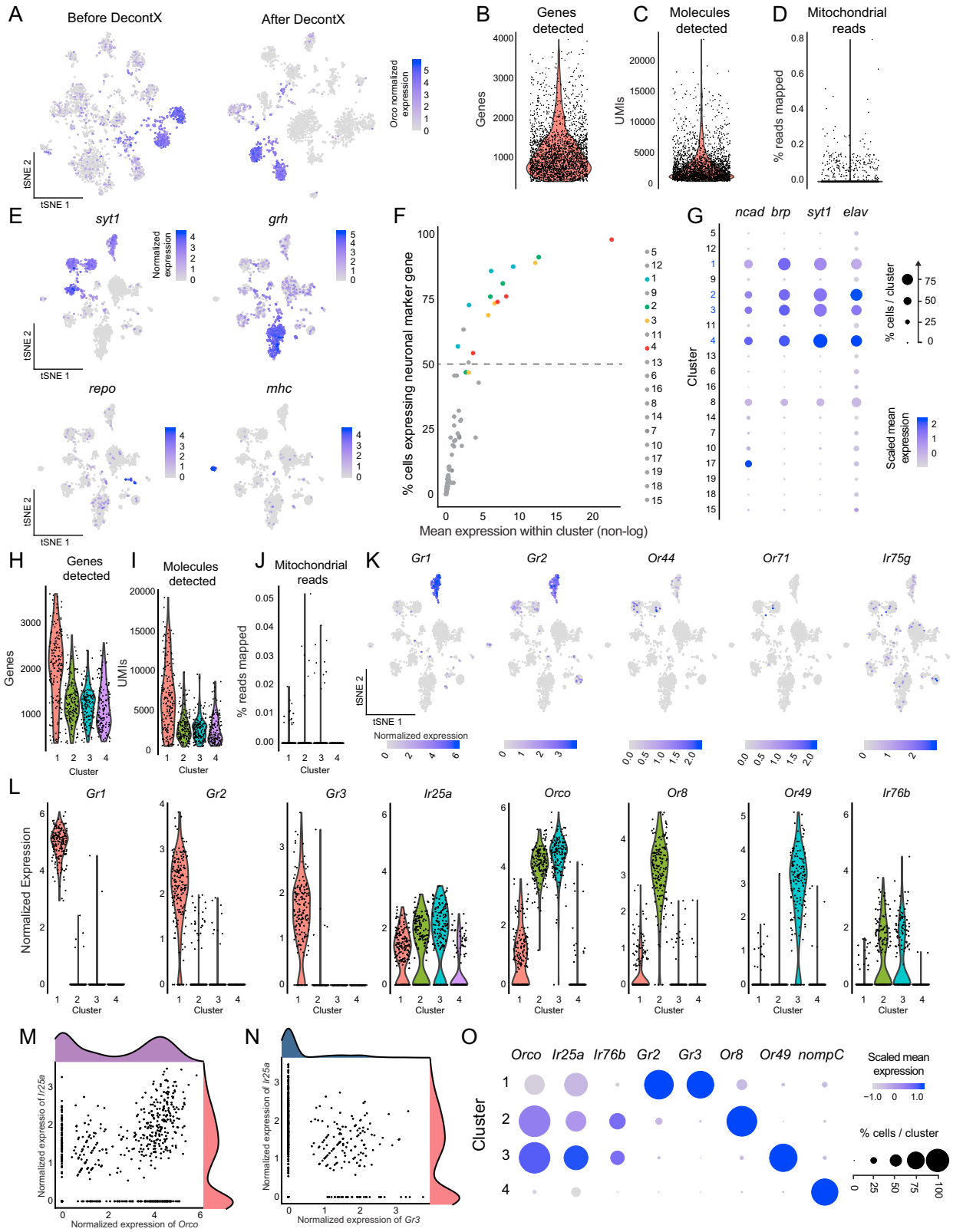

(legend on next page)

Figure S7. Maxillary palp snRNA-seq pipeline and chemoreceptor expression analysis, related to Figure 6

(A) Ambient RNA removal using DecontX, illustrated using normalized expression of *Orco* mapped onto t-distributed stochastic neighbor embedding (t-SNE) plots for maxillary palp snRNA-seq experiment. [unit for normalized expression in maxillary palp data is ln(UMI of gene*10,000/total UMI of cell+1)].

(B–D) Sample properties and distributions after filtering. Nuclei were retained that expressed between 400 and 40,000 genes (B) and fewer than 5% mitochondrial transcripts (D). Nuclei were not additionally filtered on UMIs after multiplet removal (C).

(E) Normalized expression mapped onto t-SNE plots for *syt1* as a marker for neurons, *grh* for epithelial cells, *repo* for glial cells, and *mhc* for muscle cells.

(F) Distribution of neural marker genes (*ncad, brp, syt1*, and *elav*) within clusters. Points denote expression patterns of individual neural marker genes for each cluster. Line indicates the threshold used to identify neuron clusters. Points from identified neuron clusters (1–4), where 50% of cells within a cluster expressing a 3 out of 4 defined neural markers are labeled with color [unit for mean expression in cluster is non-log of normalized expression UMI of gene*10,000/total UMI of cell+1)].

(G) Dot plot illustrating mean scaled expression (*Z* score) of neural markers used to identify neuron clusters. Clusters of identified neurons are labeled in blue (clusters 1, 2, 3, and 4).

(H) Number of genes detected per cell in neuron clusters defined in Figures S13

(I) Number of transcripts detected per cell in neuron clusters.

(J) Percent mitochondrial reads per cell in neuron clusters.

(K) Normalized expression mapped onto t-SNE plots for the indicated chemoreceptor genes.

(L) Distribution of normalized expression of the indicated chemoreceptor genes in cells within neuron clusters.

(M and N) Scatterplot depicting expression levels within individual neuron-identified cells of *Orco* and *Ir25a* (F) and *Gr3* and *Ir25a* (G).

(O) Dot plot illustrating mean scaled expression (*Z* score) and cells expressing a given gene.